

Iowa Research Online

Mitochondria-targeted therapy for metastatic melanoma

Klopping, Kyle Christohper

<https://iro.uiowa.edu/esploro/outputs/doctoral/Mitochondria-targeted-therapy-for-metastatic-melanoma/9983776783202771/filesAndLinks?index=0>

Klopping, K. C. (2015). Mitochondria-targeted therapy for metastatic melanoma [University of Iowa].
<https://doi.org/10.17077/etd.7aq38tk2>

<https://iro.uiowa.edu>

Free to read and download

Copyright © 2015 Kyle Christohper Klopping

Downloaded on 2024/04/29 06:45:34 -0500

Mitochondria-Targeted Therapy for Metastatic Melanoma

by

Kyle Christopher Klopping

A thesis submitted in partial fulfillment
of the requirements for the Doctor of Philosophy
degree in Free Radical and Radiation Biology in the
Graduate College of
The University of Iowa

December 2015

Thesis Supervisor: Associate Professor Michael K. Schultz

Copyright by

KYLE CHRISTOPHER KLOEPPING

2015

All Rights Reserved

Graduate College
The University of Iowa
Iowa City, Iowa

CERTIFICATE OF APPROVAL

PH.D. THESIS

This is to certify that the Ph.D. thesis of

Kyle Christopher Klopping

has been approved by the Examining Committee for
the thesis requirement for the Doctor of Philosophy degree
in Free Radical and Radiation Biology at the December 2015 graduation.

Thesis Committee:

Michael K. Schultz, Thesis Supervisor

Douglas R. Spitz

Apollina Goel

F. Christopher Pigge

Prabhat C. Goswami

ACKNOWLEDGEMENTS

I would first like to express my sincere appreciation for my PhD advisor and mentor Dr. Michael Schultz. His enthusiasm and passion inspire and motivate not only myself, but everyone he interacts with. His guidance and instruction have been essential to my development as a scientist. I am grateful for the support Dr. Schultz has provided me throughout my graduate education and the opportunities he has provided me to travel nationally and internationally.

I would also like to thank my PhD committee members Dr. Douglas Spitz, Dr. Apollina Goel, Dr. Christopher Pigge, and Dr. Prabhat Goswami. The expertise each member brought to my project has proved invaluable and has been essential to moving my project forward. Their comments, critiques, and recommendations have not only aided my project, but also myself as a developing scientist.

I would also like to express my gratitude for the members of the Schultz Lab. Each and every member has impacted my research project in a positive way and have been a tremendous amount of support. I appreciate all the help and advice they have provided throughout my graduate education. I would also like to thank all the high school students, undergraduate students, and medical students I have worked with through the years. I sincerely appreciate all of their hard work and dedication to my project; and it was a pleasure to work with them.

I would like to thank all the faculty, staff, and students of the Free Radical and Radiation Biology Program. Each and every member has provided support

and technical help during my graduate education and have been a valuable asset to my project and development as a scientist. I would especially like to thank the Free Radical and Radiation Biology Core Laboratory and Dr. Michael McCormick for his help and support. I would also like to thank Susan Walsh of the Small Animal Imaging Core for her assistance with my project.

I was fortunate to have the opportunity to study abroad in India during my graduate education. I am thankful for the financial support that the Indo-US Science and Technology Forum provided that allowed me to take part in this incredible experience. This experience would not have been possible without my host and mentor Dr. Baljinder Singh of the Post Graduate Institute for Medical Education and Research in Chandigarh, India. I am grateful for Dr. Singh's hospitality and the opportunity to be a part of his research team. I would also like to thank Dr. Anil Mishra of the Institute of Nuclear Medicine and Allied Sciences in Delhi, India and Dr. Sarabjit Singh of Panacea Biotech in Navi Mumbai, India. Once again, I am grateful for the opportunity to participate in their research projects and their hospitality.

I also want to express my gratitude to the departments, centers, and fellowships that have supported my graduate education financially. I would like to thank the University of Iowa Center for Biocatalysis and Bioprocessing and the Free radical and Radiation Biology Program for supporting me with their T32 training fellowships, the University of Iowa Department of Radiology, and the University of Iowa Holden Comprehensive Cancer Center.

Finally, I would not be where I am today in my education without the love and support of my family. I would especially like to thank my mother and father. They have been a constant source of support and I cannot express enough how grateful I am for them.

ABSTRACT

Melanoma incidence is increasing faster than any other cancer in the world today. Disease detected early can be cured by surgery, but once melanoma progresses to the metastatic stage it is lethal, with an overall median survival of less than one year. The poor prognosis for late stage melanoma patients is attributed to the intrinsic resistance of melanoma to all Food and Drug Administration approved melanoma therapies. Therefore, there is a critical need for novel treatment approaches that circumvent melanoma therapy resistance.

Emerging evidence suggests that differences in melanoma metabolism relative to non-malignant cells represents a potential target for therapeutic intervention. The research presented here demonstrates the potential for using triphenylphosphonium-based compounds as a new therapeutic for metastatic melanoma that is designed to take advantage of these metabolic differences. *In vitro* experiments demonstrate that triphenylphosphonium-based compounds modified with an aliphatic side chain target melanoma cell mitochondria and promote melanoma cell death via mitochondria metabolism inhibition and subsequent reactive oxygen species production. Increased reactive oxygen species production results in decreased glutathione levels and an oxidized cellular state. There is also a structure-activity relationship between TPP side chain length, metabolic disruption, and melanoma cell cytotoxicity. Further, results demonstrate that traditional *in vivo* triphenylphosphonium drug administration routes such as oral gavage, intraperitoneal injection, and

intravenous injection do not result in significant triphenylphosphonium drug tumor accumulation. However, the use of a thermosensitive hydrogel delivery system localizes triphenylphosphonium drugs directly at the melanoma tumor site and decreases melanoma tumor growth rate. These results suggest that a hydrogel-based triphenylphosphonium delivery system could potentially be a therapeutic strategy that circumvents melanoma resistance mechanisms in order to provide durable therapy for an increasing number of metastatic melanoma patients worldwide.

PUBLIC ABSTRACT

Melanoma incidence is increasing faster than any other form of cancer worldwide. Disease detected early can be cured by surgery, but late-stage melanoma is lethal. The lethality of late stage melanoma is attributed to the resistance of melanoma to all Food and Drug Administration approved melanoma treatments. Therefore, there is a critical need for novel treatments that circumvent melanoma resistance and result in long-term benefit for melanoma patients.

An alternative approach to melanoma therapy targets melanoma cell metabolism. Cellular metabolism is essential to acquire energy necessary for cellular function and survival. Further, there are fundamental differences between melanoma cell metabolism and normal cell metabolism that represent a way to selectively kill melanoma cells while sparing normal cells from toxicity.

The research presented here explores a novel class of drugs that target the metabolic differences between melanoma cells and normal cells as a way to selectively kill melanoma cells relative to normal cells. The drugs used in this study preferentially accumulate in melanoma cell mitochondria, the cellular compartment that generates energy required for proper melanoma cell function and survival. Results demonstrate that the compounds studied can be designed to inhibit mitochondria metabolism that ultimately results in melanoma cell death. Further, results demonstrate the compounds used in this study can be delivered directly to the melanoma tumor site and decrease melanoma tumor growth in an

animal model. Collectively, results highlight the potential of a mitochondria-targeted therapy for metastatic melanoma.

TABLE OF CONTENTS

LIST OF FIGURES	xiii
LIST OF ABBREVIATIONS	xvii
CHAPTER I: INTRODUCTION	1
Melanoma	1
Melanoma Initiation and Progression	1
Melanoma Statistics	4
Melanoma Treatment Options.....	5
Cellular Metabolism	8
Non-Malignant Cell Metabolism	8
Cancer Cell Metabolism	10
Melanoma Cell Metabolism	12
Cellular Antioxidant Systems	13
The Glutathione Antioxidant Network.....	14
The Thioredoxin Antioxidant Network	15
Superoxide Dismutase and Catalase	16
Triphenylphosphonium Compounds	17
Triphenylphosphonium Chemical and Mitochondria Targeting Properties.....	19
Thermosensitive Hydrogels	21
Rationale and Hypothesis	22
Significance	23
CHAPTER II: TRIPHENYLPHOSPHONIUM DERIVATIVES INHIBIT MITOCHONDRIA METABOLISM AND INDUCE MELANOMA CELL CYTOTOXICITY	30
Overview	30
Materials and Methods.....	33
Cell Culture	33
Chemicals and Reagents	34
MTT Cell Viability Assay	35
Clonogenic Cell Survival Assay.....	35
JC-1 Mitochondria Membrane Potential Assay	36
Glutathione Assay	36
DHE Oxidation Assay.....	37
Superoxide Dismutase Activity Assay	38
Catalase Activity Assay	39
GPx4 Activity Assay	39
Adenovirus Clonogenic Cell Survival Assay.....	40
NAC Clonogenic Cell Survival Assay	41

GSH and TrxR Inhibitor Clonogenic Cell Survival Assays.....	41
Intracellular ATP Concentration Measurements.....	42
Tumor Xenograft Growth.....	42
C-14 Biodistribution Studies.....	43
In Vivo Tumor Growth Studies.....	43
TPP In Vivo Toxicity Studies.....	44
Statistical Analysis.....	44
Results.....	45
Increasing TPP Side-Chain Length Decreases the Viability of Melanoma Cells.....	45
Increasing TPP Side-Chain Length Decreases the Clonogenic Survival of Melanoma Cells.....	46
Increasing TPP Side-Chain Length Decreases the Mitochondria Membrane Potential of Melanoma Cells.....	48
TPP Decreases Oxygen Consumption in Melanoma Cells.....	49
Increasing TPP Side-Chain Length Increases DHE Oxidation in Melanoma Cells.....	51
Increasing TPP Side-Chain Length Decreases Total Glutathione in Melanoma Cells.....	52
Increasing TPP Side-Chain Length Increases Oxidized Glutathione in Melanoma Cells.....	53
Increasing TPP Side-Chain Length Increases Total Glutathione in Melanoma Cell Tissue Culture Media.....	54
Increasing TPP Side-Chain Length Decreases ATP Levels in Melanoma Cells.....	55
Superoxide Dismutase and Catalase Do Not Protect Melanoma Cells from TPP-Mediated Cytotoxicity.....	56
Glutathione Peroxidase-4 Does Not Protect Melanoma Cells from TPP-Mediated Cytotoxicity.....	57
NAC Treatment Partially Protects Melanoma Cells from TPP-Mediated Cytotoxicity.....	58
Glutathione Synthesis Inhibitors Sensitize Melanoma Cells to TPP Treatment.....	59
Thioredoxin Reductase Inhibitors Enhance the Sensitivity of Melanoma Cells to TPP Treatment.....	60
TPP in vivo Biodistribution.....	60
TPP Treatment Does Not Result in Systemic Toxicity.....	62
TPP Slows Melanoma Tumor Growth When Administered via Hydrogel.....	64
Discussion.....	64

CHAPTER III: FUTURE DIRECTIONS – HYDROGEL-ADMINISTERED TPP BASED COMBINATION THERAPY FOR METASTATIC MELANOMA..... 102

Hypothesis and Specific Aims.....	102
Significance.....	103

Aim 1.....	104
Background and Rationale.....	104
Experimental Design.....	105
Anticipated Results.....	105
Alternative Approach.....	106
Aim 2.....	106
Background and Rationale.....	106
Experimental Design.....	107
Anticipated Results.....	107
Alternative Approach.....	108
 APPENDIX A: SUPPLEMENTARY DATA.....	 111
Overview.....	111
Materials and methods.....	112
Cell Culture.....	112
Chemicals and Reagents.....	113
Cell Growth Curves.....	113
Clonogenic Cell Survival Assay.....	113
Metabolic Flux Measurements.....	114
Enrichment of Mouse Liver Mitochondria.....	114
Electron Transport Chain Complex Activity Assays.....	115
Glucose Uptake Measurements.....	118
Metabolic Gene Array.....	119
Statistical Analysis.....	119
Results.....	122
Melanoma Cell Growth Curves.....	122
TPP Linear Side Chains Induce Cytotoxicity.....	122
TPP Decreases Mitochondria Electron Transport Chain Complex Activity.....	123
TPP Increases Melanoma Cell Glycolytic Activity.....	124
TPP Increases Melanoma Cell Glucose Uptake.....	125
TPP Decreases Melanoma Cell Metabolic Gene Expression.....	126
Discussion.....	136
 APPENDIX B: SYNTHESIS AND CHARACTERIZATION OF TRIPHENYLPHOSPHONIUM DERIVATIVES.....	 138
Overview.....	138
Materials and Methods.....	138
General Considerations.....	138
Azide-TPP Synthesis.....	139
Bis-TPP Synthesis.....	140
17-TPP Synthesis.....	140
21-TPP Synthesis.....	141
TPP-OH Synthesis.....	142

TPP-COOH Synthesis.....	142
Results.....	143
Azide-TPP Synthesis	143
Bis-TPP Synthesis	144
17-TPP Synthesis	144
21-TPP Synthesis	145
TPP-COOH Synthesis.....	145
TPP-OH Synthesis.....	146
Discussion	146
APPENDIX C: TRIPHENYLPHOSPHONIUM DERIVATIVE HIGH THROUGHPUT SCREENS.....	154
Overview.....	154
Materials and Methods.....	155
TPP Compound Library.....	155
MTT HTS Assay.....	155
Results.....	156
TPP High Throughput Screens	156
Discussion	157
APPENDIX D: CHELATOR-MODIFIED TRIPHENYLPHOSPHONIUM DERIVATIVES FOR PET IMAGING.....	160
Overview.....	160
Materials and Methods.....	162
TPP-DOTA Synthesis	162
TPP-NOTA Synthesis	162
TPP-PCTA Synthesis.....	163
TPP-Chelator Radiolabeling.....	163
Results.....	164
TPP-DOTA, TPP-NOTA, and TPP-PCTA Synthesis.....	164
TPP-DOTA and TPP-NOTA Radiolabeling	165
Discussion	165
REFERENCES.....	172

LIST OF FIGURES

Figure I-1: The initiation and progression of melanoma.....	26
Figure I-2: An overview of cellular metabolic pathways	27
Figure I-3: An overview of the glutathione and thioredoxin antioxidant networks	28
Figure I-4: The proposed mechanism of TPP derivatives	29
Figure II-1: The TPP derivatives examined in this study.....	72
Figure II-2: Increasing TPP side-chain length decreases the viability of A375 melanoma cells	73
Figure II-3: Increasing TPP side-chain length decreases the viability of MeWo melanoma cells	74
Figure II-4: Increasing TPP side-chain length decreases the clonogenic survival of A375 melanoma cells after 24 h treatment	75
Figure II-5: Increasing TPP side-chain length decreases the clonogenic survival of A375 melanoma cells after 48 h treatment	76
Figure II-6: Increasing TPP side-chain length decreases the mitochondria membrane potential of A375 melanoma cells	77
Figure II-7: TPP decreases oxygen consumption in melanoma cells	78
Figure II-8: Increasing TPP side-chain length increases DHE oxidation in melanoma cells	79
Figure II-9: Increasing TPP side-chain length decreases intracellular total glutathione in melanoma cells.....	80
Figure II-10: Increasing TPP side-chain length increases oxidized glutathione in melanoma cells	81
Figure II-11: TPP increases total glutathione in the tissue culture media media of melanoma cells	82
Figure II-12: Increasing TPP side-chain length decreases ATP levels in melanoma cells.....	83

Figure II-13: Melanoma cells transfected with a CuZnSOD adenovirus exhibit increased CuZnSOD activity	84
Figure II-14: Melanoma cells transfected with a MnSOD adenovirus exhibit increased MnSOD activity	85
Figure II-15: Melanoma cells transfected with a Cat adenovirus exhibit increased Cat activity	86
Figure II-16: CuZnSOD and Cat does not protect melanoma cells from TPP-mediated cytotoxicity	87
Figure II-17: MnSOD does not protect melanoma cells from TPP-mediated cytotoxicity	88
Figure II-18: Melanoma cells transfected with a GPx4 adenovirus exhibit increased GPx4 activity	89
Figure II-19: GPx4 does not protect melanoma cells from TPP-mediated cytotoxicity	90
Figure II-20: NAC treatment partially protects melanoma cells from TPP-mediated cytotoxicity	91
Figure II-21: Glutathione synthesis inhibition enhances the sensitivity of melanoma cells to TPP treatment.....	92
Figure II-22: Thioredoxin reductase inhibition enhances the sensitivity of melanoma cells to TPP treatment.....	93
Figure II-23: TPP biodistribution following intraperitoneal injection.....	94
Figure II-24: TPP biodistribution following intravenous injection.....	95
Figure II-25: TPP biodistribution following oral administration	96
Figure II-26: TPP biodistribution following peritumoral administration via a thermosensitive hydrogel	97
Figure II-27: TPP treatment does not cause bone marrow toxicity	98
Figure II-28: TPP treatment does not cause liver toxicity	99
Figure II-29: TPP does not affect blood urea nitrogen levels	100

Figure II-30: TPP decreases melanoma tumor growth rate when administered via hydrogel.....	101
Figure III-1: Vemurafenib enhances the sensitivity of BRAF mutant melanoma cells to TPP treatment.....	110
Figure A-1: The TPP structures examined in supplementary experiments	128
Figure A-2: A375 melanoma cell growth curve	129
Figure A-3: MeWo melanoma cell growth curve	130
Figure A-4: TPP linear side-chains induce cytotoxicity	131
Figure A-5: TPP inhibits mitochondria electron transport chain activity	132
Figure A-6: TPP increases melanoma cell glycolytic activity	133
Figure A-7: TPP increases melanoma cell glucose uptake	134
Figure A-8: TPP decreases melanoma cell metabolic gene expression.....	135
Figure B-1: Azide-TPP mass spectroscopy confirmation of the product.....	148
Figure B-2: Bis-TPP mass spectroscopy confirmation of the product.....	149
Figure B-3: 17-TPP mass spectroscopy confirmation of the product.....	150
Figure B-4: 21-TPP mass spectroscopy confirmation of the product.....	151
Figure B-5: TPP-OH mass spectroscopy confirmation of the product	152
Figure B-6: TPP-COOH mass spectroscopy confirmation of the product.....	153
Figure C-1: TPP high throughput melanoma versus non-malignant cell viability assay	158
Figure C-2: The chemical structures of lead TPP compounds identified in high throughput screens that result in the greatest differential cytotoxicity in melanoma versus non-malignant cells	159
Figure D-1: TPP-DOTA mass spectroscopy confirmation of the product.....	167
Figure D-2: TPP-NOTA mass spectroscopy confirmation of the product.....	168

Figure D-3: TPP-PCTA mass spectroscopy confirmation of the product	169
Figure D-4: TPP-DOTA radio-HPLC trace	170
Figure D-5: TPP-NOTA radio-HPLC trace	171

LIST OF ABBREVIATIONS

2-NBDG: 2-deoxy-2-[(7-nitro-2,1,3-benzoxadiazol-4-yl)amino]-D-glucose

2-VP: 2-vinylpyridine

Ad: Adenovirus

ADP: Adenosine diphosphate

APC: Antigen presenting cell

ALP: Alkaline phosphatase

ALT: Alanine transaminase

ATP: Adenosine triphosphate

AUR: Auranofin

BCS: Bathocupriome disulfonic acid

BILI: Bilirubin

BSA: Bovine serum albumin

BSO: L-Buthionine sulfoximine

BUN: Blood urea nitrogen

CAT: Catalase

CBC: Complete blood count

Ci: Curie

CMV: Cytomegalovirus

CO₂: Carbon dioxide

CPI: Cardiac perfusion imaging

CTLA-4: Cytotoxic T-lymphocyte antigen-4

CuZnSOD: Copper-zinc superoxide dismutase

DCIP: Dichlorophenolindophenol

DETAPAC: Diethylenetriaminepentaacetid acid

DHE: Dihydroethidium

DMEM: Dulbecco's modified eagle medium

DMSO: Dimethyl sulfoxide

DNA: Deoxyribonucleic acid

DNTB: 5,5'-dithiobis-2-nitrobenzoic acid

EcSOD: Extracellular superoxide dismutase

ESI-MS: Electrospray ionization mass spectrometry

ETC: Electron transport chain

FADH: Flavin adenine dinucleotide

FBS: Fetal bovine serum

FCCP: Carbonyl cyanide 4-(trifluoromethoxy)phenylhydrazone

FDA: Food and Drug Administration

G-6-PH: Glucose-6-phosphate

GLUTs: Glucose transporters

GPx: Glutathione peroxidase

GR: Glutathione reductase

GSH: Glutathione

GSSG: Glutathione disulfide

HCT: Hematocrit

HGB: Hemoglobin

H₂O₂: Hydrogen peroxide

HPLC: High performance liquid chromatography

I.P.: Intraperitoneal

I.V.: Intravenous

JC-1: 5,6-dichloro-2-[(*E*)-3-(5,6-dichloro-1,3-diethyl-1,3-dihydro-2*H*-benzimidazol-2-ylidene)-1-prop-1-enyl]-1,3-diethyl-1*H*-benzimidazolium iodide

LC-MS: Liquid chromatography-mass spectrometry

LYMPH: Lymphocytes

MAPK: Mitogen activated protein kinase

MHC: Major histocompatibility complex

MnSOD: Manganese superoxide dismutase

MOI: Multiplicity of infection

MONO: Monocyte

MTT: 3-(4,5-dimethylthiazol-2-yl)-2,5-diphenyltetrazolium Bromide

NAC: *N*-acetyl-L-cysteine

NAD: Nicotinamide adenine dinucleotide

NADPH: Nicotinamide adenine dinucleotide phosphate

NBT: Nitroblue tetrazolium

NEUT: Neutrophil

O₂: Oxygen

O₂^{•-}: Superoxide

[•]OH: Hydroxyl radical

PBS: Phosphate buffered saline

PCR: Polymerase chain reaction

PD-1: Programmed death receptor-1

PET: Positron emission tomography

PCOOH: Phosphatidylcholine hydroperoxide

PPP: Pentose phosphate pathway

Prx: Peroxiredoxin

RBC: Red blood cell

RET: Reticulocyte

RGP: Radial growth phase

RNA: Ribonucleic acid

ROOH: Organic hydroperoxide

ROS: Reactive oxygen species

SF: Surviving fraction

SOD: Superoxide dismutase

TCA: Citric acid cycle

TNB: 2-nitro-5-thiobenzoate

TPP: Triphenylphosphonium

Trx: Thioredoxin

TRxR: Thioredoxin reductase

UV: Ultraviolet

VGP: Vertical growth phase

WBC: White blood cell

VEGF: Vascular endothelial growth factor

CHAPTER I: INTRODUCTION

Melanoma

Melanoma is a form of skin cancer that arises from melanocytes located in the epidermis of the skin. Once melanoma progresses to the metastatic stage it is lethal and results in poor patient outcome. Poor patient outcome is due to the lack of durable melanoma therapies attributed to the resistance of melanoma tumors to treatment. Ongoing efforts have recently resulted in new Food and Drug Administration (FDA) approved melanoma therapies, but patient prognosis remains poor. There remains a critical need for the development of novel treatment strategies to circumvent melanoma resistance in order to provide durable, long-term treatment for an increasing number of melanoma patients worldwide.

Melanoma Initiation and Progression

Melanoma is the most aggressive form of skin cancer and incidence is increasing worldwide [1, 2]. Although melanoma accounts for less than 4% of all dermatological cancers, it results in the largest number of skin cancer deaths [3-5]. Melanoma arises from melanocytes that are located in the epidermis of the skin [2, 5-8]. Melanocytes are cells that produce melanin that is responsible for skin and hair color and are regulated by keratinocytes located in the epidermis [2,

5, 6, 9, 10]. When exposed to ultraviolet (UV) radiation, keratinocytes secrete factors that signal melanocytes to produce melanin that ultimately results in the tanning process that protects us from the harmful effects of UV radiation [2, 5, 6, 9, 10]. Melanoma initiation begins when melanocytes escape keratinocyte regulation due to genetic mutations, growth factor production, and loss of adhesion receptors that allow them to proliferate and spread and form a benign nevus (common mole) or dysplastic nevus [2, 4, 11]. Nevi can then enter the radial-growth-phase (RGP), which generally occurs in the epidermis but sometimes can minimally invade the dermis [2, 8, 11]. Following RGP, RGP cells can enter the vertical growth phase (VGP) where nodules of cells invade the dermis and gain lethal metastatic potential [2, 8, 11].

Although melanomas generally follow this pattern of progression, RGP and VGP can develop directly from melanocytes and nevi and can progress directly to metastatic melanoma [2]. In fact, melanoma is distinguished from other solid tumors due to its ability to rapidly metastasize [12-14]. Melanoma tumors less than 2 mm thick have the ability to invade the dermis, intravasate into the lymphatics or vasculature, travel to distant organs, and extravasate into the parenchyma in order to form metastatic lesions [8, 12, 13, 15]. One reason melanoma readily metastasizes is due to the fact that they have high expression of cell adhesion molecules on their outer surface that allows them to migrate and invade the dermis and undergo intravasation [12, 14, 16, 17]. It has also been shown that expression of these cell adhesion molecules help regulate the activity of enzymes such as matrix metalloproteinases that break down the basement

membrane and extracellular matrix which promotes invasion [7, 12, 13]. Melanoma cell adhesion molecules also allow melanoma cells to clump in circulation, thus protecting inner cells from sheer stress and immunosurveillance [12, 18, 19]. Once melanoma cells undergo intravasation, they share many antigens with vascular endothelial cells as well [12, 18, 19]. This allows them to survive physical forces in circulation, adhere to vessel walls, and extravasate [12, 18-20]. Further, endothelial cells express different cell adhesion molecules depending on the organ type that can lead to site specific metastasis depending on the expression levels of that same cell adhesion molecule on melanoma cells [12, 19, 20].

Another factor that promotes melanoma metastasis is the ability of melanoma cells to adapt to a distant organ site microenvironment, stimulate angiogenesis, and stimulate lymphanogenesis [12, 13, 21]. Evidence demonstrates that metastatic melanoma cells respond and adapt to the organ site they metastasize to and acquire characteristics of that organ (e.g. alter gene expression to mimic gene expression patterns of the organ they have metastasized to) [12, 22, 23]. In order to induce angiogenesis, metastatic melanoma cells express interleukin-8, a chemokine that stimulates endothelial cell migration by acting as a ligand for interleukin-8 receptors expressed on the microvasculature that stimulates endothelial cell proliferation and migration [12, 13, 21]. Metastatic melanoma cells also express basic fibroblast factor and vascular endothelial growth factor (VEGF) that induce angiogenesis and tumor cell proliferation [12, 21, 24]. Much in the same way as melanoma cells stimulate

angiogenesis, melanoma cells upregulate biomolecules (e.g., lipid lysophosphatidic acid, vascular endothelial growth factor C) that aid in lymphangiogenesis as well [12, 25, 26]. The upregulation of molecules associated with angiogenesis and lymphangiogenesis provide the nutrients and oxygen needed for tumor development [12, 27, 28].

Finally, melanoma cells are characterized by the ability to avoid immune surveillance that ultimately contributes to their aggressiveness and ability to metastasize despite being one of the most immunogenic cancer types [12, 13, 29, 30]. Melanoma cells also secrete cytokines that inhibit an immune response against them [12, 13, 31, 32]. Further, melanoma cells have the ability to inhibit T-cell responses by blocking T-cell receptors and by overcoming immune response checkpoints through increased expression of the cytotoxic T-lymphocyte associated antigen-4 (CTLA-4) and programmed death receptor-1 (PD-1) among others [12, 30, 33]. The stages of melanoma initiation and progression are shown in **Figure I-1**.

Melanoma Statistics

Melanoma incidence is increasing worldwide and is expected to result in 73,870 new diagnoses and 9,940 deaths in 2015 in the United States alone [34-40]. From 1950 to 2000, melanoma incidence has increased by 619% and is now the 5th most common cancer in men and 7th in women [35, 40, 41]. Projections indicate that by 2030 the number of new melanoma cases will be around 112,000 without improved treatment approaches or public education [35].

Further, melanoma treatment costs \$3.3 billion annually in the United States alone [35]. Fortunately, localized, early stage melanomas can be cured by surgical resection, which results in a 98.3% five-year survival rate [35, 37, 42]. Once melanoma progresses to the metastatic stage the five-year survival rate drops to < 20% [35]. These facts and figures highlight the need for new and improved detection and therapeutic strategies for metastatic melanoma.

Melanoma Treatment Options

Prior to 2011, the only FDA approved melanoma therapies were dacarbazine and high dose interleukin-2 [5, 36, 38, 41, 43]. Dacarbazine was FDA approved in 1975 and is a DNA alkylating agent that was considered the standard of care [44, 45]. Dacarbazine success is limited due to a low patient response rate and lack of survival benefit [36, 44, 45]. Interleukin-2 is a lymphokine that activates T cells, natural killer cells, and cytokine release by lymphocytes that was FDA approved in 1998 [5, 44, 45]. Similar to dacarbazine, the interleukin-2 patient response rate is low and does not result in a durable response [5, 36, 44-46]. Further, interleukin-2 is accompanied by harsh side effects in patients [5, 36, 44-46].

Recently much excitement has been generated in the melanoma field, with six new FDA approved targeted or immune-based therapies in the past five years [5, 37, 38, 43]. Ipilimumab is a human monoclonal antibody that blocks CTLA-4 that was FDA approved in 2011 [5, 45, 46]. T-lymphocytes are stimulated in response to tumor antigens to inhibit tumor progression [5, 45, 46].

During T cell activation, a tumor antigen is presented on the surface of an antigen presenting cell (APC) and a T-cell receptor binds to the APC antigen [5, 46-48]. Next, CD-28 found on T-cells bind to the B7 co-stimulatory receptor on the APC which signals further T-cell activation [46-48]. CTLA-4 is found on T-cells and melanoma cells and acts as a negative co-stimulatory molecule for T-cell activation by outcompeting CD-28 for binding to B7, thus inactivating T-cell stimulation and a way for melanoma cells to avoid immune detection [36, 46-48]. Ipilimumab binds to CTLA-4 and prevents it from binding B7 and subsequently prevents a decrease in T-cell activation [36, 46-48]. In phase III clinical trials, ipilimumab increased overall survival compared to control groups, but the patient response rate was modest [5, 36, 45, 46].

In 2011, vemurafenib was also FDA approved for the treatment of melanoma [5, 45, 49]. Vemurafenib is a BRAF inhibitor, and gene mutated in ~50% of melanoma patients [3, 36, 45, 49, 50]. Vemurafenib inhibits a V600E mutation (valine for glutamic acid substitution), which is the most common BRAF mutation found in melanoma patients [36, 45, 49]. Mutations in BRAF lead to constitutive activation of the mitogen-activated protein kinase (MAPK) (RAS/RAF/MEK/ERK) pathway that results in cell proliferation and pro-survival [36, 49, 50]. Phase III studies demonstrated that vemurafenib achieves a large response rate (>50%) in melanoma patients, but the duration of response is relatively short [3, 5, 45, 49]. Dabrafenib is a second V600E BRAF inhibitor that was FDA approved in 2013 [5, 45, 49]. This BRAF inhibitor also achieved a large response rate in melanoma patients but again the duration of response was

relatively short in patients with stage III or IV melanoma [5, 45, 49]. Tramatenib is a MEK inhibitor that was FDA approved in 2013 for patients harboring a V600E or a V600K (valine for lysine substitution) BRAF mutation [5, 40, 45, 49]. Again, melanoma patient response rate was high but the duration of response was relatively short [40, 45, 49].

Nivolumab is an immune-based therapy that was FDA approved in 2014 [5, 40]. Nivolumab is a human monoclonal antibody that binds programmed PD-1 [40, 45]. Similar to CTLA-4, PD-1 is a receptor found on T-cells and melanoma cells that acts as a negative regulator of T-cell activation when bound to B7 found on APCs or tumor cells and inhibits an immune response against cancer cells [51, 52]. Nivolumab binds PD-1 and prevents this decrease in immune response [45, 51, 52]. In phase III trials, nivolumab achieved a higher response rate than previous immunotherapies with fewer adverse effects [40, 45]. Pembrolizumab is second PD-1 inhibitor FDA approved in 2014 [5, 40, 53]. This therapy also achieves a high response rate similar to nivolumab [5, 40, 53]. Overall survival data on nivolumab and pembrolizumab is not yet available.

The recent FDA approval of new melanoma therapies has yielded promising results, but patient response rate and therapy resistance continues to be a barrier to durable melanoma therapy. Trials are ongoing investigating the use of combination therapies with the new FDA approved melanoma drugs as a way to target multiple pathways in order to achieve higher patient response rates and improve overall survival. Collectively, results of clinical trials support the

continued development of novel treatments that circumvent melanoma resistance mechanisms in order to improve patient response rate and treatment efficacy.

Cellular Metabolism

All cells require energy sources in order to survive and proliferate [54-57]. Cells extract energy from nutrients (carbohydrates, fatty acids, amino acids) in order to generate energy in the form of adenosine triphosphate (ATP) that is used to fuel cellular processes and biosynthetic needs [54, 55]. Cellular metabolism is generally broken down into three processes: glycolysis, the citric acid cycle (TCA), and oxidative phosphorylation. Interestingly, cancer cells (including melanoma) exhibit different metabolic properties compared to non-malignant cells that can potentially be exploited as a way to selectively kill melanoma cells relative to non-malignant cells and circumvent melanoma therapy resistance. An overview of cellular metabolism can be found in **Figure I-2**.

Non-Malignant Cell Metabolism

The main energy source in cells is glucose [50, 54, 55, 58, 59]. Glucose undergoes glycolysis, a series of enzyme-catalyzed reactions occurring in the cytosol, where glucose is converted into pyruvate [50, 54, 55, 58, 60]. Glycolysis consists of two phases; a “prep” phase that requires ATP and a “payoff” phase that generates ATP [55, 60, 61]. A total of four ATP are generated per molecule

of glucose during glycolysis, but two ATP are required for the prep phase, yielding a net of two ATP per molecule of glucose [55, 59, 60, 62].

In addition to conversion to pyruvate, a portion of glucose can be shunted through the pentose phosphate pathway (PPP) following conversion to glucose-6-phosphate (G-6-PH) [55, 62, 63]. The PPP consists of an oxidative phase and a non-oxidative phase [55, 63]. The oxidative phase of the PPP generates the reducing equivalent nicotinamide adenine dinucleotide phosphate (NADPH) necessary for fatty acid and steroid synthesis and the reduction of the antioxidant glutathione (GSH)/glutathione peroxidase (GPx)/glutathione reductase (GR) system and the thioredoxin (Trx)/peroxiredoxin (Prx)/thioredoxin reductase (TRxR) system [55, 63-65]. The non-oxidative phase of the PPP generates pentoses necessary for the synthesis of nucleic acids, nucleotides, and coenzymes [55, 63-65].

Under anaerobic conditions, pyruvate generated by glycolysis is converted to lactate via lactate dehydrogenase [55, 59, 60]. Under aerobic conditions, pyruvate is oxidized to acetyl-CoA that enters the TCA [50, 55, 56, 58, 60]. During the TCA in the mitochondria, acetyl-CoA is oxidized to form carbon dioxide (CO₂), flavin adenine dinucleotide (FADH₂), nicotinamide adenine dinucleotide (NADH), and water [55, 56, 59, 60, 62, 66]. NADH and FADH₂ generated from the TCA are used as a source of electrons for the electron transport chain (ETC) and the process of oxidative phosphorylation [50, 55, 56, 59, 60]. The ETC consists of four complexes: NADH:ubiquinone oxidoreductase (complex I), succinate:ubiquinone oxidoreductase (complex II),

ubiquinone:cytochrome c oxidoreductase (complex III), and cytochrome c oxidase (complex IV) [55, 67, 68]. The first electron entry point into the ETC is at complex I, where NADH donates two electrons to NADH dehydrogenase, which then transfers those electrons to ubiquinone [55, 59, 68, 69]. At complex II, succinate is oxidized by succinate dehydrogenase to fumarate and generates FADH₂. Electrons are transferred from FADH₂ to ubiquinone [55, 59, 68, 69]. At complex III, electrons are transferred from ubiquinone to cytochrome c [55, 67, 68]. Finally, complex IV involves the transfer of electrons from cytochrome c to oxygen (O₂) to form water [50, 55, 59, 67, 68].

The movement of electrons through the electron transport chain complexes results in the translocation of protons from the mitochondria matrix to the mitochondria intermembrane space which results in a proton gradient [50, 55, 59, 69, 70]. This establishes a proton motive force or negative voltage potential with the inside of the mitochondria having a larger negative charge than the intermembrane space [55, 59, 69, 70]. The proton motive force drives protons back into the mitochondria matrix through ATP synthase, which results in the conversion of adenosine diphosphate (ADP) and phosphate to ATP [50, 55, 59, 69, 70]. The oxidation of one molecule of glucose molecule by oxidative phosphorylation can yield up to 36 molecules of ATP [55, 62].

Cancer Cell Metabolism

Non-malignant cells primarily rely on oxidative phosphorylation to generate ATP in the presence of O₂ [56, 60, 69]. Otto Warburg observed that

cancer cells primarily rely on glycolysis and produce large amounts of lactate even in the presence of sufficient amounts of oxygen known as “aerobic glycolysis” or the “Warburg Effect.” [50, 56, 58, 60, 64, 71, 72]. The conversion of glucose to lactate only yields two ATP, whereas oxidative phosphorylation yields up to 36 ATP per molecule of glucose [56, 59, 60, 64].

One possible explanation for the metabolic switch to a less efficient form of ATP production is that tumors have hypoxic areas that are limited in O₂ [50, 56, 60, 66]. This would prevent proper ETC activity; therefore the switch to glycolysis is a way to generate ATP and survive in hypoxic and normoxic tumor environments [50, 56, 60, 64, 71]. Glycolysis also leads to lactate formation that aids in cancer cell invasion and metastasis by disruption of the extracellular matrix [64, 66, 71]. Normal cells also do not take up nutrients unless signaled to do so by growth factors that prevents uncontrolled proliferation [56, 66]. Cancer cells on the other hand acquire genetic mutations that overcome this growth factor dependence on nutrient uptake which results in uncontrolled uptake and metabolism of nutrients that fuel cell growth and proliferation [56, 66, 71]. In fact, a host of genetic mutations or gene expression changes have been identified in genes that regulate metabolic enzyme expression in cancer cells that lead to increased glycolytic activity [17, 64, 66, 69, 71]. Glycolysis and the PPP also generate metabolic intermediates that are important for biosynthesis necessary for cancer cells to survive and proliferate [58, 64, 71].

Lastly, it is believed that as many as 0.1-1 % of the electrons that enter the ETC are released at complexes I and III due to inefficiencies in ETC activity

in non-malignant cells [73-76]. In cancer cells, this inefficiency in electron transfer is exacerbated and results in more electrons escaping from the ETC [77-80]. This results in one-electron reductions of O₂ to superoxide (O₂^{•-}), which then reacts to form hydrogen peroxide (H₂O₂) and other organic hydroperoxides (ROOH) [50, 76, 81, 82]. In response to this increase in reactive oxygen species (ROS), increased glucose uptake and upregulated glucose metabolism in cancer cells relative to normal cells (including melanoma) is recognized as a mechanism that not only supports increased survival and proliferation needs, but also detoxifies ROS in cancer cells [83-85]. During glucose metabolism, glucose is metabolized to glucose-6-phosphate that is either converted to pyruvate through glycolysis or shunted through the PPP in order to generate NADPH from NADP⁺ and pentoses necessary for nucleotide and cofactor biosynthesis [63, 81, 83-87]. NADPH provides the reducing equivalents for the antioxidant GSH/GPx/GR and Trx/Prx/TRxR systems that scavenge ROS and protect cells from cytotoxic oxidative stress [63-65, 83-87].

Melanoma Cell Metabolism

Proliferating cancer cells exhibit distinct differences in metabolism relative to non-malignant cells [58, 64, 86, 88, 89]. While decreased oxidative phosphorylation and increased glycolysis is a generalized cancer-cell-specific metabolic trait, emerging evidence suggests that melanoma cells maintain sustained (or increased) mitochondria oxidative phosphorylation rates by using energy reducing equivalents derived from fatty acid oxidation and the TCA [50,

90-93]. Evidence of upregulated gene expression associated with fatty acid metabolism, TCA, and oxidative phosphorylation in melanoma cells, further supports the assertion that oxidative phosphorylation along with glycolysis is active in metastatic melanoma cells [90-92].

An important consequence of increased oxidative phosphorylation in melanoma cells is hyperpolarization of the mitochondria membrane potential in cancer cells relative to non-malignant cells due to increased ETC activity [57, 94-97]. Hyperpolarization (or increased electronegative membrane potential) of melanoma cell mitochondria membranes represents a physical difference in melanoma cells relative to non-malignant cells that can be targeted for drug delivery and a potential way to circumvent melanoma therapy resistance.

Cellular Antioxidant Systems

Increased cellular levels of ROS (e.g., $O_2^{\bullet-}$ and H_2O_2) can result in oxidative stress if there is an imbalance between ROS production and removal [98, 99]. Elevated ROS and subsequent oxidative stress can result in damage to cellular components such as DNA, protein oxidation, lipid oxidation, and enzyme deactivation and their cofactors [98]. Cells have antioxidant systems comprised of small molecular weight antioxidants and antioxidant enzymes that are crucial for a variety of cellular functions including ROS scavenging. The two main antioxidant systems in cells are GSH and Trx [77, 100]. These networks provide reducing equivalents for DNA synthesis, thiol-redox homeostasis, oxidative stress defense, protein folding, regulation of cell growth, and regulation of

apoptosis [63, 87, 101-103]. NADPH serves as the reducing equivalent for both GSH and Trx [63, 65, 87, 104]. Although the GSH and Trx system share similar functions, they are separate entities and differ in their preferred substrates [101, 105, 106]. The GSH and Trx systems do support each other [e.g., Trx can reduce oxidized GSH (GSSG)]; therefore disruption of either impacts the other [87, 101, 105-108]. Cancer cells (including melanoma) have demonstrated increased levels of GSH and Trx that are associated with therapy resistance [77, 83, 84, 102-104, 109]. Therefore, the GSH and Trx networks represent potential targets for enhancing the sensitivity of cancer cells to chemotherapy treatment. A diagram of the GSH and Trx systems can be found in **Figure I-3**.

In addition to the GSH and Trx antioxidant networks, cells also have the antioxidant enzymes superoxide dismutase (SOD) and catalase (Cat). Superoxide dismutase converts $O_2^{\cdot-}$ to H_2O_2 and O_2 and Cat neutralizes H_2O_2 to water and O_2 [98, 110-112]. Collectively, these antioxidant enzymes scavenge and detoxify ROS and significantly influence the redox state within cells, which can affect many biological processes such as cell proliferation and death [99, 110].

The Glutathione Antioxidant Network

Glutathione is the major thiol redox buffer found in cells at an average concentration of 1-11 mM [87, 113, 114]. GSH is a tripeptide that has a thiol-containing cysteine residue and forms inter-molecular disulfides with other GSH proteins when oxidized [87, 100, 115]. GSH is synthesized primarily in the

cytosol from glutamate, glycine, cysteine, and the enzymes γ -glutamylcysteine synthetase and glutathione synthetase [87, 109, 113, 116, 117]. GPx oxidizes GSH and Grx reduces oxidized GSSG back to two GSH with NADPH as the reducing equivalent [104, 105, 107].

L-buthionine sulfoximine (BSO) is an inhibitor of γ -glutamylcysteine synthetase, the rate-limiting step in GSH synthesis [83, 102, 104, 118]. Many groups have evaluated BSO and subsequent GSH depletion as a potential combination therapy with various chemotherapeutic agents for cancer therapy [83, 84, 104, 109].

The Thioredoxin Antioxidant Network

The Trx system is a second major thiol redox buffer found in cells at a concentration of 1-10 μ M [87]. Trx is a small redox active protein with two active thiol-containing selenocysteine residues that form intra-molecular disulfides when oxidized [87, 100, 107]. Trx is oxidized with the aid of the enzyme Prx and TRxR reduces Trx with NADPH as the reducing equivalent [15, 103, 105, 107, 119]. TRxR is a selenium containing oxidoreductase that catalyzes the NADPH-dependent reduction of Trx [105, 120].

Auranofin (AUR) is a gold compound FDA approved for rheumatoid arthritis [83, 119, 121]. Auranofin has also demonstrated anti-cancer properties [103, 104, 119, 121]. Auranofin reacts with selenocysteine and cysteine; therefore it is believed to inhibit the selenocysteine containing TRxR [103, 119-121]. Similar to BSO, many groups have looked at AUR as a potential enhancer

of cell killing when combined with other chemotherapeutic agents [83, 84, 103, 120, 122].

Superoxide Dismutase and Catalase

Superoxide is a ROS that is generated by the ETC, xanthine oxidases, NAD(P)H oxidases, nitric oxide synthases, and cytochrome P450s [98, 110, 123]. Elevated intracellular levels of $O_2^{\bullet-}$ can result in cellular oxidative stress if not scavenged by antioxidant systems. Elevated ROS and subsequent oxidative stress can result in damage to cellular components such as DNA, protein oxidation, lipid oxidation, and enzyme deactivation and their cofactors [98, 123]. Superoxide dismutase is an antioxidant enzyme that converts $O_2^{\bullet-}$ to H_2O_2 and O_2 [98, 99, 110-112]. Mammalian cells have three different forms of SOD: EcSOD, CuZnSOD, and MnSOD [99, 110, 111]. EcSOD is found in the plasma membrane of cells [110, 111]. CuZnSOD is found in the cytoplasm, nucleus, and mitochondria inner membrane [110-112]. Finally, MnSOD is found in the mitochondria matrix [110, 111]. The H_2O_2 generated by the dismutation of $O_2^{\bullet-}$ can then be converted to water and O_2 by the enzyme Cat [98, 110, 111]. If H_2O_2 generated by the dismutation of $O_2^{\bullet-}$ is not converted to water, it can react with reduced iron to form the very reactive hydroxyl ($\bullet OH$) radical. Collectively, the enzymes SOD and Cat aid to scavenge and detoxify ROS in order to alleviate oxidative stress and influence cell survival and proliferation.

Triphenylphosphonium Compounds

Mitochondria dysfunction has been implicated in a number of diseases including cancer and interest in targeting mitochondria for cancer therapy has increased over the past few years [57, 95, 124]. One class of mitochondria targeted agents that have received considerable attention as a potential cancer therapy is based on a lipophilic cation, triphenylphosphonium (TPP). TPP-based compounds have been used for decades to study mitochondria biophysics, membrane potential, and to target mitochondria for cellular imaging and disease therapy [125-127]. TPP compounds have primarily been used *in vivo* for the delivery of biologically active molecules such as ROS-scavenging antioxidants (e.g., vitamin E, ubiquinone, α -lipoic acid) to the mitochondria, a major source of ROS that has been associated with the progression of multiple diseases and disorders [123, 128-130]. MitoQ is a TPP compound linked to an antioxidant ubiquinone moiety by a ten-carbon linker [126, 130, 131]. MitoQ preferentially accumulates on the matrix surface of the inner mitochondria membrane, where the quinone moiety inserts into the inner mitochondria membrane and is redox-cycled between its quinol antioxidant form and quinone form by the ETC [130]. MitoQ primarily accumulates in the heart and liver when administered to mice orally, with some accumulation in the brain and muscle [128-130]. Importantly, animal studies demonstrate that 500 μ M MitoQ administered orally via drinking for up to 28 weeks is well tolerated in mice [130]. In human clinical trials, MitoQ has been evaluated as a treatment to slow Parkinson's disease and hepatitis C

infection mediated liver damage; two diseases associated with mitochondria dysfunction and oxidative stress [131, 132]. In a clinical trial designed to determine if MitoQ slows Parkinson's disease progression, 128 untreated Parkinson's disease patients were randomized into treatment groups and orally administered 40 mg MitoQ, 80 mg MitoQ, or placebo daily for up to 12 months and evaluated for Parkinson's disease progression [131]. Unfortunately, there were no differences in Parkinson's disease progression between MitoQ treatment and placebo groups [131]. A phase II clinical trial was also conducted to determine if MitoQ treatment decreases liver damage in patients with hepatitis C infection [132]. In this trial, 30 patients who did not respond or were unsuitable candidates for the hepatitis C standard of care were randomized into treatment groups and administered 40 mg, 80 mg, or placebo once daily for 28 days [132]. Patients were analyzed for serum aminotransferase (alanine transaminase and aspartate aminotransferase) levels and hepatitis C ribonucleic acid (RNA) viral load levels [132]. Results demonstrated a significant decrease in serum alanine transaminase and aspartate transaminase levels in MitoQ treatment versus placebo groups from baseline compared to day 28 [132]. There were no differences in hepatitis C RNA viral load levels, which argues that MitoQ affects hepatitis C virus mediated liver damage and not the virus itself [132]. Importantly, MitoQ side effects were mild in both trials [131, 132].

Although most TPP studies to date utilize TPP as a targeting agent to deliver a biologically active moiety to mitochondria (e.g., Mito Q), the potential for the use of linear-side-chain-modified TPP compounds as anticancer agents has

only recently been realized [93, 127]. The utility of side-chain-modified TPP derivatives as anticancer agents comes from their ability to preferentially accumulate within mitochondria and disrupt mitochondria metabolism to mediate cytotoxicity due to their chemical properties and the biochemical properties of mitochondria. Targeting the differences in mitochondria metabolism between melanoma cells and non-malignant cells could represent a therapeutic avenue to circumvent melanoma resistance. A diagram of TPP accumulation in mitochondria can be found in **Figure I-4**.

Triphenylphosphonium Chemical and Mitochondria Targeting Properties

TPP compounds are hydrophobic cationic molecules that can pass through cellular membranes without the need for ionophores or carrier proteins due to their hydrophobicity [125, 129, 133, 134]. In contrast to hydrophilic compounds, the activation energy required to facilitate TPP passage through the hydrophobic core of lipid membranes is much lower [125, 126, 135]. The activation energy has two main components: a repulsive electrostatic energy component (Born energy) and attractive hydrophobic forces [125, 126, 136]. The Born energy is the enthalpy input needed to remove solvating water molecules from cations as they move from an aqueous environment to the lipid membrane [125, 134, 136]. The enthalpy input for TPP is low because the ionic radius of TPP is large and has a delocalized positive charge [125, 134-136]. This results in weakened solvation and a lower electric field at the TPP surface that can polarize water molecules [125, 134, 136]. Hydrophobic force is the energy

necessary to move an uncharged molecule identical in size and hydrophobicity from the aqueous environment to the lipid membrane core [136]. In the case of lipophilic TPP cations, this force is attractive due to the loss of water structure in moving a large hydrophobic surface area molecule into a lipid [125, 136]. The larger the hydrophobic surface area, the larger the effect [125, 136]. Therefore, increasing the hydrophobic surface area through rational modifications to TPP increases the lipophilicity and membrane uptake as well [133, 137-139]. In fact, evidence demonstrates that TPP derivatives modified with linear aliphatic side chains adsorb to the inner mitochondria membrane where the side chain anchors into the mitochondria membrane [133, 138, 139]. Further, evidence demonstrates that the longer and more hydrophobic the TPP side chain, the more TPP anchors into the mitochondria membrane [133, 138, 139].

The positive charge of TPP cations also facilitates TPP movement through biological membranes due to the plasma and mitochondria membrane potentials [125, 129, 133, 140]. The plasma membrane has a voltage potential of -30 to -60 mV and the mitochondria membrane potential is -150 to -180 mV [129, 133, 140, 141]. TPP mitochondria accumulation increases 10-fold for every 61.5 mV of membrane potential at 37 °C [125, 129, 142]. This leads to a 100 to 500-fold increase in TPP accumulation in the mitochondria [125, 129, 142].

Interestingly, evidence demonstrates that melanoma cells have increased oxidative phosphorylation activity [50, 90-93]. This increased activity leads to hyperpolarization of the mitochondria membrane potential in melanoma cells relative to non-malignant cells [57, 94]. This hyperpolarization of melanoma cell

mitochondria membranes results in increased TPP accumulation in the mitochondria of melanoma cells and represents a difference between melanoma and non-malignant cells and could potentially result in the selective killing of melanoma cells while minimizing off-target effects in non-malignant cells.

Thermosensitive Hydrogels

The potential of TPP compounds to translate clinically as a cancer therapeutic will depend largely on the *in vivo* biodistribution and concentration achievable at the tumor site due to the lipophilicity of TPP; and this could be a barrier to successful cancer therapy. Traditional routes of drug administration [e.g., oral, intravenous (I.V.), intraperitoneal (I.P.)] typically require drugs with hydrophilic properties for biodistribution to target sites (e.g., tumors) [137, 143]. However, these routes of administration are expected to lead to TPP accumulation in off-target sites (e.g., mitochondria-rich heart and liver), TPP metabolism in the gut and liver, and TPP drug excretion without tumor accumulation [57, 124, 128, 141, 143-146].

A novel approach to TPP drug administration involves the use of a thermosensitive hydrogel. Thermosensitive hydrogels exist in a water-like state at low temperatures and form a gel at body temperature [146-148]. Hydrogels are biodegradable (3 day half-life) and allow for the controlled release of a substance directly at a desired site *in vivo* [147]. Much preclinical work has explored the potential for the use of hydrogels to direct the delivery of numerous

biologics and drugs (e.g., insulin, antimicrobials, pain medications, growth factors, peptides, cells, radiopharmaceuticals) to specific *in vivo* sites [147, 149-153]. Recent preclinical research efforts have evaluated the use of thermosensitive hydrogels for the delivery of chemotherapeutic agents directly to the tumor site, thereby minimizing potential off target effects observed with many cancer therapies [146-148]. Further, hydrogels consist of hydrophilic polymers and are miscible with hydrophobic drugs such as TPP-based compounds [146, 148]. Hydrogels can also be loaded with multiple drugs in order to develop combination therapies that could potentially circumvent melanoma resistance [146, 148].

Rationale and Hypothesis

All cells require energy in order to survive and proliferate. Therefore, it is possible to inhibit cellular metabolism and take away the ability of a cell to make energy in the form of ATP in order to induce cell death. It is well established that cancer cells (including melanoma) have high glucose metabolism compared to non-malignant cells. Although cancer cells exhibit increased glucose metabolism, it is traditionally believed that cancer cells exhibit slightly decreased rates of aerobic respiration (Warburg effect). However data demonstrate that melanoma cells are not purely glycolytic, but in fact have sustained or increased mitochondrial oxidative phosphorylation. A consequence of heightened oxidative phosphorylation rates in melanoma cells is hyperpolarization of the mitochondria

membrane potential, with the inner mitochondria membrane having a more negative charge than the intermembrane space. This difference in mitochondria membrane potential in melanoma versus non-malignant cells represents a potential way to target and selectively kill melanoma cells relative to non-malignant cells. It is also known that TPP derivatives modified with linear side chains have the ability to target this negative voltage potential and preferentially accumulate in the mitochondria, disrupt mitochondria metabolism, and induce cytotoxicity. Further, TPP accumulation in mitochondria and their cytotoxic effects is dependent on the chemical composition of TPP compounds.

Based on this knowledge of the TPP mitochondria targeting properties and effects on mitochondria metabolism and cytotoxicity, the central hypothesis of this work is that TPP derivatives can be rationally designed to include molecular side chains that will better facilitate TPP accumulation within melanoma cell mitochondria, disrupt melanoma cell mitochondria metabolism, increase ROS species generation, and induce cytotoxicity. Further, TPP can be combined with drugs that inhibit the GSH and Trx antioxidant systems necessary for critical cellular processes such as ROS scavenging in order to enhance the sensitivity of melanoma cells to TPP treatment.

Significance

Metastatic melanoma incidence is increasing faster than any other form of cancer worldwide. No treatment affords durable, long-term benefit with minimal

side effects to melanoma patients attributed to the intrinsic resistance of melanoma to treatment. This highlights the need for novel therapies that potentially circumvent melanoma resistance in order to provide durable benefit for an increasing number of melanoma patients worldwide.

The research presented here is significant because it targets differences in cellular metabolism between non-malignant and melanoma cells that is absolutely essential for melanoma cell survival. No FDA approved therapy for melanoma targets cellular metabolism. Further, TPP compounds have long been utilized for mitochondria targeting applications, but only recently has their potential as chemotherapeutic agents been investigated. Few groups have evaluated how alterations to the TPP molecular side chain impact the effects of TPP compounds on melanoma cell mitochondria metabolism and survival or established a structure-activity relationship between TPP side chain length and effect on melanoma cell mitochondria metabolism and survival. Finally, the research presented here takes advantage of a thermosensitive hydrogel delivery system. No studies have evaluated the different routes of administration that result in the greatest accumulation of TPP in tumors relative to non-malignant tissues or utilized a thermosensitive hydrogel for TPP drug administration. This delivery system has a broad range of applications and opens up vast opportunities for combination therapies since multiple drugs can be loaded into hydrogel delivery systems. Importantly, heightened metabolic activity is a generalizable trait among many cancer types. Therefore a TPP hydrogel delivery

system could serve as a therapy not only for metastatic melanoma, but rather a broad range cancer types and patients worldwide.

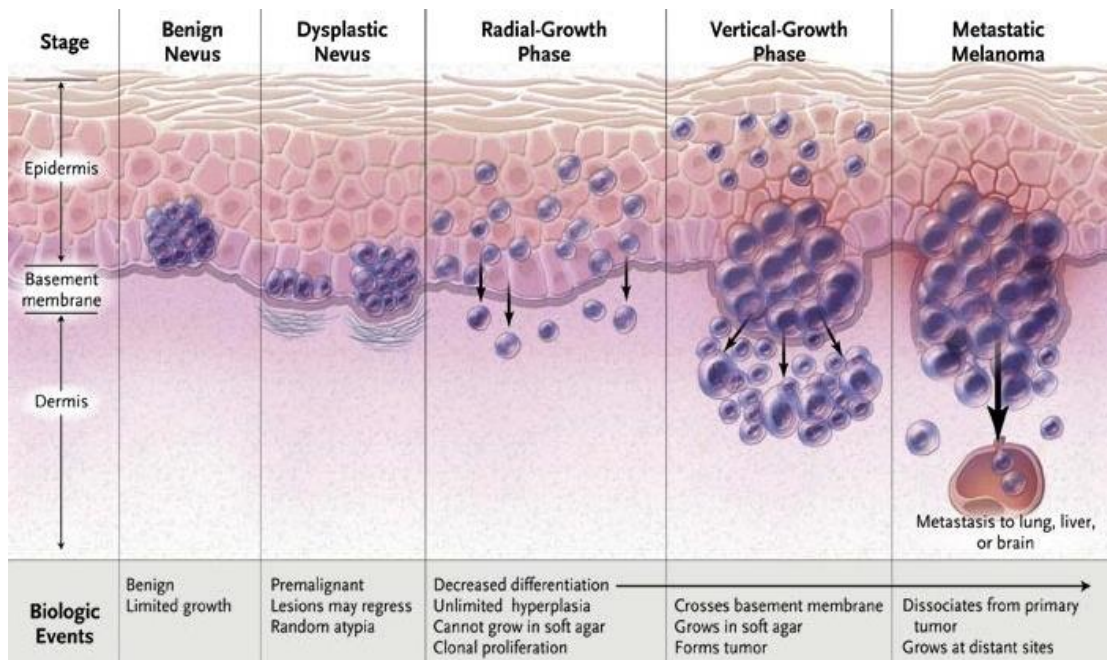


Figure I-1: The initiation and progression of melanoma.

Reproduced with permission from Miller, A.J. and M.C. Mihm, Jr., *Melanoma*. N Engl J Med, 2006. 355(1): p. 51-65. Copyright Massachusetts Medical Society.

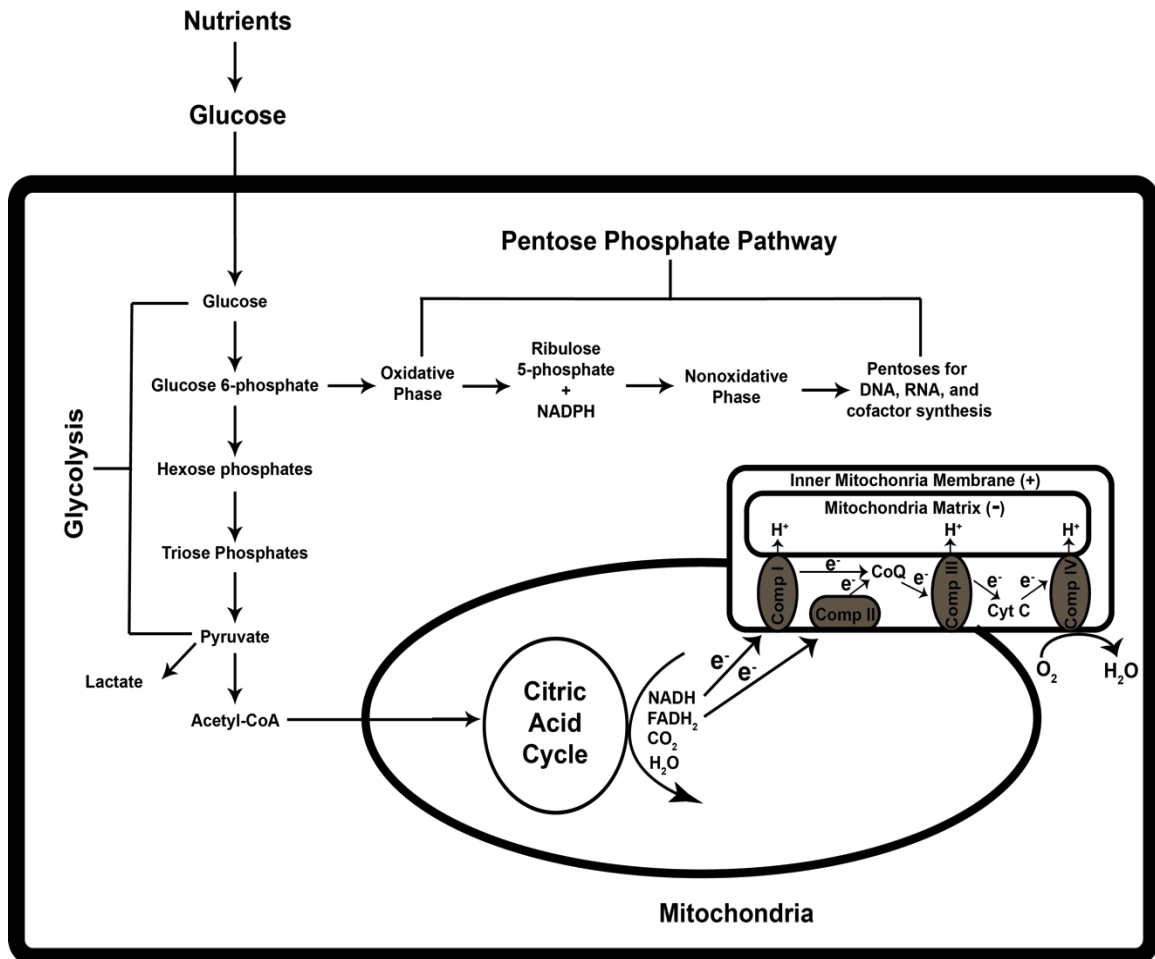


Figure I-2: An overview of cellular metabolic pathways.

Adapted from Lehninger, A.L., The molecular organization of mitochondrial membranes. *Adv Cytopharmacol*, 1971. 1: p. 199-208 and Harrigan, G.G., G. Maguire, and L. Boros, *Metabolomics in alcohol research and drug development*. *Alcohol Res Health*, 2008. 31(1): p. 26-35.

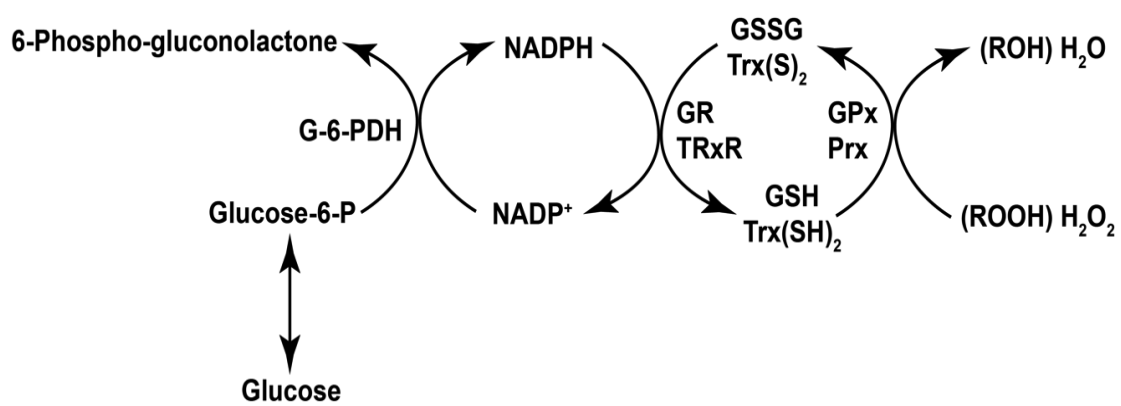


Figure I-3: An overview of the glutathione and thioredoxin antioxidant networks.

Adapted from Li, L., et al., Combined inhibition of glycolysis, the pentose cycle, and thioredoxin metabolism selectively increases cytotoxicity and oxidative stress in human breast and prostate cancer. *Redox Biol*, 2015. 4: p. 127-35.

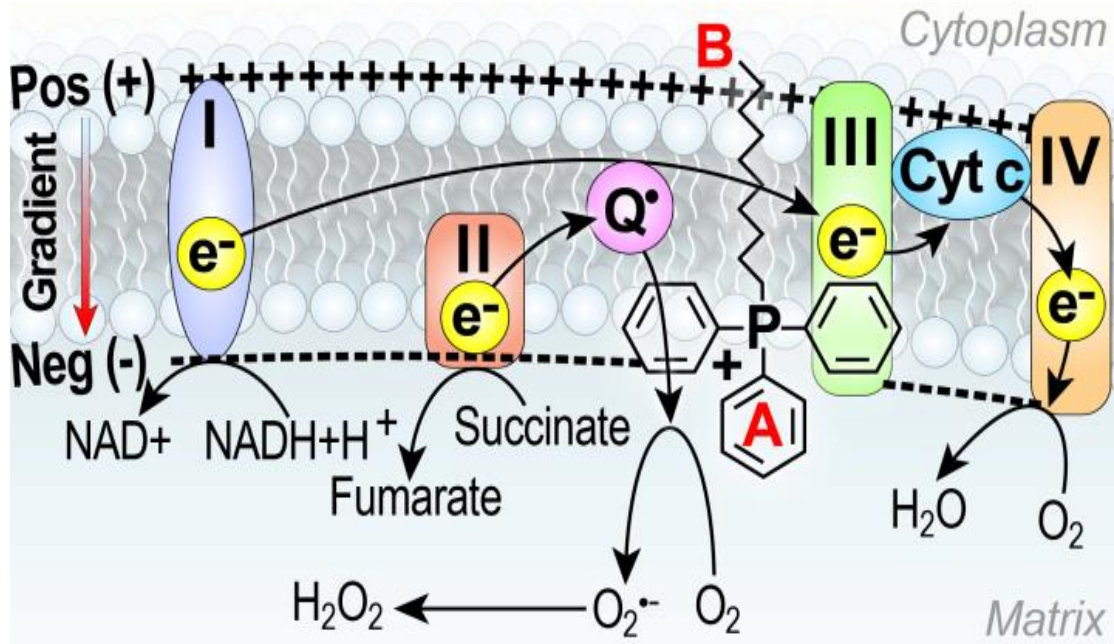


Figure I-4: The proposed mechanism of TPP derivatives.

(A) The positively charged “head” of TPP brings the molecule into the mitochondria matrix due to the hyperpolarized membranes in melanoma cell mitochondria; (B) The uncharged aliphatic side chain of TPP anchors the molecule into the inner mitochondrial membrane disrupting the flow of electrons between electron transport chain complexes (drawn here at complex III) leading to increased reactive oxygen species formation.

CHAPTER II: TRIPHENYLPHOSPHONIUM DERIVATIVES INHIBIT MITOCHONDRIA METABOLISM AND INDUCE MELANOMA CELL CYTOTOXICITY

Overview

While most cancer cells are characterized by decreased aerobic respiration and increased glycolysis (Warburg effect), evidence demonstrates that melanoma cells maintain sustained (or increased) mitochondria oxidative phosphorylation [50, 90-93]. Increased oxidative phosphorylation results in hyperpolarization of the mitochondria membrane potential in melanoma cells relative to non-malignant cells [57, 94]. Hyperpolarization (or increased electronegative membrane potential) of melanoma cell mitochondria membranes represents a physical difference in melanoma cells relative to non-malignant cells that can be targeted for drug delivery.

Increased or sustained oxidative phosphorylation in melanoma cells (relative to non-malignant cells) also results in increased ETC generated ROS that can lead to cytotoxic oxidative stress [76, 81, 84]. It is believed that cancer cells increase glucose uptake and glucose metabolism relative to normal cells not only to support increased energy needs, but to detoxify ROS in cancer cells as well [83-85]. Increased glycolysis results in more G-6-PH channeled through the PPP in order to generate NADPH that provides the reducing equivalents for the antioxidant GSH/GPx/GR and Trx/Prx/TRxR systems that scavenge ROS

[81, 83-86]. Molecular agents that are designed to exploit these metabolic differences (e.g., ETC activity, glucose metabolism, GSH, Trx) are receiving increased attention as the potential for interventions that target mitochondria is recognized [83, 84, 86, 92, 154]. However, because the metabolic requirements of normal proliferating cells are (in principle) the same as cancer cells, a limitation of metabolic inhibitors for cancer therapy is systemic toxicity [69, 86, 88, 154]. Based on this knowledge, drugs and routes of drug delivery that target cancer vs. non-malignant cells *in vivo* will largely determine the probability of success for therapies targeting cancer cell mitochondria and cellular metabolism.

TPP-based drugs have recently been investigated as anticancer agents due to their ability to preferentially accumulate within mitochondria by way of the hyperpolarized mitochondria membrane potential [124-126, 129]. TPP molecules pass through the mitochondria membrane and move down the negative mitochondria membrane voltage potential due to a positive charge delocalized over the large lipophilic TPP moiety [124-126, 129]. The high metabolic activity of melanoma cells results in a hyperpolarized mitochondria membrane potential relative to non-malignant cells, thus leading to greater TPP accumulation in cancer cell mitochondria relative to non-malignant cells and a way to selectively target melanoma relative to non-malignant cells [57, 94]. While several TPP-based compounds that utilize TPP as a targeting agent to deliver a biologically active moiety to mitochondria have been reported that appear to have potential as anticancer agents, few studies have investigated the effect of rational modifications to the molecular side chain “linker” of TPP-based

variants alone and the potential impact of linker changes on mitochondria metabolism and cytotoxicity [93, 127, 133, 139]. Further, the precise mechanism of action of these compounds on mitochondria metabolism and cancer cell cytotoxicity remains debated [93, 134]. Regardless of TPP mechanism of action, it is evident that the potential of TPP compounds to translate clinically as a cancer therapeutic will depend largely on the *in vivo* biodistribution and concentration achievable at the tumor site due to the lipophilicity of TPP; and this could be a barrier to successful cancer therapy.

The research proposed here investigates the development of small molecule TPP derivatives for metastatic melanoma therapy. Specifically, studies were performed to investigate the effect of increases in length of an aliphatic molecular side chain modification to the TPP-base functional mitochondria-targeting group. Changes in cytotoxicity to melanoma cells that resulted from an increase in side chain length from 5 to 16 carbons and the specific effects of TPP derivatives modified with molecular side chains on mitochondria metabolism were explored (**Figure II-1**). The effect of TPP side chain length on GSH and redox status in melanoma cells was also evaluated. Further, combination studies using inhibitors of GSH and Trx were explored as a way to enhance the sensitivity of melanoma cells to TPP treatment. To address the potential issue of TPP tumor accumulation due to TPP lipophilicity, different routes of TPP administration were explored to determine which route results in the greatest TPP drug accumulation in melanoma tumors and the potential of a

thermosensitive-hydrogel delivery system to administer a TPP derivative directly to the tumor site and its effects on melanoma tumor growth rate.

In vitro experiments demonstrate that increasing the length of the aliphatic molecular side chain on TPP-based compounds increases their cytotoxicity in metastatic melanoma cells. Further, TPP compounds disrupt mitochondria metabolism; decrease GSH levels, and increase cellular oxidation. There is also a structure-activity relationship between TPP side chain length and disrupted metabolism. Further, inhibitors of the cellular antioxidants GSH and Trx enhance the sensitivity of melanoma cells to TPP treatment. *In vivo* experiments demonstrate hydrogel-administered TPP results in effective drug delivery to subcutaneous melanoma xenografts and decreases melanoma tumor growth rate in mice with no observable off-target toxicities. These findings suggest that disruption of mitochondria metabolism using hydrogel-delivered TPP compounds can kill melanoma cells while minimizing off-target effects in non-malignant cells.

Materials and Methods

Cell Culture

A375 (catalog no. CRL-1619) and MeWo (catalog no. HTB-65) human melanoma cells were obtained from American Type Culture Collection (Manassas, VA). A375 cells were cultured in Gibco Dulbecco's Modified Eagle Medium (DMEM; Gibco, Life Technologies, Carlsbad, CA) containing 10% fetal

bovine serum (FBS; Gibco) and 1% penicillin/streptomycin (Gibco). MeWo cells were cultured in 1:1 DMEM:Ham's F12 Nutrient Mixture (Gibco) containing 10% FBS and 1% penicillin/streptomycin. Cells were maintained at 37 °C in a humidified 5% CO₂ incubator and detached with 0.25% trypsin-EDTA (Gibco). Experiments were performed with cells at or below passage twenty.

Chemicals and Reagents

Triphenylphosphonium compounds were obtained from Alpha Aesar (Ward Hill, MA). L-buthionine sulfoximine (BSO), auranofin (AUR), N-acetyl-L-cysteine (NAC), and 3-(4,5-dimethylthiazol-2-yl)-2,5-diphenyltetrazolium bromide (MTT) were purchased from Sigma Chemical Co. (St. Louis, MO). Hydrogel was complements of Dr. Dongrim Seoul and Dr. Tae-Hong Lim at the University of Iowa. TPP and AUR were all dissolved in the smallest volume of dimethylsulfoxide (DMSO) required to solubilize the compounds, while BSO was dissolved in water. NAC was dissolved in water and brought to pH 7 with sodium bicarbonate. 5,6-dichloro-2-[(*E*)-3-(5,6-dichloro-1,3-diethyl-1,3-dihydro-2*H*-benzimidazol-2-ylidene)-1-prop-1-enyl]-1,3-diethyl-1*H*-benzimidazolium iodide (JC-1) and dihydroethidium (DHE) were purchased from Molecular Probes (Eugene, OR). Replication deficient adenovirus with human CuZnSOD cDNA (Ad-CuZnSOD) driven by the cytomegalovirus (CMV) promoter was obtained from the University of Iowa DNA Vector Core (Iowa City, IA). Replication deficient adenovirus with human MnSOD, Cat, and GPx4 cDNA (Ad-MnSOD, Ad-

Cat, Ad-GPx4) driven by the CMV promoter was obtained from ViraQuest Inc. (Iowa City, IA).

MTT Cell Viability Assay

A375 (20,000 cells/well) and MeWo (40,000 cells/well) cells were plated in 96-well tissue culture plates for 24 h. Cells were then treated with TPP (0.5-2.0 μ M) for 24-72 h. Following treatment, media was aspirated and MTT (5 mg/mL dissolved in 1X phosphate buffered saline (PBS) was added to each well and incubated for 1 h [155]. MTT was then aspirated and DMSO was added to each well to dissolve the formazan salt. The absorbance of the formazan solution was measured using a plate reader (Tecan spectrafluor plus) at 590 nm.

Clonogenic Cell Survival Assay

A375 cells were plated in 60 mm tissue culture dishes at a density of 150,000 cells/dish and incubated for 48 h. Cells were then treated with 0.25-1.0 μ M TPP for 24-48 h. Following drug treatment, cells were trypsinized and plated at a density of 500 cells/dish and incubated for 2 weeks. Colonies were then fixed with 70% ethanol, stained with Coomassie blue G250 (Sigma) in 45% methanol and 10% acetic acid, and counted. Only colonies \geq 50 cells were counted. Surviving fraction (SF) was calculated using the following formula: SF = (number of colonies counted)/(number of cells seeded x plating efficiency).

JC-1 Mitochondria Membrane Potential Assay

A375 cells were plated in 60 mm culture dishes at a density of 150,000 cells/dish and incubated for 24 h. Cells were treated with TPP (0.5-2.0 μ M) for 1 h. Cells were then washed and incubated with 2.0 μ M JC-1 in 1X PBS containing 5 mM pyruvate for 1 h. Control dishes were treated with 1.0 μ M carbonyl cyanide 4-(trifluoromethoxy)phenylhydrazone (FCCP; Sigma) 30 min prior to measurement. Cells were washed, pelleted, and suspended in 1X PBS. Cells were analyzed using a Becton Dickinson LSR II Flow cytometer at 530 nm and 590 nm. Data from 10,000 events were collected and mean fluorescence intensity was analyzed using Flowjo software. Background fluorescence was corrected to the auto-fluorescence of unlabeled cells.

Glutathione Assay

A375 cells were plated in 60 mm tissue culture dishes at a density of 150,000 cells/dish and incubated for 48 h. Cells were treated with 1.0 μ M TPP for 24 h. Cells were then washed twice in ice-cold 1X PBS and scraped in 5% sulfosalicylic acid and stored at -80 °C for future use. Samples were then thawed on ice and spun at 10,000 for 5 min in order to remove precipitated protein. The supernatant was collected and volume recorded. The precipitated protein was dissolved in 0.1 N sodium hydroxide (NaOH) with 1% sodium dodecyl sulfate (SDS) for future use in protein estimation. Total glutathione

(GSH and GSSG) was measured in supernatants using a 5,5'-dithiobis-2-nitrobenzoic acid (DNTB; Sigma) spectrophotometric recycling assay as previously described [156, 157]. For these assays, GR, NADPH, ddH₂O, and DNTB are added in excess. Two molecules of GSH react with DNTB to make GSSG and two molecules of 2-nitro-5-thiobenzoate (TNB). NADPH then reduces GSSG back to two molecules of GSH. The formation of two TNB molecules produces a yellow color; therefore the rate of yellow color formation is proportional to total glutathione levels (GSH + GSSG). In order to determine the proportion of total glutathione that is GSSG, the supernatant is treated with 2-vinylpyridine (2-VP) for 2 h. GSH is conjugated by 2-VP, therefore reduced GSH can be determined by subtracting GSSG from total glutathione. The rate of color change was measured using a DU spectrophotometer at 412 nm for 2.5 min. Data was normalized to protein content determined by the bicinchoninic acid assay.

DHE Oxidation Assay

A375 cells were plated in 60 mm tissue culture dishes at a density of 150,000 cells/dish and incubated for 48 h. Cells were treated with 1.0 μ M TPP for 1.5 h. Cells were then washed, trypsinized, and resuspended with 10 μ M DHE in 1X PBS containing 5 mM pyruvate for 30 min. Control dishes were treated with 10 μ M antimycin A (Sigma) 30 min prior to measurement. Samples were analyzed using a Becton Dickinson FACScan flow cytometer at 488 nm

excitation and 585/42 nm emission. Data from 10,000 events were collected and mean fluorescence intensity was analyzed using Flowjo software. Background fluorescence was corrected the auto-fluorescence of unlabeled cells.

Superoxide Dismutase Activity Assay

A375 cells were plated in 60 mm tissue culture dishes at a density of 150,000 cells/dish and incubated for 48 h. Cells were then transfected with Ad-CuZnSOD or Ad-MnSOD for 24 h in serum free media. The adenovirus was then removed and full media replaced for 24 h. Cells were then washed twice in ice-cold 1X PBS and scraped in 5% sulfosalicylic acid and stored at -80 °C for future use. Pellets were thawed on ice and resuspended in diethylenetriaminepentaacetid acid (DETAPAC). Superoxide dismutase activity was determined as previously described [158]. For these assays, $O_2^{\bullet-}$ is generated by xanthine oxidase, which then reduces nitroblue tetrazolium (NBT), resulting in the formation of a blue color that can be measured spectrophotometrically in a DU700 spectrophotometer at 560 nm. Bathocupriome disulfonic acid is added to the system in order to prevent to prevent metal interference. Increasing concentrations of SOD convert $O_2^{\bullet-}$ to H_2O_2 and O_2 and results in the inhibition of the rate of NBT reduction. MnSOD activity is determined by adding 5 mM sodium cyanide for 45 min in order to inhibit CuZnSOD activity. CuZnSOD activity is determined by subtracting the MnSOD activity from the total SOD activity. All protein levels were determined by the

Lowry assay. Activity is expressed as units SOD/mg protein, where one unit of SOD is the amount of protein that results in 50% of maximum inhibition.

Catalase Activity Assay

A375 cells were plated in 60 mm tissue culture dishes at a density of 150,000 cells/dish and incubated for 48 h. Cells were then transfected with Ad-Cat for 24 h in serum free media. The adenovirus was then removed and full media replaced for 24 h. Cells were then washed twice in ice-cold 1X PBS and scraped in 5% sulfosalicylic acid and stored at -80 °C for future use. Pellets were thawed on ice and resuspended in DETAPAC. Catalase activity was determined by measuring the rate of H₂O₂ decay in a DU700 spectrophotometer at 240 nm in 50 mM potassium phosphate buffer (pH 7.0). Activity is expressed as *mk* units per mg protein⁻¹. All protein levels were determined by the Lowry assay.

GPx4 Activity Assay

A375 cells were plated in 60 mm tissue culture dishes at a density of 150,000 cells/dish and incubated for 48 h. Cells were then transfected with Ad-GPx4 for 24 h in serum free media. The adenovirus was then removed and full media replaced for 24 h. Cells were then washed twice in ice-cold 1X PBS and scraped in 5% sulfosalicylic acid and stored at -80 °C for future use. Pellets

were thawed on ice and resuspended in DETAPAC. GPx4 activity was measured as previously described [159, 160]. For these assays, glutathione reductase (GR), glutathione (GSH), NADPH, and phosphatidylcholine hydroperoxide (PCOOH) are added to the samples in excess. PCOOH oxidizes GSH via the enzyme GPx4 to form GSSG and PCOH. GSSG is then reduced by NADPH via the enzyme GR to reform GSH. The rate of NADPH oxidation can be measured spectrophotometrically with a DU700 spectrophotometer at 340 nm. One unit of GPx4 activity is defined as the amount of enzyme catalyzing 1 μM of NADPH per min and is expressed as milliunits per mg protein⁻¹. All protein levels were determined by the Bradford assay.

Adenovirus Clonogenic Cell Survival Assay

A375 cells were plated in 60 mm tissue culture dishes at a density of 150,000 cells/dish and incubated for 48 h. Cells were then transfected with adenovirus (Ad-CuZnSOD, Ad-MnSOD, Ad-Cat, Ad-GPx4) for 24 h in serum free media. The adenovirus was then removed and full media replaced for 24 h. Cells were then treated with 1 μM TPP for 24 h. Following drug treatment, cells were trypsinized and plated at a density of 500 cells/dish and incubated for 2 weeks. Colonies were then fixed with 70% ethanol, stained with Coomassie blue G250 in 45% methanol and 10% acetic acid, and counted. Only colonies ≥ 50 cells were counted. Surviving fraction (SF) was calculated using the following

formula: $SF = (\text{number of colonies counted})/(\text{number of cells seeded} \times \text{plating efficiency})$.

NAC Clonogenic Cell Survival Assay

A375 cells were plated in 60 mm tissue culture dishes at a density of 150,000 cells/dish and incubated for 48 h. Cells were then treated with 1.0 μM TPP alone or in combination with 20 mM NAC for 24 h. Following drug treatment, cells were trypsinized and plated at a density of 500 cells/dish and incubated for 2 weeks. Colonies were then fixed with 70% ethanol, stained with Coomassie blue G250 in 45% methanol and 10% acetic acid, and counted. Only colonies ≥ 50 cells were counted. Surviving fraction (SF) was calculated using the following formula: $SF = (\text{number of colonies counted})/(\text{number of cells seeded} \times \text{plating efficiency})$.

GSH and TrxR Inhibitor Clonogenic Cell Survival Assays

A375 cells were plated in 60 mm tissue culture dishes at a density of 150,000 cells/dish and incubated for 48 h. Cells were then treated with 0.5 μM TPP alone or in combination with 100 μM BSO or 1.0 μM AUR for 24 h. Following drug treatment, cells were trypsinized and plated at a density of 500 cells/dish and incubated for 2 weeks. Colonies were then fixed with 70% ethanol, stained with Coomassie blue G250 in 45% methanol and 10% acetic

acid, and counted. Only colonies ≥ 50 cells were counted. Surviving fraction (SF) was calculated using the following formula: $SF = (\text{number of colonies counted})/(\text{number of cells seeded} \times \text{plating efficiency})$.

Intracellular ATP Concentration Measurements

A375 cells were plated in 60 mm tissue culture dishes at a density of 150,000 cells/dish and incubated for 48 h. Cells were treated with 1.0 μM TPP for 24 h. Cells were then pelleted and counted. A cell suspension containing 50,000 cells was added to the wells of a 96-well opaque wall tissue culture plate. Reagent from a CellTiterGlo ATP kit (Promega) was added to lyse the cells and initiate the luminescence reaction. Luminescence was measured on a SpectraMax microplate reader. A standard curve of ATP concentration vs. luminescence signal was generated with adenosine 5'-triphosphate (ATP) disodium salt hydrate (Sigma). A standard curve was generated with each ATP assay; intracellular ATP concentration was calculated from the corresponding standard curve run on that individual day using cell number and cell volume, as measured by cell sizing function on Moxi Z automated cell counter (Orflow).

Tumor Xenograft Growth

Female 4-week-old athymic-nu/nu mice were purchased from Harlan Laboratories (Indianapolis, IN) and housed in the Animal Care Facility at the University of Iowa. The Institutional Animal Care and Use Committee at the

University of Iowa approved all animal studies and procedures (ACURF # 1308161). For subcutaneous xenografts, mice were injected with 500,000 A375 cells in LEDV-free matrigel basement membrane matrix (Corning). Tumor volumes were calculated using the following equation: $(\text{length} \times \text{width}^2)/2$. Mice bearing tumors >15 mm in any direction or tumor ulceration were euthanized.

C-14 Biodistribution Studies

A 12-TPP compound labeled with ^{14}C at the alpha-carbon position was purchased from American Radiolabeled Chemicals (St. Louis, MO). Animals bearing A375 xenografts were administered 2.5 μCi of ^{14}C labeled 12-TPP via tail vein injection, oral gavage, intraperitoneal injection, or hydrogel peritumorally. Animals were sacrificed at 0.5 h, 3 h, 12 h, 24 h, or 48 h post ^{14}C -12-TPP administration. Organs were harvested, dried, ground, and counted using a liquid scintillation counter (Packard). Activity was normalized to the total activity recovered in the analysis and represented as normalized activity per gram of tissue.

In Vivo Tumor Growth Studies

Athymic nu/nu mice bearing A375 melanoma xenografts (~5x5 mm in size) were administered 12-TPP suspended in hydrogel peritumorally at a 10 μM concentration. Injections were made twice weekly for three weeks. Tumor size and body weight were measured at the times of injection. Animals losing <10%

of their body weight were administered 200 μ L saline IP. Tumor volumes were calculated using the following equation: $(\text{length} \times \text{width}^2)/2$.

TPP In Vivo Toxicity Studies

Female SCID hairless mice were treated with 100 μ M 10-TPP (or vehicle control) in their drinking water. Mice were weighed daily to monitor body weight loss to see if treatments were well tolerated. Animals losing <10% of their body weight were administered 200 μ L saline IP. After 17 days, mice were sacrificed and blood was drawn via a cardiac puncture and diluted with Sysmex buffer and analyzed for CBC differentials via Sysmex XT2000i Automated Hematology Analyzer per manufacturer instructions. For liver and kidney pathology, blood was immediately placed in plasma separator tubes containing heparin. After centrifugation the plasma was sent on ice to Radil Labs (Columbia, MO) for further analysis.

Statistical Analysis

Statistical significance for *in vitro* studies with more than three groups was determined using one-way analysis of variance (ANOVA) with post hoc analyses using the Tukey's honestly significant difference test for multiple comparisons. Statistical significance for *in vitro* studies with less than three groups was done using a Student's t test. Homogeneity of variance was assumed at 95 % confidence interval. Results with $p < 0.05$ were considered significant. Statistical

analysis was performed using SPSS Statistics Version 21 (IBM). For *in vivo* tumor growth studies, linear mixed effects regression models were used to estimate and compare group-specific tumor growth curves. Pairwise comparisons were performed to identify specific group differences in the growth curves. All tests were two-sided and carried out at the 5% level of significance. Analyses were performed with SAS v9.4 (Cary, NC).

Results

Increasing TPP Side-Chain Length Decreases the Viability of Melanoma Cells

Evidence suggests that TPP derivatives modified with linear side chains preferentially accumulate in cancer cell mitochondria and induce cytotoxicity. In order to explore the effect of changes to TPP aliphatic side chain length on melanoma cell viability, MTT cell viability assays were performed utilizing TPP variants with side chain lengths of 5-, 10-, and 16- carbon atoms. For these experiments, A375 (**Figure II-2**) and MeWo (**Figure II-3**) melanoma cells were treated with TPP derivatives for 24 h, 48 h, and 72 h at a 0.5 μ M concentration. MTT analysis of the cell populations following these treatments showed an observable, but relatively mild effect on melanoma cell viability and proliferation resulting from a 24 h incubation period for all chain lengths studied; however, the effect on melanoma cells as a result of incubation with 5-TPP was minimal at all incubation periods employed for these experiments. On the other hand, the viability of melanoma cells when incubated with 10-TPP and 16-TPP decreased

significantly with increasing incubation periods relative to 5-TPP and control, with the highest levels of cytotoxicity for 10-TPP and 16-TPP occurring after 72 h of incubation. These results support the hypothesis that lengthening of the aliphatic side chain of TPP derivatives promotes greater reductions in metastatic melanoma cell viability. It is also well established that MTT reduction is largely dependent on mitochondria NAD(P)H-dependent oxidoreductase and dehydrogenase activity of metabolically active cells [161]. Therefore, these results suggest that the decreased melanoma cell viability could be attributed to TPP targeting of melanoma cell mitochondria and subsequent decrease in mitochondria activity.

*Increasing TPP Side-Chain Length Decreases the Clonogenic Survival of
Melanoma Cells*

Clonogenic survival assays were performed in addition to viability assays to determine the effect TPP side chain length on melanoma cell reproductive ability. Changes in clonogenic survival with increases in incubation time and concentration were examined for TPP variants with side chain lengths of 5-, 8-, 10-, 12-, 14-, and 16- carbon atoms. For these experiments, A375 melanoma cells were treated with TPP derivatives for 24 h (**Figure II-4**) and 48 h (**Figure II-5**) at 0.25 μ M, 0.5 μ M, or 1.0 μ M concentrations. Clonogenic survival analysis strongly suggests that inclusion of longer length side chains imparts greater reductions in melanoma cell clonogenic survival. There was no decrease in

melanoma cell clonogenic survival after a 0.25 μM 24 h TPP treatment for all chain lengths studied; and the effect on melanoma cells as a result of incubation with 5-TPP was minimal at all incubation periods and concentrations employed for these experiments. On the other hand, the clonogenic survival decreased roughly 10-20% with each increase in chain length from 8 to 16 carbons in cells treated with TPP at a 0.5 μM concentration. A similar pattern was observed at a 1.0 μM concentration, with greater clonogenic cell killing compared to the 0.5 μM concentration. In cells treated for 48 h with TPP compounds, a decrease in clonogenic survival (<10%) was observed for 8-TPP at a 0.5 μM concentration, which decreased to approximately 50% at a 1.0 μM concentration. Cells treated with 10-TPP for 48 h exhibited roughly a 30% decrease in clonogenic survival at a 0.25 μM concentration and total clonogenic cell death at a 1.0 μM concentration. Greater than 60% clonogenic cell death was observed in cells treated with 12-, 14-, or 16-TPP at a 0.25 μM concentration for 48 h and increased to nearly complete clonogenic cell death at a 0.5 μM concentration. These results demonstrate that lengthening of the aliphatic side chain of TPP derivatives promotes greater reductions in melanoma cell clonogenic survival. Further, there is a time and concentration dependence on TPP-induced clonogenic melanoma cell death.

Increasing TPP Side-Chain Length Decreases the Mitochondria Membrane Potential of Melanoma Cells

The major utility of TPP compounds as a potential anticancer agent comes from their ability to target mitochondria. In order to determine if TPP derivatives modified with linear side chains accumulate in melanoma cell mitochondria and affect mitochondria membrane potential; and if there is a structure-activity relationship between side chain length and mitochondria membrane potential; JC-1 mitochondria membrane potential assays were performed. Changes in mitochondria membrane potential with increases in concentration were examined for TPP variants with side chain lengths of 5-, 10-, and 16- carbon atoms. For these experiments, A375 melanoma cells were treated with TPP derivatives for 1 h at 0.5 μ M, 1.0 μ M, or 2.0 μ M concentrations. Results demonstrate that cells treated with 5-TPP did not exhibit a loss of mitochondria membrane potential at all concentrations tested relative to untreated controls (**Figure II-6**). There was approximately a 30% decrease in mitochondria membrane potential in cells treated with 10- and 16-TPP at a 0.5 μ M concentration. Cells treated with 10-TPP showed about a 50% decrease in mitochondria membrane potential relative to untreated controls at 1.0 and 2.0 μ M concentrations. Cells treated with 16-TPP at 1.0 μ M and 2.0 μ M concentrations demonstrated roughly a 60-70% decrease in mitochondria membrane potential relative to untreated cells. These results support that TPP derivatives target the mitochondria of melanoma cells and decrease mitochondria membrane potential. Importantly, since 5-TPP had

no effect on mitochondria membrane potential, but 10- and 16-TPP did, these data support that the loss of membrane potential is not due to the cationic TPP moiety, but rather the TPP side chain insertion into the mitochondria membrane. Further, the mitochondria are not completely depolarized when treated with TPP. This finding argues that the decrease in melanoma cell viability and clonogenic survival is not simply attributed to total mitochondria membrane depolarization or disruption, but presumably a disruption in mitochondria metabolism.

TPP Decreases Oxygen Consumption in Melanoma Cells

Results demonstrate that TPP derivatives preferentially accumulate in melanoma cell mitochondria and decrease melanoma cell mitochondria membrane potential. These results suggest that TPP induced cytotoxicity to melanoma cells functions through mitochondria metabolism disruption. However, the precise mechanism of action of TPP on mitochondria metabolism is unknown. In order to determine if a 12-TPP derivative acts as an uncoupler or inhibitor of the ETC, metabolic flux measurements using a Seahorse Bioscience XF96 extracellular flux analyzer were performed [133]. 12-TPP was chosen because previous studies demonstrated that inclusion of side chains longer than 12-TPP did not improve the effects of TPP on melanoma cell metabolism. For these experiments, A375 human melanoma cells were treated with or without 12-TPP (1.0 μ M) followed by the sequential addition of oligomycin to determine mitochondria ATP-linked oxygen consumption, FCCP to determine mitochondria

reserve capacity, and antimycin A/rotenone to determine non-mitochondria sources of oxygen consumption. Results demonstrate that baseline oxygen consumption in A375 human melanoma cells is high compared to other published values for many types of cancer cells and non-cancerous cells (*e.g.*, generally less than 50 amole sec⁻¹ cell⁻¹) (**Figure II-7**) [162]. This finding supports the idea that melanoma cells have high or sustained oxygen consumption rates (OCR) and ETC activity and provides rationale for a mitochondria-targeted therapy. Immediately upon addition of 12-TPP, OCR decreased compared to cells that did not receive 12-TPP treatment. Since ETC uncouplers generally result in an increase in oxygen consumption; this finding suggests TPP acts as an inhibitor of the ETC. When oligomycin was added to cells that were not treated with 12-TPP, there was a sharp decrease in oxygen consumption. There was only a minimal decrease in oxygen consumption in cells treated with 12-TPP following addition of oligomycin. This finding argues that TPP acts as an inhibitor of the ETC, presumably by decreasing ATP-linked oxygen consumption. Addition of FCCP resulted in an increase in oxygen consumption in cells that were not treated with 12-TPP; but no increase in oxygen consumption was observed in cells treated with 12-TPP. This suggests that 12-TPP has inhibited the movement of electrons through the ETC, presumably decreased proton pumping across the mitochondria inner membrane and subsequent decreased membrane potential and taken away the ability of cells to consume oxygen at complex IV that is linked to ATP production. Finally, addition of antimycin A/rotenone resulted in a further decrease in oxygen

consumption in cells that did not receive 12-TPP treatment and is likely attributed to non-mitochondria sources of oxygen consumption. No further decreases in oxygen consumption were observed in cells that received 12-TPP treatment. This suggests that the decrease in oxygen consumption is due to 12-TPP treatment and ETC inhibition rather than non-mitochondria sources. These results demonstrate that TPP specifically disrupts melanoma cell mitochondria metabolism via inhibition of ATP-linked oxygen consumption.

Increasing TPP Side-Chain Length Increases DHE Oxidation in Melanoma Cells

Metabolic flux data support that a 12-TPP compound decreases melanoma cell oxygen consumption. However, metabolic flux analysis demonstrated that although 12-TPP decreases oxygen consumption, cells still consume oxygen at a high rate ($\sim 60 \text{ amol sec}^{-1} \text{ cell}^{-1}$). A potential consequence of TPP oxygen consumption disruption is an increase in ROS [76, 82, 124, 129, 163]. It is believed that in non-malignant cells, as many as 0.1-1 % of the electrons that enter the ETC leak off the ETC and generate $\text{O}_2^{\bullet-}$, which then reacts to form H_2O_2 and ROOH [73-76]. By preventing the movement of electrons through the ETC with 12-TPP despite continued oxygen consumption, it is possible that more electrons leak off the ETC and result in the formation of more $\text{O}_2^{\bullet-}$ that goes on to form other free radical species affecting the redox state of melanoma cells. To evaluate how TPP treatment affects the redox state of melanoma cells DHE oxidation assays were performed based on the idea that

TPP based drugs increase free radical species generation in melanoma cells that results in a more oxidized cellular state (**Figure II-8**). For these experiments, cells were incubated with 5-, 8-, 10-, 12-, 14-, or 16-TPP at a concentration of 1.0 μ M for 1.5 h. Treatment with 5-TPP and 8-TPP did not cause an increase in DHE oxidation. Alternatively, treatment with 10-, 12-, 14-, and 16-TPP caused a significant two to three-fold increase in DHE oxidation relative to controls. No statistical difference could be discerned between the observed DHE oxidation resulting from 10-TPP through 16-TPP treatments under the conditions of these experiments. These findings support that TPP inhibition of oxidative phosphorylation results in an increase in ROS that oxidize melanoma cells. Further, increased DHE oxidation is dependent on TPP side-chain length.

Increasing TPP Side-Chain Length Decreases Total Glutathione in Melanoma Cells

Glutathione functions as a cellular antioxidant that scavenges ROS and maintains cellular redox potential [102]. DHE oxidation studies demonstrate that TPP derivatives disrupt oxidative metabolism, which results in increased ROS in melanoma cells. Based on these findings, TPP treatment could potentially affect GSH levels in melanoma cells. For these experiments, A375 human melanoma cells were treated with 5-, 8-, 10-, 12-, 14-, or 16-TPP for 24 h at a 1 μ M concentration. Following treatment, cells were analyzed for total GSH content (GSH + GSSG) (**Figure II-9**). Results demonstrate that cells treated with 5-TPP

did not exhibit a significant decrease in total GSH compared to control cells. Cells treated with TPP derivatives modified with side chains of eight carbons or longer had ~ 50% less total GSH than untreated cells. These results demonstrate that TPP derivatives decrease intracellular GSH content in melanoma cells, and there is a structure-activity relationship between decreased GSH and TPP chain length. Results also establish a link between TPP ETC disruption and increased ROS generation that oxidizes and depletes intracellular GSH levels. Further, this data identifies a potential exploitable target (*e.g.*, GSH and Trx) for combination therapies with TPP that could enhance the sensitivity of melanoma cells to TPP treatment.

Increasing TPP Side-Chain Length Increases Oxidized Glutathione in Melanoma Cells

Previous studies that measured total GSH (GSH + GSSG) demonstrated that TPP derivatives with side chains of eight carbons or longer decrease total GSH in melanoma cells. Previous studies also demonstrate that TPP treatment increases DHE oxidation, presumably through mitochondria metabolism disruption and subsequent ROS production. This increase in ROS is expected to oxidize GSH to GSSG in cells. To determine what percentage of total GSH is GSSG in melanoma cells, A375 human melanoma cells treated with 5-, 8-, 10-, 12-, 14-, or 16-TPP for 24 h at a 1 μ M concentration were analyzed for GSSG content (**Figure II-10**). Results demonstrate that melanoma cells treated with 5-

TPP did not have a significant increase in GSSG compared to control cells. Cells treated with TPP derivatives modified with side chains of eight carbons or longer had ~ 2-2.5x more GSSG than untreated cells. These results demonstrate that TPP derivatives increase the amount of GSSG cells, presumably due to TPP-mediated ROS production. Further, there is a structure activity relationship between TPP chain length and increased GSSG.

*Increasing TPP Side-Chain Length Increases Total Glutathione in Melanoma Cell
Tissue Culture Media*

Total and oxidized GSH studies demonstrated that TPP treatment decreases total GSH (GSH + GSSG) in melanoma cells, and there is an increase in the percentage of GSH that is GSSG. Normally, GSSG is transported out of cells through GSH transporters [117, 164-169]. Next, studies were performed to evaluate how TPP treatment affects total GSH in the media of cells treated with TPP. For these studies, A375 human melanoma cells were treated with 5-, 8-, 10-, 12-, 14-, or 16-TPP for 24 h at a 1 μ M concentration. The media cells were cultured in was then analyzed for total GSH content (**Figure II-11**). Results demonstrate that the media from cells treated with 5-, 8-, and 10-TPP did have significant increases in total GSH content. Interestingly, cells treated with 12-, 14-, and 16-TPP did not have significant increases in total GSH in the media. These results demonstrate that TPP derivative do disrupt GSH metabolism and

increase total GSH in the media; and there is a structure-activity relationship between total GSH in the media and TPP chain length.

Increasing TPP Side-Chain Length Decreases ATP Levels in Melanoma Cells

Total GSH measurements in the media from cells treated with 1.0 μ M 5-, 8-, 10-, 12-, 14-, or 16-TPP for 24 h demonstrated that the media from cells treated with 5-, 8-, and 10-TPP had increased total GSH. Interestingly, the media collected and analyzed from cells treated with 12-, 14-, and 16-TPP did not have increased total GSH in the media. Evidence demonstrates that GSSG is transported out of cells by GSH transporters. Further, these GSH transporters are ATP-dependent [117, 164-169]. In order to determine why 5-, 8-, and 10-TPP did result in increased total GSH in the media, while 12-, 14-, and 16-TPP did not, ATP measurements were made to determine how TPP treatment affects melanoma cell ATP levels and to potentially explain the differences in GSH transport out of cells that is dependent on ATP. For these experiments, A375 human melanoma cells were treated with 1.0 μ M 5-, 8-, 10-, 12-, 14-, or 16-TPP for 24 h. Following treatment cells were analyzed for intracellular ATP concentration using a luminescence based ATP assay (**Figure II-12**). Results demonstrate that there is a relationship between TPP side chain length and decreased intracellular ATP concentration, with inclusion of longer side chains resulting in larger decreases in intracellular ATP concentrations. There was a

chain length dependent decrease in ATP levels as the TPP side chain length was increased from five to ten carbons. TPP side chain lengths of twelve carbons or longer resulted in the largest decreases in intracellular ATP levels. Further, since GSH transport is dependent on ATP, these results could explain why media from cells treated with 5-, 8-, and 10-TPP has increased total GSH, whereas media from cells treated with 12-, 14-, and 16-TPP does not. There could also be a side chain length (between 10-12 carbons) that is the optimal length that results in melanoma cell mitochondria disruption, ROS generation, GSH metabolism disruption, and cytotoxicity.

Superoxide Dismutase and Catalase Do Not Protect Melanoma Cells from TPP-Mediated Cytotoxicity

Previous studies demonstrate that TPP derivatives disrupt mitochondria metabolism and decrease ATP-linked oxygen consumption, which results in increased DHE oxidation. Superoxide is the main ROS generated by the ETC chain, which is then converted to H₂O₂. In order to determine if TPP ETC disruption is specifically increasing O₂^{•-} or H₂O₂ levels in melanoma cells, and if O₂^{•-} or H₂O₂ and subsequent oxidative stress is the mechanism for TPP mediated toxicity, clonogenic rescue studies were performed to determine if cells transfected with SOD and Cat adenoviruses scavenge and detoxify O₂^{•-} and H₂O₂ and protect melanoma cells from TPP mediated cytotoxicity. For these experiments, A375 cells were transfected with 50 MOI Ad-MnSOD, 100 MOI Ad-CuZnSOD, or 100 MOI Ad-Cat alone or in combination. These MOIs were

selected because activity assays determined that these were the lowest MOIs that resulted in the greatest SOD and Cat activity in A375 cells (**Figures II-13, II-14, and II-15**). Following transfection, cells were treated with 1 μ M 12-TPP for 24 hours in the CuZn-SOD experiment, and with 1 μ M 16-TPP for 24 hours in the Mn-SOD experiment. Cells were then analyzed for clonogenic survival (**Figures II-16 and II-17**). Results demonstrate that CuZn-SOD, Mn-SOD, and Cat overexpression did not protect melanoma cells from TPP mediated toxicity. These results suggest that $O_2^{\bullet-}$ and H_2O_2 are not the specific ROS species generated following TPP treatment under these experimental conditions.

Glutathione Peroxidase-4 Does Not Protect Melanoma Cells from TPP-Mediated Cytotoxicity

Previous rescue studies demonstrated that SOD and Cat do not protect cells from TPP-mediated cytotoxicity. Next, rescue studies were performed using GPx4 adenoviruses to determine if GPx4 can protect melanoma cells from TPP treatment. GPx4 converts H_2O_2 , ROOH, and lipid hydroperoxides to water or alcohols using GSH as a cofactor [170, 171]. For these experiments, A375 cells were transfected with 100 MOI Ad-GPx4, a MOI that results in high GPx4 activity (**Figure II-18**). Following transfection, cells were treated with 1 μ M 10-, 12-, 14-, or 16-TPP for 24 hours. Cells were then analyzed for clonogenic survival (**Figure II-19**). Results demonstrate that although there appears to be a trend towards improved clonogenic survival, only 16-TPP + GPx4 was significant

compared to 16-TPP alone. These results support that H₂O₂, ROOH, and lipid hydroperoxides likely are not the cause of TPP-mediated cytotoxicity.

*NAC Treatment Partially Protects Melanoma Cells from TPP-Mediated
Cytotoxicity*

Previous data demonstrate that TPP treatment results in decreased intracellular GSH and consequently results in an oxidized cellular state in melanoma cells. In order to support that TPP induced cytotoxicity functions through ETC inhibition that subsequently results in increased ROS generation, cellular oxidation, and GSH depletion, NAC clonogenic rescue studies were performed. NAC is an ROS scavenging antioxidant and provides cysteine residues necessary for GSH synthesis [114, 172, 173]. For these experiments, A375 melanoma cells were treated with 5-16 TPP (1 μ M) alone or in combination with 20 mM NAC for 24 h. Following treatment, cells were plated and analyzed for clonogenic survival (**Figure II-20**). Results demonstrate that NAC is able to rescue TPP induced decreases in clonogenic survival by ~30 %. These results suggest that TPP compounds disrupt the ETC, which causes electrons to leak off the ETC and generate ROS species that oxidize GSH and subsequently creates an oxidized cellular state and cytotoxicity. Restoration of GSH protects cells from TPP treatment, therefore it appears that TPP compounds disrupt GSH metabolism.

Glutathione Synthesis Inhibitors Sensitize Melanoma Cells to TPP Treatment

To test these working hypotheses that GSH inhibition can sensitize melanoma cells to TPP, clonogenic assays were performed using A375 human melanoma cells. Cells were treated with TPP derivatives (0.5 μM) with chain lengths of 10-16 carbons (these compounds result in the greatest reduction in GSH) alone or in combination with 100 μM BSO. Results demonstrate that BSO enhances the effect of TPP treatment in A375 cells (**Figure II-21**). Cells treated with 10-TPP alone resulted in roughly 70% clonogenic survival, whereas 10-TPP and BSO resulted in about 20% clonogenic survival. Cells treated with 12-TPP alone exhibited approximately 50% clonogenic survival, compared to roughly 10% clonogenic survival when combined with BSO. The addition of BSO improved clonogenic cell killing by >60% compared to cells treated with 14-TPP or 16-TPP alone as well. These results demonstrate that TPP decreases GSH, and additional decreases in GSH enhance the effects of TPP clonogenic cell killing. Collectively, these results support the hypothesis that TPP derivatives increase ROS production through ETC inhibition, which in turn decreases intracellular GSH. Additional agents that further inhibit GSH enhance the sensitivity of melanoma cells to TPP treatment and could be a potential combination therapy.

Thioredoxin Reductase Inhibitors Enhance the Sensitivity of Melanoma Cells to TPP Treatment

To test these working hypotheses that TrxR inhibition can sensitize melanoma cells to TPP, clonogenic assays were performed using A375 human melanoma cells. Cells were treated with TPP derivatives (0.5 μ M) with chain lengths of 10-16 carbons (these compounds result in the greatest reduction in GSH) alone or in combination with 1.0 μ M AUR (**Figure II-22**). Results demonstrate that the addition of AUR improved cell killing by >60% compared to cells treated with 10-, 12-, 14-, or 16-TPP alone. These results demonstrate that TPP decreases GSH, and additional decreases in GSH and Trx enhance the effects of TPP clonogenic cell killing. Collectively, these results support the hypothesis that TPP derivatives increase ROS production through ETC inhibition, which in turn decreases intracellular GSH. Additional agents that further inhibit GSH and Trx enhance the sensitivity of melanoma cells to TPP treatment and could be a potential combination therapy.

TPP in vivo Biodistribution

In vitro data support that TPP-based compounds have the potential for use as chemotherapeutic agents. Despite the potential of TPP compounds as anti-cancer agents *in vitro*, no studies to date have demonstrated significant tumor accumulation of TPP compounds *in vivo* or analyzed routes of

administration that result in the highest level of tumor accumulation versus normal tissue. To address these issues, a ^{14}C labeled 12-TPP was utilized to determine where 12-TPP accumulates *in vivo* following administration via oral gavage, I.V. injection, I.P. injection, or a thermosensitive hydrogel. 12-TPP was chosen because previous studies demonstrated that inclusion of side chains longer than 12-TPP did not improve the effects of TPP on melanoma cell metabolism. Further, inclusion of longer TPP side chains increases the lipophilicity of TPP and presumably will decrease TPP bioavailability. In order to determine the biodistribution of ^{14}C -12-TPP following I.P., I.V., oral, and hydrogel administration, mice bearing A375 melanoma xenografts were administered 2.5 μCi of ^{14}C -12-TPP. Animals were sacrificed at 0.5 h, 3 h, 12 h, 24 h, or 48 h post ^{14}C -12-TPP administration. Organs were harvested, dried, ground, and counted by liquid scintillation. Results demonstrate the ^{14}C -12-TPP administered via I.P. injection did not result in bioaccumulation in the blood, brain, muscle, or tumor up to 48 h post-injection (**Figure II-23**). Heart uptake of 12-TPP was maximal at 48 h post-injection, while liver uptake was highest 0.5 h post injection and steadily decreased until 48 h post injection. Accumulation was also observed in the kidney, lung, spleen, and bladder up to 48 h post injection. Administration of ^{14}C -12-TPP via I.V. injection resulted in no uptake in the blood, brain, or bladder (**Figure II-24**). Tumor accumulation increased up to 48 h, although it was low compared to other organs analyzed. Heart, kidney, and muscle accumulation peaked at 48 h while liver, lung, and spleen accumulation peaked immediately post injection and steadily decreased thereafter. Oral administration of ^{14}C -12-

TPP led to accumulation in all organs up to 48 h post injection except the blood (**Figure II-25**). A general pattern of steady increases in ^{14}C -12-TPP accumulation was observed, with peak organ accumulation generally occurring 48 h post injection. Tumor accumulation of ^{14}C -12-TPP was still quite low compared to other organs analyzed. Contrary to the I.P., I.V., and oral routes of administration, ^{14}C -12-TPP administered via thermosensitive hydrogel resulted in roughly >10x the amount of detectable ^{14}C -12-TPP in tumors as early as 3 h post injection and up to 48 h post injection (**Figure II-26**). Importantly, little accumulation of ^{14}C -12-TPP was evident in all other organs analyzed at all time points. This data strongly suggests that I.P., I.V., and oral administration routes of TPP does not result in favorable accumulation in melanoma tumors compared to off-target organs. This data also strongly supports the use of thermosensitive hydrogels for TPP delivery to tumors with little to no off-target bioaccumulation.

TPP Treatment Does Not Result in Systemic Toxicity

In vivo efficacy studies demonstrated that 12-TPP administered peritumorally via hydrogel significantly decreases melanoma tumor growth rate compared to untreated mice and appeared to be well tolerated in animals. Biodistribution studies also demonstrated that 12-TPP administered via hydrogel located to the tumor with minimal accumulation in other organs; whereas orally administered 12-TPP did result in 12-TPP accumulation in off-target organs. In order to identify any potential systemic toxicity due to TPP treatment, 100 μM 10-

TPP was administered to mice orally (biodistribution studies indicate that this administration route results in TPP accumulation in off-target organs) via drinking water for 16 days. Following treatment, animals were sacrificed and blood was drawn via cardiac puncture for analysis of bone marrow, liver, and kidney toxicity.

CBC differential analysis was conducted on drawn blood to determine how 10-TPP treatment affects white blood cell and red blood cell counts (**Figure II-27**). There were no statistical differences in neutrophil, lymphocyte, and monocyte (white blood cells) counts in the treatment versus control mice. There were no significant differences in hemoglobin levels, percent hematocrit, and percent reticulocytes in treatment versus control groups indicating red blood cells are not affected by 10-TPP treatment. For liver toxicity analysis, bilirubin, albumin, alkaline phosphatase, and alanine transaminase levels were measured (**Figure II-28**). There were no significant differences between treatment and control mice for all four liver toxicity parameters indicating 10-TPP does not induce liver toxicity. Finally, blood urea nitrogen levels were measured as another indicator of liver toxicity and kidney function (**Figure II-29**). Again no significant differences were found in blood urea nitrogen levels in control versus treatment mice, indicating 10-TPP does not cause liver or kidney damage. Collectively, these results demonstrate that TPP is well tolerated in mice and does not cause systemic toxicity. Further, since oral administration does lead to off-target TPP accumulation whereas hydrogel TPP administration does not, the risk of systemic toxicity is even lower for a hydrogel TPP delivery system.

TPP Slows Melanoma Tumor Growth When Administered via Hydrogel

TPP biodistribution studies demonstrate that a thermosensitive hydrogel delivery system results in 12-TPP-melanoma tumor accumulation as early as 0.5 h post injection and up to 48 h post injection. In order to evaluate the potential for the use of a hydrogel delivery system to administer TPP directly at the tumor site in order to decrease melanoma tumor growth rate, 12-TPP was administered peritumorally via hydrogel to athymic nude mice bearing A375 human melanoma tumors (**Figure II-30**). Mice were treated with 10 μ M 12-TPP or vehicle control twice weekly for three weeks. Tumor size and animal weight was measured at each injection. Animals were sacrificed after three weeks of treatment due to the development of treatment resistance. Results show that *in vivo* treatment with 12-TPP via hydrogel peritumorally significantly suppressed melanoma tumor growth rate compared to untreated control mice following three weeks of treatment. Further, mice maintained body weight and treatment appeared to be well tolerated. These results suggest that a TPP-hydrogel delivery system has the potential as an effective and tolerable therapy for the treatment of metastatic melanoma.

Discussion

Melanoma is one of the most aggressive and lethal forms of cancer whose incidence is increasing worldwide [36-40]. Melanoma is now the 5th and 7th most

common cancer type in men and woman in the United States alone [40]. While melanoma identified early can be cured by surgery, metastatic disease is lethal with a median survival of less than one year [37, 42]. Prior to 2011, the only FDA approved melanoma therapies were dacarbazine and high dose interleukin-2, yet both do not improve the median overall survival [36-38, 43]. Recently, much excitement has been generated in the melanoma field, with six new FDA approved targeted or immune-based therapies approved in the past five years [37, 38, 43]. Despite the approval of new FDA approved therapies for melanoma, patient response and therapy resistance continue to be a barrier to durable melanoma therapy [36-38, 42, 43]. These observations clearly demonstrate the need to explore novel therapies for metastatic melanoma.

The research presented here involves the development of targeted therapies for metastatic melanoma that are designed to target differences in melanoma metabolism relative to non-malignant cells that have the potential to circumvent melanoma drug resistance to provide melanoma-cell specific cell killing and durable benefit to melanoma patients. TPP-based drugs can be designed to target tumor cell hyperpolarized mitochondria membranes and disrupt mitochondria and cellular metabolism that leads to melanoma cell death. The goal of this study is to develop a more detailed mechanistic understanding of the potential for TPP-based drugs for treatment of metastatic melanoma and to determine routes of TPP administration that result in the highest accumulation of TPP in melanoma tumors and lead to decreased melanoma tumor growth rate.

The mitochondria targeting qualities of positively charged lipophilic TPP-based compounds have long-been known and TPP-based variants have been investigated as antitumor agents. For example, a screen of a 10,000-compound small-molecule library identified three TPP derivatives of varying side-chain structural composition that promoted tumor cell cytotoxicity [127]. Based on *in vitro* results, these authors selected a TPP compound with a side-chain group consisting of a 3-carbon length chain (with an internal alkene double bond) for *in vivo* testing [127]. These results contrast our findings concerning the correlation between molecular side-chain length and melanoma cell cytotoxicity. For example, our results suggest that a side-chain length of as many as eight carbon atoms is relatively non-toxic to melanoma cells. On the other hand, our results are consistent with the idea presented by other groups that the molecular structure of the TPP-side chain can be manipulated to enhance cancer cell cytotoxicity [93]. More precisely, we find that increasing the length of an aliphatic side chain increases the cytotoxicity profile of TPP-based compounds. We further find that the cytotoxicity of TPP-based drugs that have been modified to include an aliphatic side chain is time and dose dependent. These results suggest that these TPP based compounds (modified with an aliphatic side chain) have the potential to induce cell killing at lower concentrations than previously studied with longer incubation periods, which contributes to a more detailed understanding of the potential to establish a therapeutic window for TPP-based treatments *in vivo*.

We further demonstrate that TPP targets cancer cell mitochondria and decreases the mitochondria membrane potential, and that decreased membrane potential depends upon TPP chain length. Despite the fact it is well established that TPP compounds target the mitochondria, their mechanism of action on cellular bioenergetics and cytotoxicity is widely debated [93]. Further, TPP mechanism of action is likely dependent on the dose of TPP used *in vitro* [133]. For example, evidence demonstrates that low micromolar concentrations of the penetrating TPP cations, such as the TPP-antioxidant MitoQ, uncouple mitochondria respiration [133, 174, 175]. On the other hand, our data support that TPP derivatives at a 1.0 μM concentration do not uncouple mitochondria respiration, but rather inhibit ATP-linked oxygen consumption. Further, studies demonstrate that inclusion of longer TPP side chains impart greater effects on OCR [93, 133, 139].

Interestingly, evidence demonstrates that melanoma cells have sustained or heightened oxidative phosphorylation activity. A significant consequence of heightened oxidative phosphorylation in cancer cells (relative to non-malignant cells) is an increase in ROS. It is believed that as many as 0.1-1% of the electrons that enter the ETC are inadvertently released at complexes I and III due to inefficiencies in ETC activity in non-malignant cells [73-75]. In cancer cells, increased ETC activity leads to increases in one-electron reduction of oxygen to $\text{O}_2^{\cdot-}$, which then reacts to form H_2O_2 and other organic ROOH [76, 81, 82]. Our results show that TPP disrupts ATP-linked oxygen consumption. This disruption presumably leads to more electrons leaking off the ETC chain that

forms more $O_2^{\cdot-}$ and H_2O_2 that goes on to generate more ROS. Results demonstrated that TPP increased DHE oxidation in a chain-length-dependent manner, with longer chains resulting in more DHE oxidation compared to shorter chains presumably due to ETC inhibition and subsequent ROS production. Interestingly, rescue studies performed with the $O_2^{\cdot-}$ and H_2O_2 scavenging SOD, Cat, and GPx4 adenoviruses did not protect melanoma cells from TPP-mediated cytotoxicity. The results suggest that under these experimental conditions, $O_2^{\cdot-}$ and H_2O_2 are not likely the ROS that result in TPP cytotoxicity. Therefore, the increase in DHE oxidation is presumably due to TPP causing electrons to leak off the ETC and oxidizing everything in the local environment.

Next, since GSH functions as a cellular antioxidant that scavenges free radicals and maintains cellular redox potential and balance, it is likely that an increase in DHE oxidation due to TPP ETC inhibition and ROS production will result in GSH depletion. Indeed, results demonstrate that TPP depletes intracellular total GSH. Results also show that TPP treatment results in increased intracellular GSSG. Further, the media from cells treated with TPP compounds also had elevated levels of total GSH. When GSH is oxidized to GSSG, it is transported out of cells. Interestingly, elevated total media GSH was only observed in cells treated with 5-, 8-, and 10-TPP and not in cells treated with 12-, 14-, or 16-TPP. One possible explanation for these results is that GSH transport is carried out by GSH transporters and is an ATP-dependent process. We next measured ATP levels in melanoma cells treated with TPP. We found that TPP derivatives decrease intracellular ATP concentrations, and that

inclusion of longer side chain lengths on TPP resulted in larger decreases in ATP levels, where 12-, 14-, and 16-TPP caused the greatest decrease in intracellular ATP. Since GSH transport is ATP dependent, these results could explain why 5-, 8-, and 10-TPP result in elevated media total GSH, whereas 12-, 14-, and 16-TPP do not. Clonogenic rescue studies demonstrate that NAC is able to rescue TPP induced cytotoxicity, which suggests that TPP causes cytotoxicity due to ETC disruption, subsequent ROS generation, and GSH depletion, which results in an oxidized cellular state. Since TPP compounds increase ROS levels and decrease total GSH in melanoma cells, we hypothesized that further decreases in GSH or Trx could enhance the sensitivity of melanoma cells to TPP treatment. Similar to other published studies, results demonstrate that addition of the GSH synthesis inhibitor BSO or the TRxR inhibitor AUR in fact do significantly enhance the sensitivity of melanoma cells to TPP treatment. Collectively, these results strongly suggest that TPP compounds disrupt oxygen consumption, increases ROS levels, and disrupts GSH metabolism.

In order to contribute to development of TPP for melanoma therapy *in vivo*, we evaluated the route of administration that results in the highest TPP tumor accumulation. This is a critical step in the translation of TPP clinically, because to our knowledge, no group has actually shown that TPP significantly accumulates in tumors and which route of administration results in the greatest accumulation of TPP. Further, the extent of uptake of TPP in cancer cells and cancer cell mitochondria is dependent upon the hydrophobicity of TPP drugs. The anchoring of the TPP side chain into the mitochondria membrane and effect

on mitochondria and cellular metabolism is also dependent on the lipophilicity of TPP [133]. This could be a major barrier to clinical translation because drugs require some amount of hydrophilicity in order to favorably biodistribute to target organs *in vivo*. It should also be noted that TPP concentrations utilized *in vitro* in many publications to date have not yet been determined to be reasonably achievable following metabolism and clearance in an animals or humans [133]. Further, systemic administration (*e.g.*, I.P., I.V., oral) is expected to lead to TPP accumulation in off-target sites (*e.g.*, mitochondria-rich heart and liver), TPP metabolism in the gut, and TPP drug excretion without tumor/tissue accumulation. Based on this knowledge, we administered a ¹⁴C-12-TPP via I.P. injection, I.V. injection, and oral gavage. We also explored new and potentially exciting alternative approach to drug administration by using a thermosensitive-hydrogel that exists in a water-like state at low temperatures and forms a gel at physiological temperature, allowing for the controlled release of a lipophilic drug at a desired site (*e.g.*, directly at the tumor site). Biodistribution results demonstrate that TPP did not significantly accumulate in melanoma tumors following administration of 12-TPP via I.V. injection, I.P. injection, or oral gavage. However, TPP administered via hydrogel peritumorally was detectable at significant levels at 48 h post injection in melanoma tumors, with minimal accumulation in off target organs. These findings suggest that hydrogel-based TPP delivery system could be an alternative administration route to conventional routes of drug administration and result in TPP concentrated directly at the tumor site. In order to identify potential normal tissue toxicity associated with TPP

treatment, mice were administered TPP via drinking water, and route of TPP administration that results in off-target TPP accumulation according to our biodistribution studies. There was no apparent liver, kidney, or bone marrow toxicity after 17 days of treatment. We next wanted to see if 12-TPP administered via hydrogel could decrease melanoma tumor growth rate with minimal off target affects. Results show that 12-TPP administered via hydrogel to mice bearing A375 melanoma tumors decreased tumor growth rates compared to untreated mice up to three weeks of treatment. These results demonstrate that a thermosensitive hydrogel can effectively deliver TPP directly at a melanoma tumor site and decrease melanoma tumor growth rate with minimal adverse effects in non-malignant tissues. Importantly, heightened metabolism is a generalizable cancer trait; therefore a TPP-hydrogel could be broadly applicable to many cancer types and patients. Further, hydrogel delivery systems are capable of delivering a payload directly at the tumor site and therefore limit systemic toxicity associated with chemotherapy. A hydrogel delivery system could also be loaded with multiple anti-cancer agents in order to target multiple cellular components and a way to circumvent cancer resistance [148]. Hydrogel loaded with TPP could also be applied to tumor margins following surgical resection and potentially decrease the likelihood of tumor recurrence. Lastly, a hydrogel-based TPP delivery system could potentially be injected at superficial tumor sites and minimize scarring often associated with surgical resection. Collectively, our results highlight the potential for a TPP hydrogel delivery system for the therapy of cancer patients worldwide.

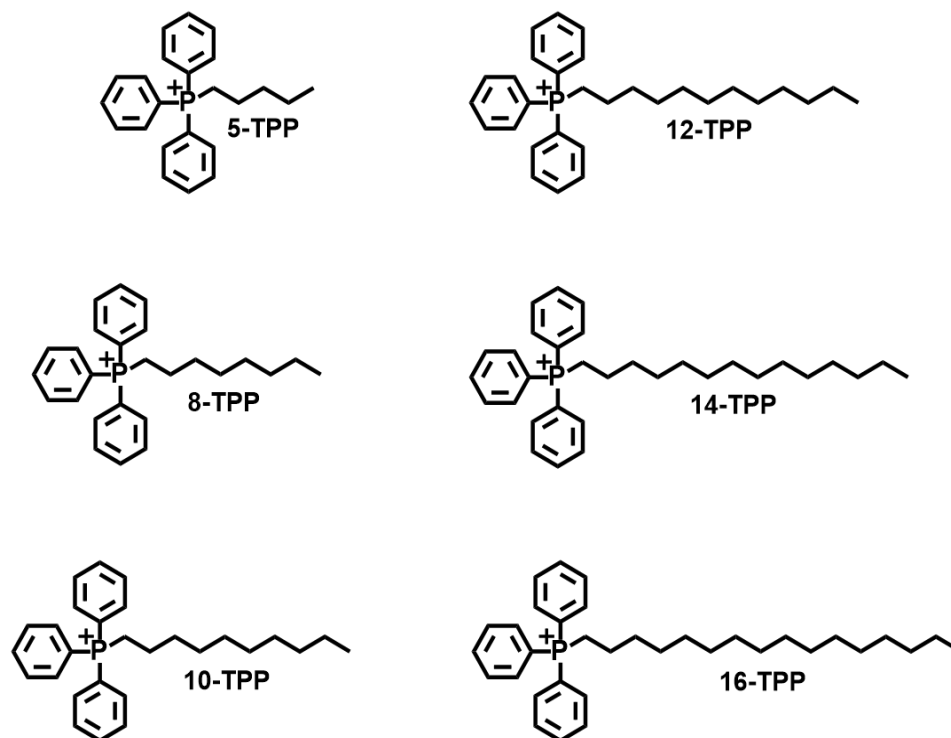


Figure II-1. The TPP derivatives examined in this study.

The positive charge of the central TPP phosphorous atom is delocalized over the lipophilic TPP moiety, contributing to the mitochondria-targeting characteristic of TPP variants. It is hypothesized that the molecular composition of the TPP side chain inserts into the mitochondrial membrane, which disrupts mitochondria metabolism.

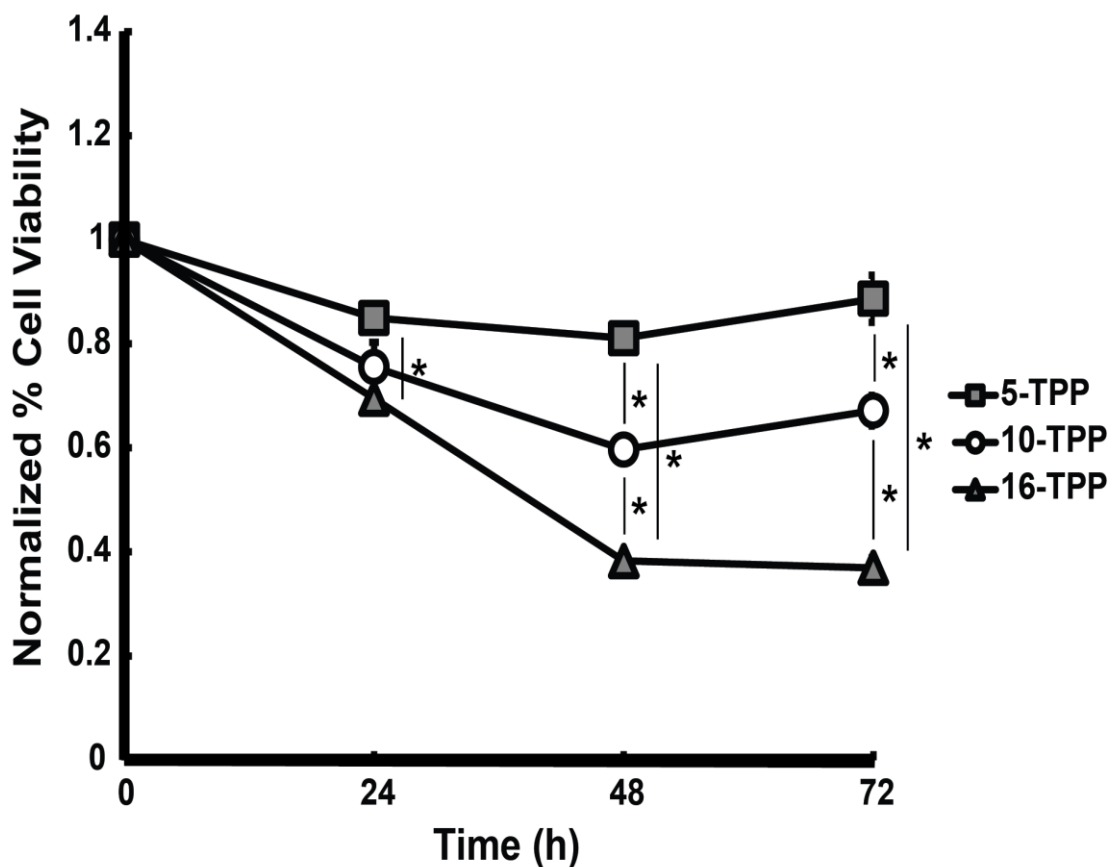


Figure II-2. Increasing TPP side-chain length decreases the viability of A375 melanoma cells.

A375 melanoma cells were plated in 96-well plates and incubated for 24 h. Cells were then treated with 0.5 μ M 5-, 8-, 10-, 12-, 14-, or 16-TPP for 24 h, 48 h or 72 h and analyzed for cell viability by the MTT method. Error bars represent the standard error of the mean (* significant relative to control, $p < 0.05$, $N = 4$). Results demonstrate that TPP derivatives decrease A375 melanoma cell viability; and there is a structure-activity relationship between TPP side chain length and decreased viability. Further, there is a time and concentration dependence on TPP induced decreases in A375 melanoma cell viability.

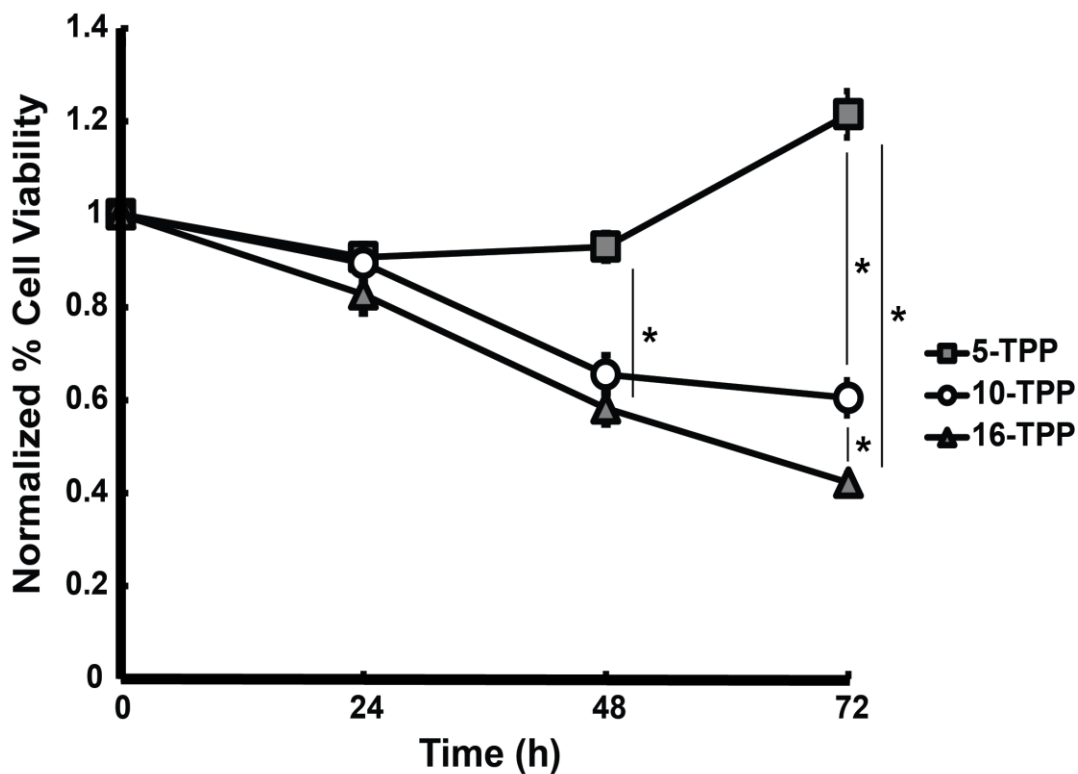


Figure II-3. Increasing TPP side-chain length decreases the viability of MeWo melanoma cells.

MeWo melanoma cells were plated in 96-well plates and incubated for 24 h. Cells were then treated with 0.5 μ M 5-, 8-, 10-, 12-, 14-, or 16-TPP for 24 h, 48 h or 72 h and analyzed for cell viability by the MTT method. Error bars represent the standard error of the mean (* significant relative to control, $p < 0.05$, $N = 4$). Results demonstrate that TPP derivatives decrease MeWo melanoma cell viability; and there is a structure-activity relationship between TPP side chain length and decreased viability. Further, there is a time and concentration dependence on TPP induced decreases in MeWo melanoma cell viability.

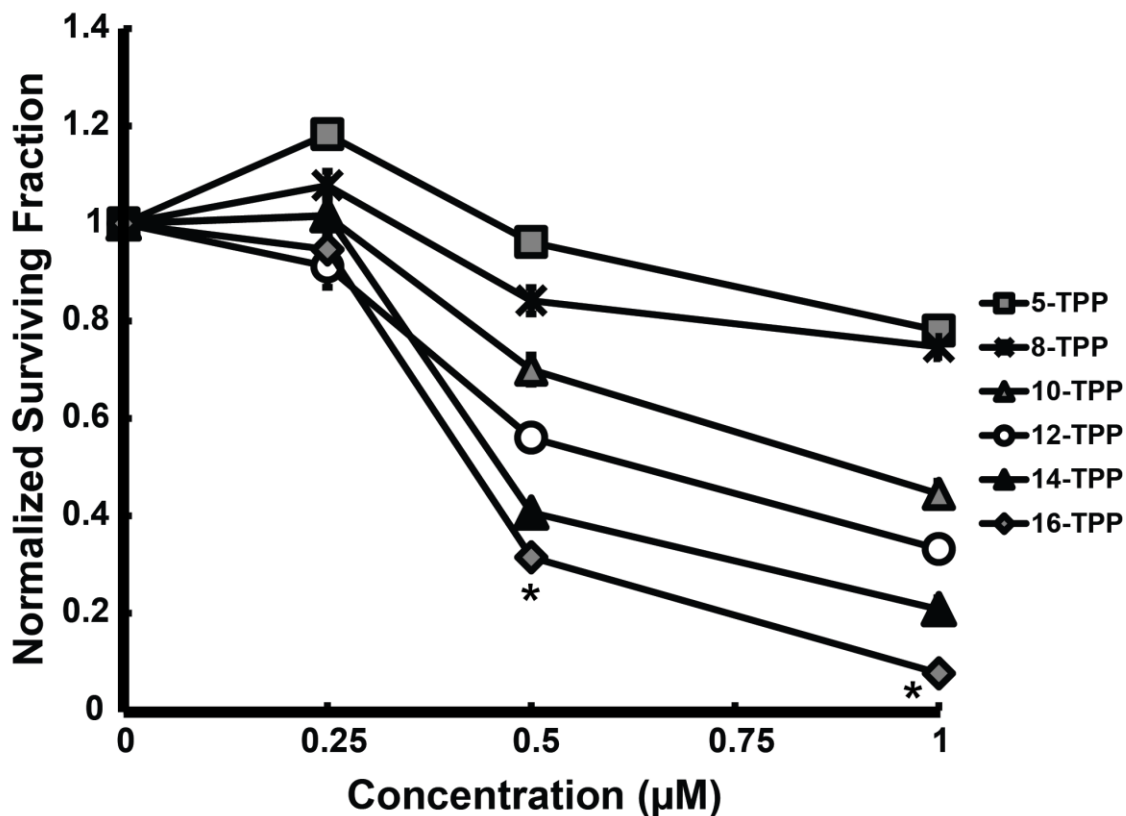


Figure II-4. Increasing TPP side-chain length decreases the clonogenic survival of A375 melanoma cells after 24 h treatment.

A375 human melanoma cells were plated in 60 mm tissue culture dishes and incubated for 48 h. Cells were then treated with 0.25 µM, 0.5 µM or 1.0 µM 5-, 8-, 10-, 12-, 14-, or 16-TPP for 24 h and analyzed for clonogenic survival. Error bars represent the standard error of the mean (* represents when 10-, 12-, 14-, and 16-TPP were significant relative to 5-TPP and 8-TPP, $p < 0.05$, $n = 3$ from 2 separate experiments, $N = 6$). Results demonstrate that TPP derivatives decrease melanoma cell clonogenic survival after 24 h treatment; and there is a structure-activity relationship between TPP side chain length and decreased clonogenic survival.

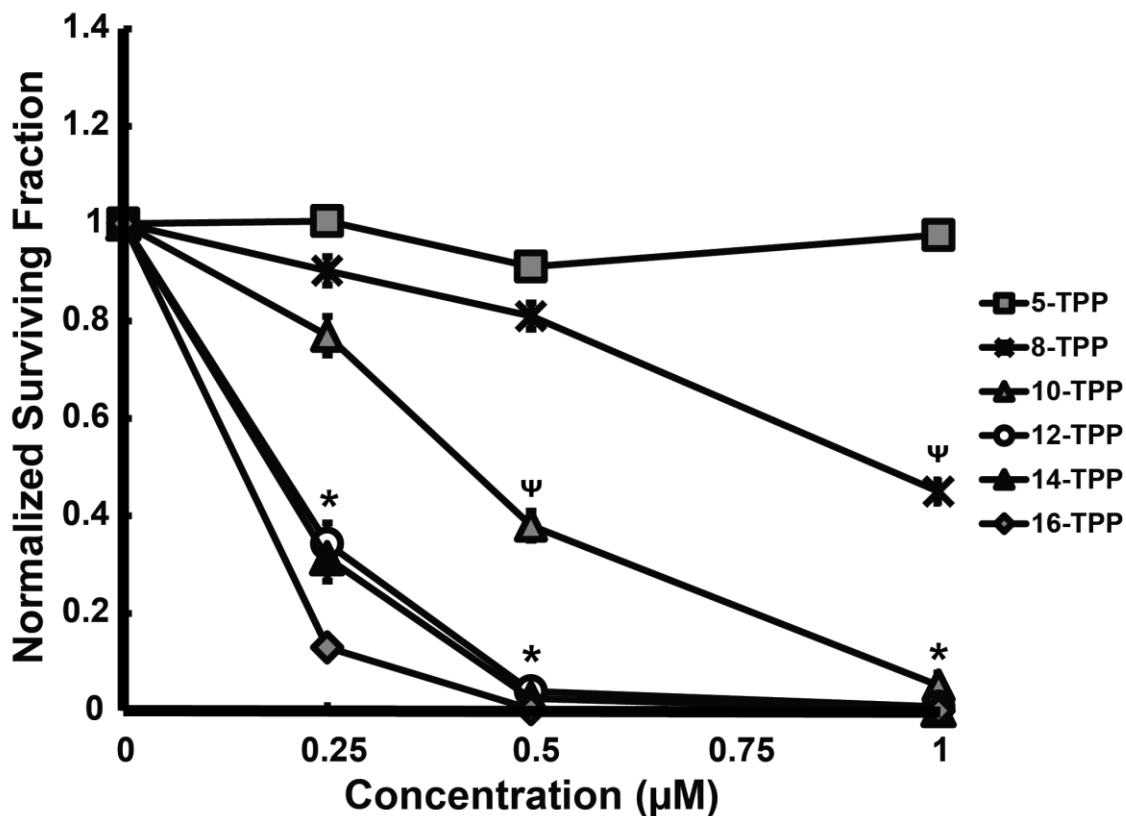


Figure II-5: Increasing TPP side-chain length decreases the clonogenic survival of A375 melanoma cells after 48 h treatment.

A375 human melanoma cells were plated in 60 mm tissue culture dishes and incubated for 48 h. Cells were then treated with 0.25 µM, 0.5 µM or 1.0 µM 5-, 8-, 10-, 12-, 14-, or 16-TPP for 48 h and analyzed for clonogenic survival. Error bars represent the standard error of the mean (* represents when 12-, 14-, and 16-TPP were significant relative to 5-TPP and 8-TPP, Ψ represents when 10-TPP was significant relative to 5-TPP and 8-TPP, $p < 0.05$, $n = 3$ from 2 separate experiments, $N = 6$). Results demonstrate that TPP derivatives further decrease melanoma cell clonogenic survival after 48 h treatment compared to 24 h; and there is a structure-activity relationship between TPP side chain length and decreased clonogenic survival.

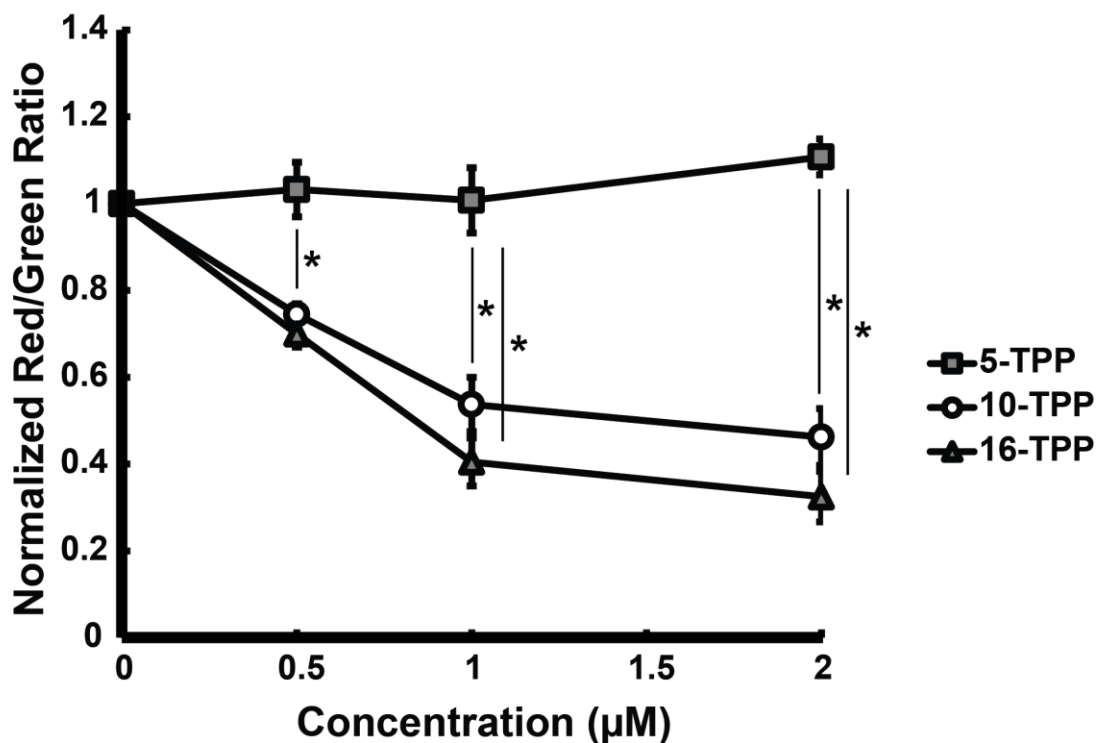


Figure II-6. Increasing TPP side-chain length decreases the mitochondria membrane potential of A375 melanoma cells.

A375 human melanoma cells were plated in 60 mm tissue culture dishes and incubated for 24 h. After incubation, cells were treated with a 5-, 10-, or 16-TPP for 1 h. Cells were then incubated with the mitochondria membrane potential fluorescent probe JC-1 for 30 min. Following labeling, cells were analyzed by flow cytometry. Error bars represent the standard error of the mean (* significant relative to control, $p < 0.05$, $n = 2$ from 2 separate experiments; $N = 4$). Results suggest that TPP derivatives preferentially accumulate in A375 cell mitochondria and decrease mitochondria membrane potential. Further, there is a structure-activity relationship between TPP chain length and decreased mitochondria membrane potential.

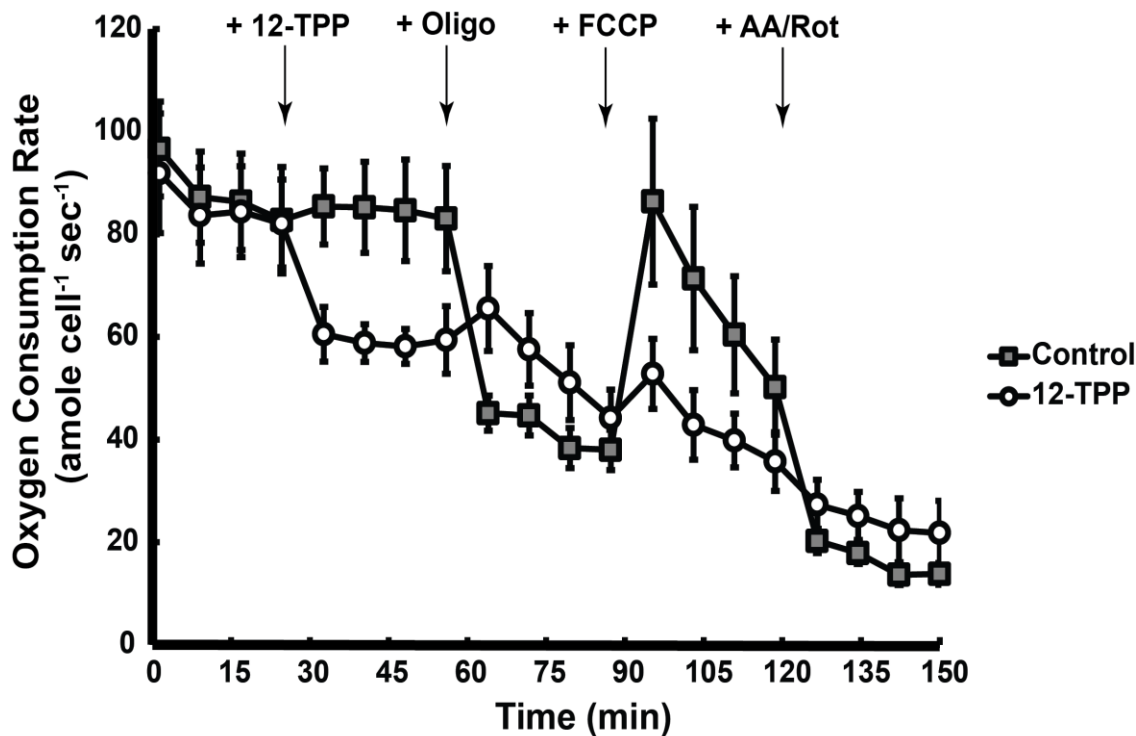


Figure II-7. TPP decreases oxygen consumption in melanoma cells.

A375 melanoma cells were plated in XF96 plates and incubated for 48 h. Oxygen consumption rate (OCR) measurements were made using a Seahorse Bioscience XF96 extracellular flux analyzer in 15 min increments for 150 min. (1) 12-TPP was injected at the 20 min mark followed by the sequential addition of (2) oligomycin, (3) FCCP, and (3) antimycin A and rotenone. Results show that 12-TPP treatment decreases ATP-linked oxygen consumption in A375 melanoma cells. Error bars represent the standard error of the mean (N = 4). These results support the hypothesis that TPP interferes with mitochondria oxidative metabolism, which results in decreased ATP-linked oxygen consumption.

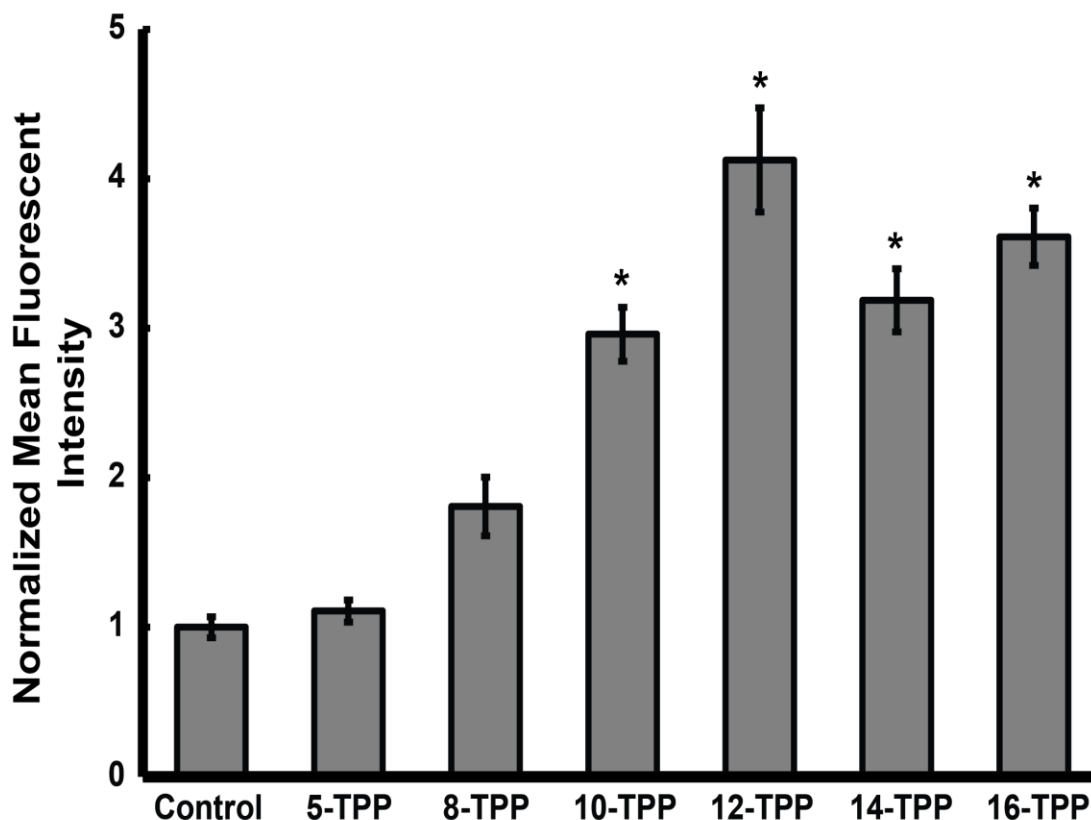


Figure II-8: Increasing TPP side-chain length increases DHE oxidation in melanoma cells.

A375 human melanoma cells were plated in 60 mm tissue culture dishes and incubated for 48 h. After incubation, cells were treated with TPP derivatives at a 1.0 μM concentration for 1.5 h. Cells were then incubated with the oxidation-sensitive DHE fluorescent probe for 30 min. After labeling, cells were analyzed by flow cytometry. Error bars represent the standard error of the mean (* significant relative to control, $p < 0.05$, $n = 3$ from 2 separate experiments, $N = 6$). Results indicate that TPP leads to increased DHE oxidation and increased DHE oxidation is dependent on TPP chain length. Further, these results suggest that TPP results in an oxidized cellular state, presumable due to ETC inhibition, which increases ROS levels.

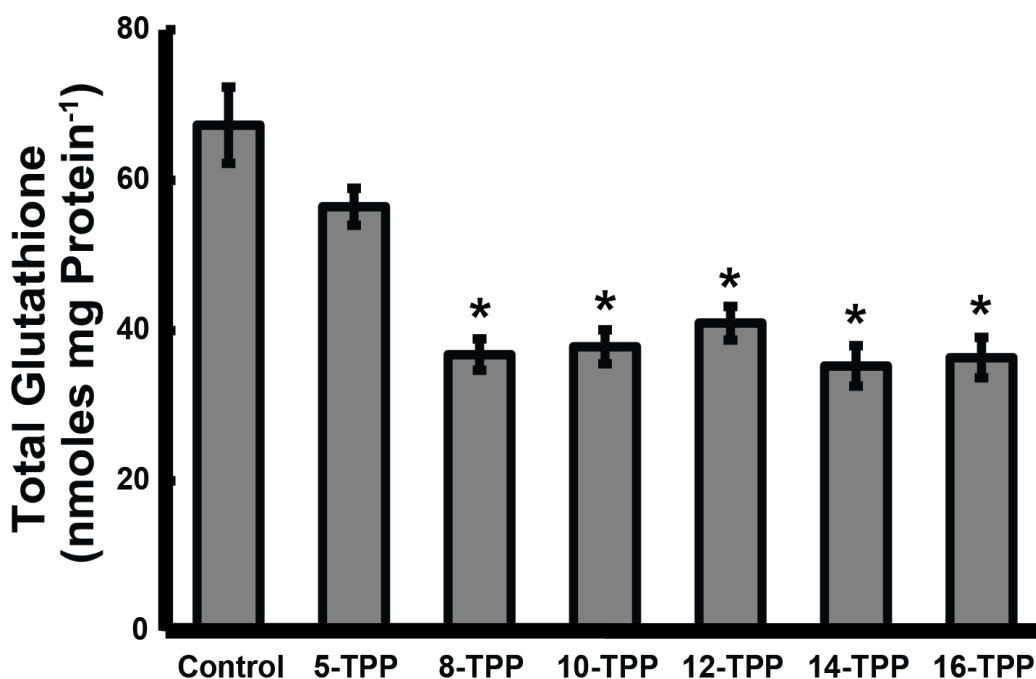


Figure II-9: Increasing TPP side-chain length decreases intracellular total glutathione levels in melanoma cells.

A375 melanoma cells were plated in 60 mm tissue culture dishes and incubated for 48 h. After incubation, cells were treated with 1.0 μ M 5-, 8-, 10-, 12-, 14- or 16-TPP for 24 h and analyzed for total cellular glutathione (GSH + GSSG) content. Error bars represent the standard error of the mean (* significant relative to control, $p < 0.05$, $N = 3$). Results demonstrate that TPP derivatives decrease GSH in melanoma cells and decreased GSH is TPP chain length dependent.

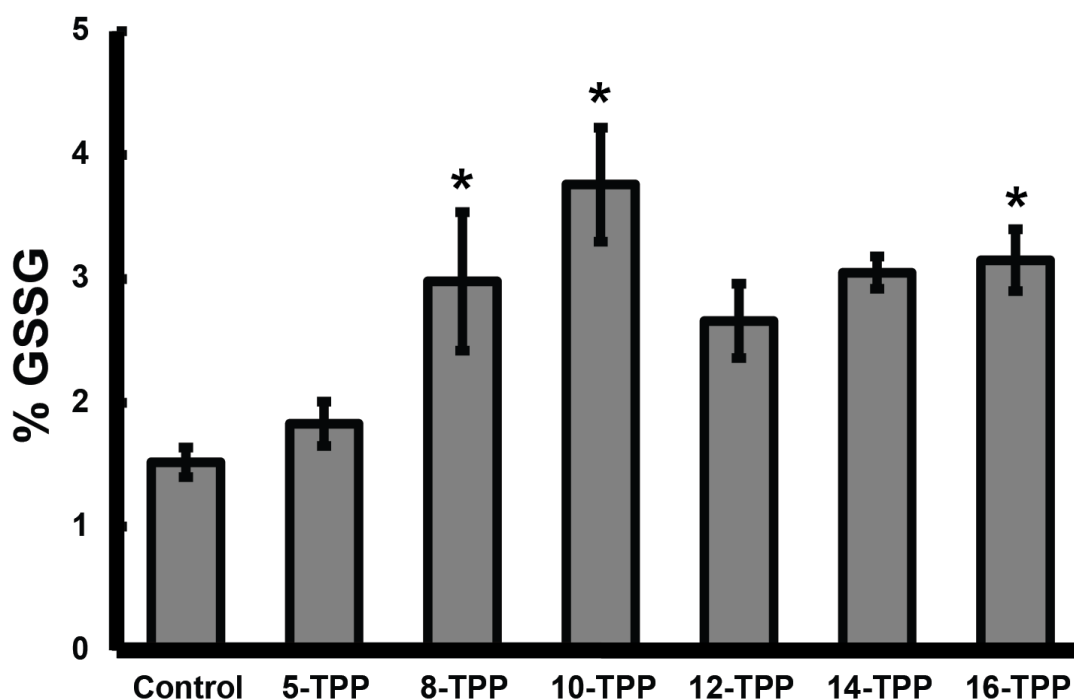


Figure II-10: Increasing TPP side-chain length increases oxidized glutathione in melanoma cells.

A375 melanoma cells were plated in 60 mm tissue culture dishes and incubated for 48 h. After incubation, cells were treated with 1.0 μ M 5-, 8-, 10-, 12-, 14- or 16-TPP for 24 h and analyzed for percent of glutathione that is oxidized (GSSG). Error bars represent the standard error of the mean (* significant relative to control, $p < 0.05$, $N = 3$). Results demonstrate that TPP derivatives increase GSSG in cells and increased GSSG is TPP chain length dependent.

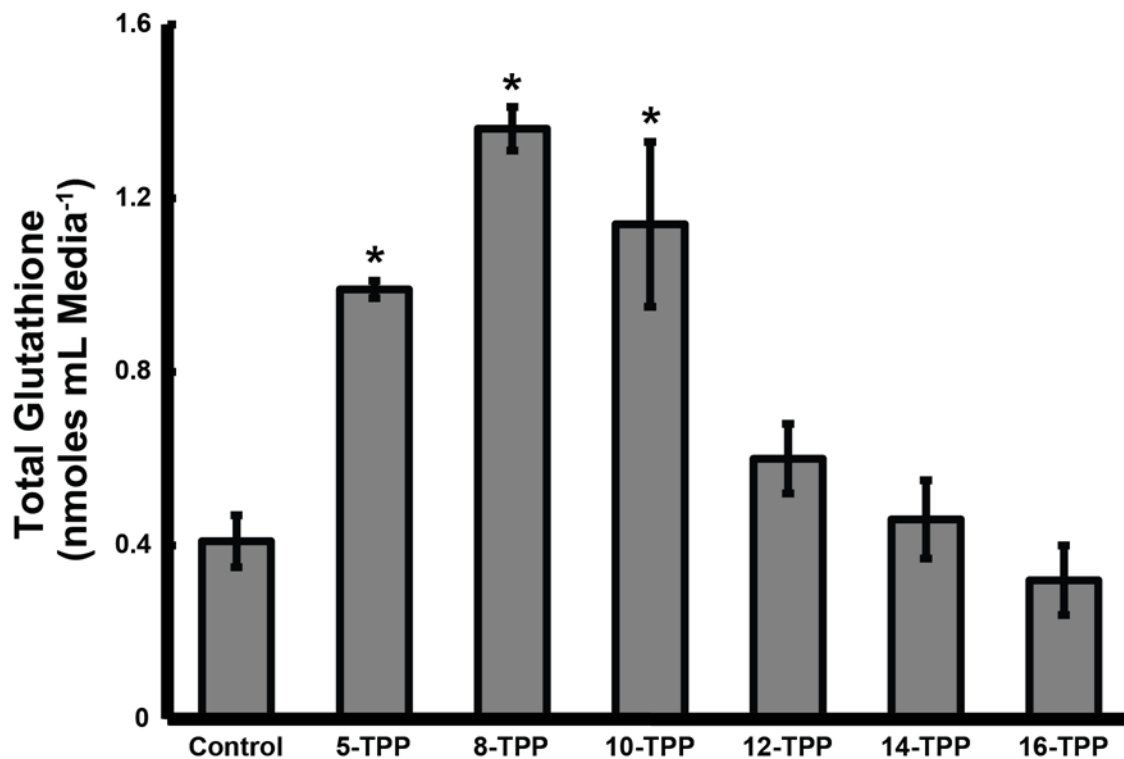


Figure II-11: TPP increases total glutathione in the tissue culture media of melanoma cells.

A375 melanoma cells were plated in 60 mm tissue culture dishes and incubated for 48 h. After incubation, cells were treated with 1.0 μ M 5-, 8-, 10-, 12-, 14- or 16-TPP for 24 h. The culture media was then collected and analyzed for total glutathione (GSH + GSSG). Error bars represent the standard error of the mean (* significant relative to control, $p < 0.05$, $N = 3$). Results demonstrate that 5-, 8-, and 10-TPP increase total GSH in the media, whereas 12-, 14-, and 16-TPP do not.

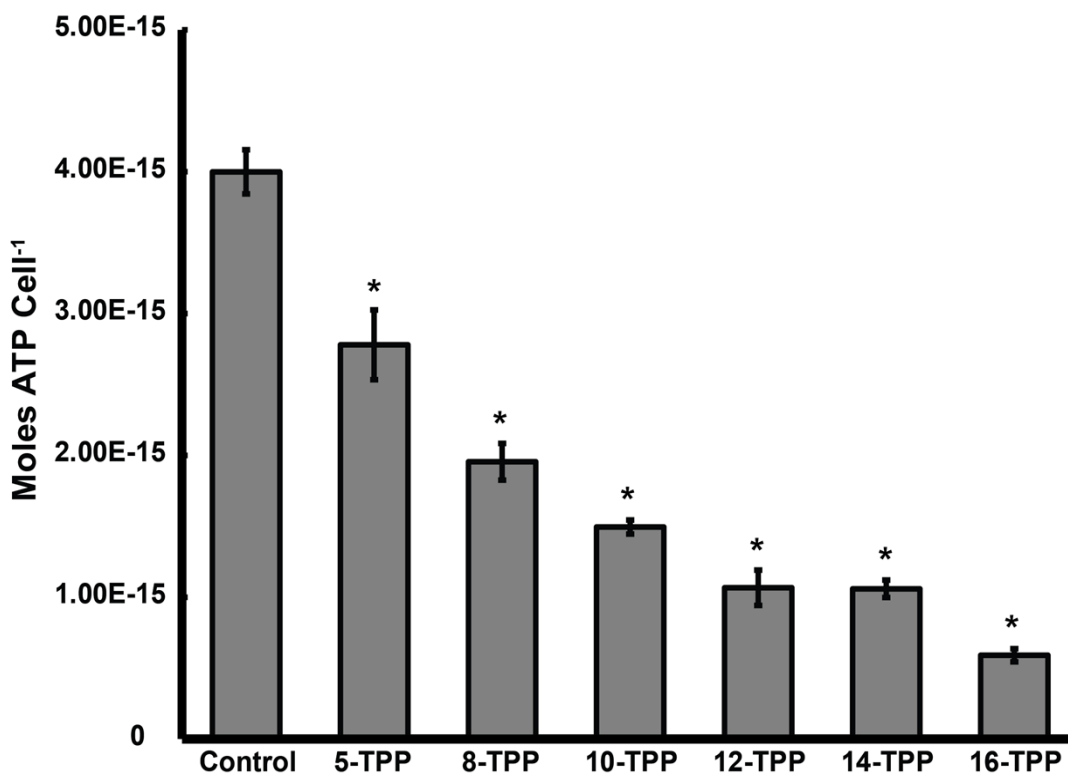


Figure II-12: Increasing TPP side-chain length decreases ATP levels in melanoma cells.

A375 human melanoma cells were plated in 60 mm tissue culture dishes and incubated for 48 h. Cells were then treated with TPP derivatives at a 1.0 μM concentration for 24 h. Following incubation with test compounds, intracellular ATP levels were analyzed with a luminescent-based ATP kit. Luminescence was measured using a microplate reader. Error bars represent the standard error of the mean (* significant relative to control, $p < 0.05$, $n = 3$ from 2 separate experiments, $N = 6$). Results demonstrate that TPP derivatives decrease intracellular ATP levels and there is a structure-activity relationship between TPP chain length and decreased intracellular ATP levels.

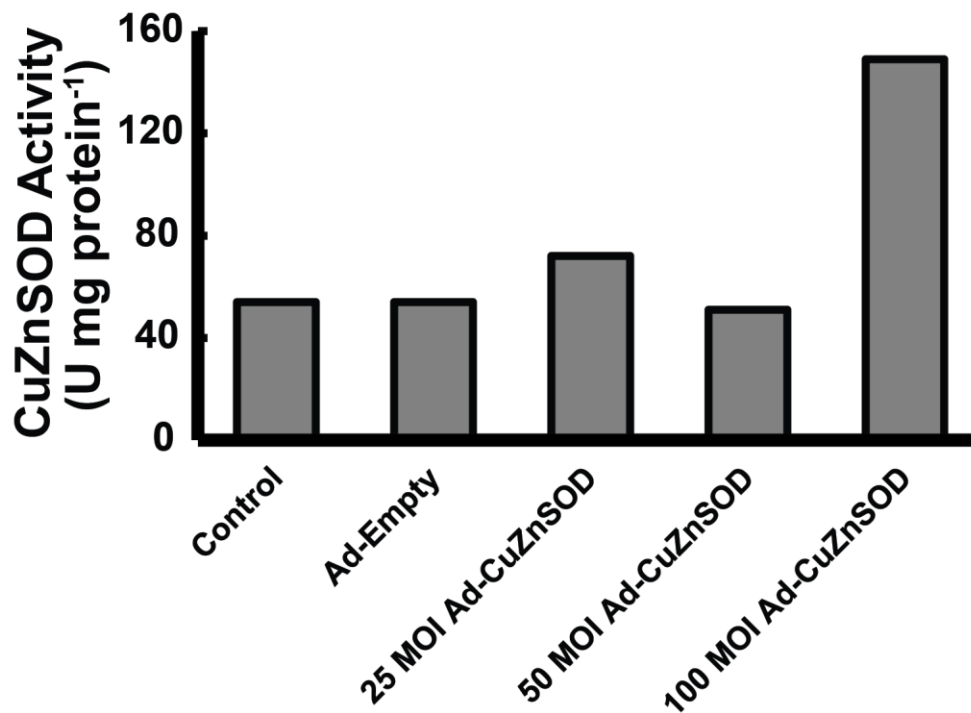


Figure II-13: Melanoma cells transfected with a CuZnSOD adenovirus exhibit increased CuZnSOD activity.

A375 cells were plated in 60 mm tissue culture dishes and incubated for 48 h. Cells were then transfected with Ad-CuZnSOD for 24 h in serum free media. The adenovirus was then removed and full media replaced for 24 h. Cells were then analyzed for CuZnSOD activity by measuring the rate of NBT reduction by $O_2^{\bullet -}$ spectrophotometrically. N = 1.

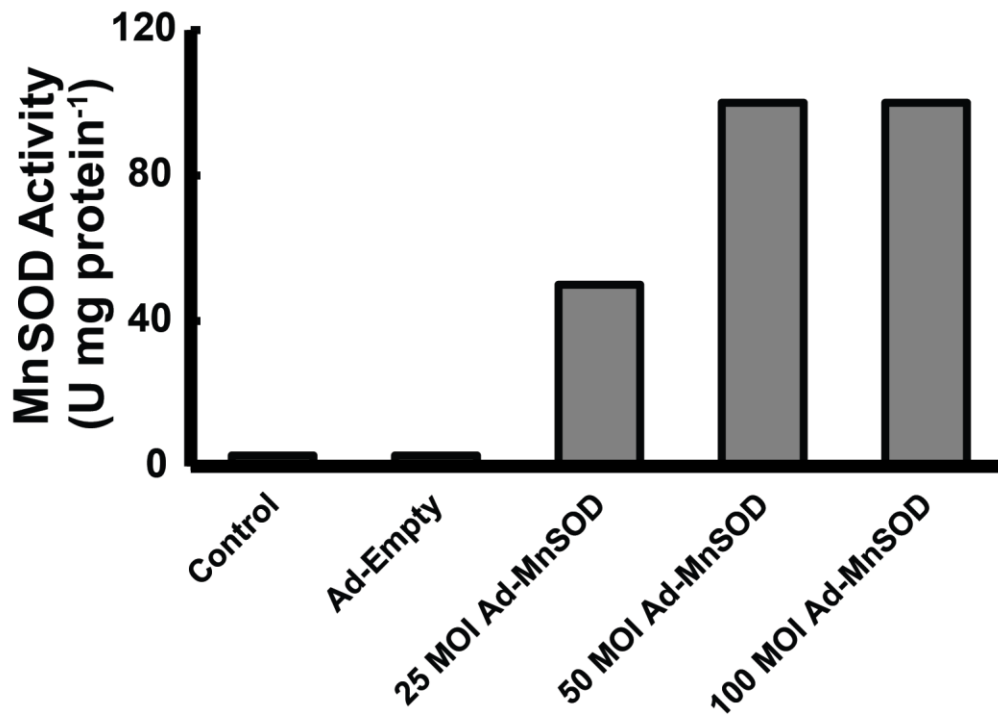


Figure II-14: Melanoma cells transfected with a MnSOD adenovirus exhibit increased MnSOD activity.

A375 cells were plated in 60 mm tissue culture dishes and incubated for 48 h. Cells were then transfected with Ad-MnSOD for 24 h in serum free media. The adenovirus was then removed and full media replaced for 24 h. Cells were then analyzed for MnSOD activity by measuring the rate of NBT reduction by $O_2^{\bullet-}$ spectrophotometrically. N = 1.

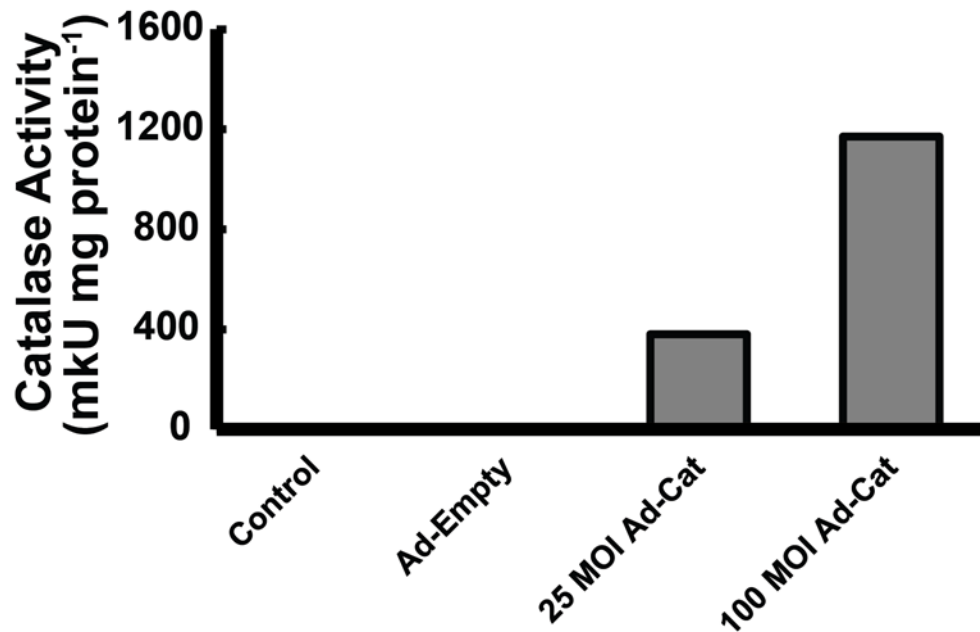


Figure II-15: Melanoma cells transfected with a Cat adenovirus exhibit high Cat and activity.

A375 cells were plated in 60 mm tissue culture dishes and incubated for 48 h. Cells were then transfected with Ad-Cat for 24 h in serum free media. The adenovirus was then removed and full media replaced for 24 h. Cells were then analyzed for Cat activity by measuring the rate of H₂O₂ decay spectrophotometrically. N = 1.

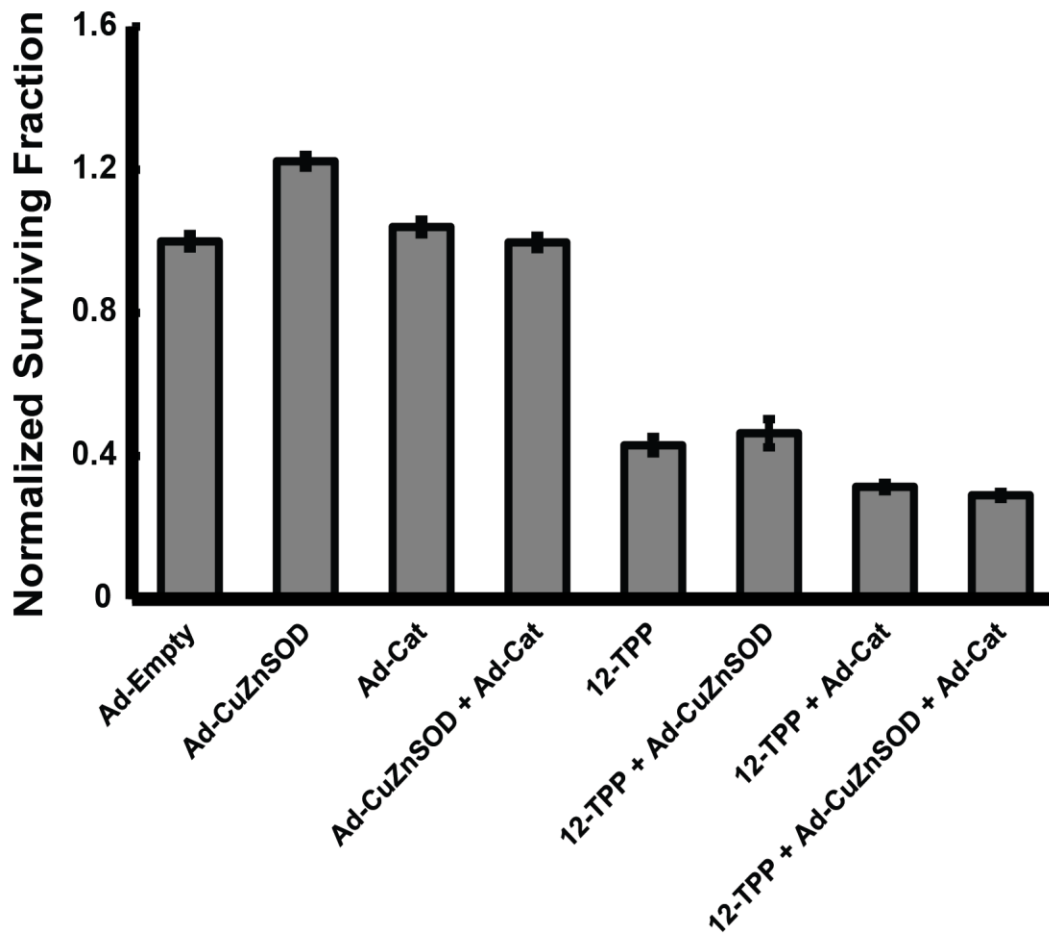


Figure II-16: CuZnSOD and Cat do not protect melanoma cells from TPP-mediated cytotoxicity.

A375 cells were plated in 60 mm tissue culture dishes and incubated for 48 h. Cells were then transfected with adenovirus (Ad-CuZnSOD and Ad-Cat) for 24 h in serum free media. The adenovirus was then removed and full media replaced for 24 h. Cells were then treated with 1 μ M 12-TPP for 24 h. Following drug treatment, cells were plated for a clonogenic survival assay. Results demonstrate that CuZnSOD or Cat do not protect melanoma cells from TPP-mediated cytotoxicity. Error bars represent the standard error of the mean (N = 3).

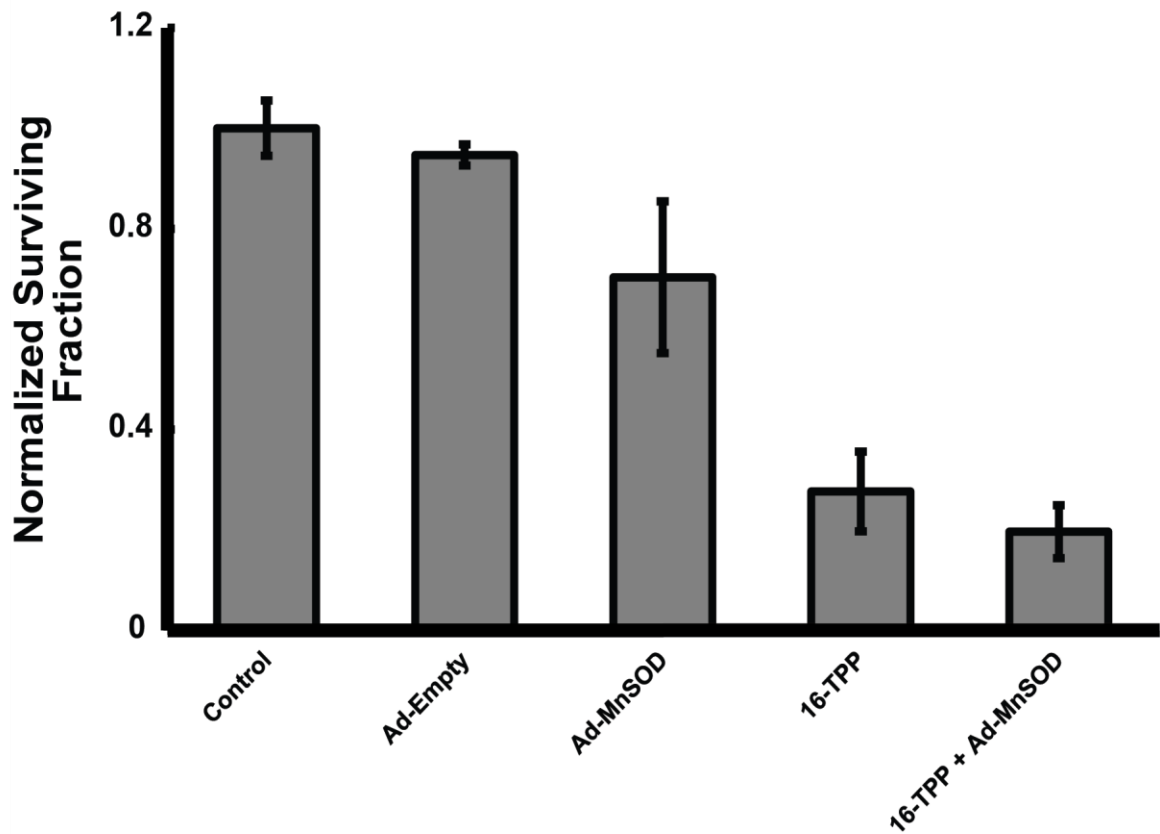


Figure II-17: MnSOD does not protect melanoma cells from TPP-mediated cytotoxicity.

A375 cells were plated in 60 mm tissue culture dishes and incubated for 48 h. Cells were then transfected with adenovirus (Ad-MnSOD) for 24 h in serum free media. The adenovirus was then removed and full media replaced for 24 h. Cells were then treated with 1 μ M 16-TPP for 24 h. Following drug treatment, cells were plated for a clonogenic survival assay.

Results demonstrate that MnSOD does not protect melanoma cells from TPP-mediated cytotoxicity. (n = 3 from 2 separate experiments; N = 6).

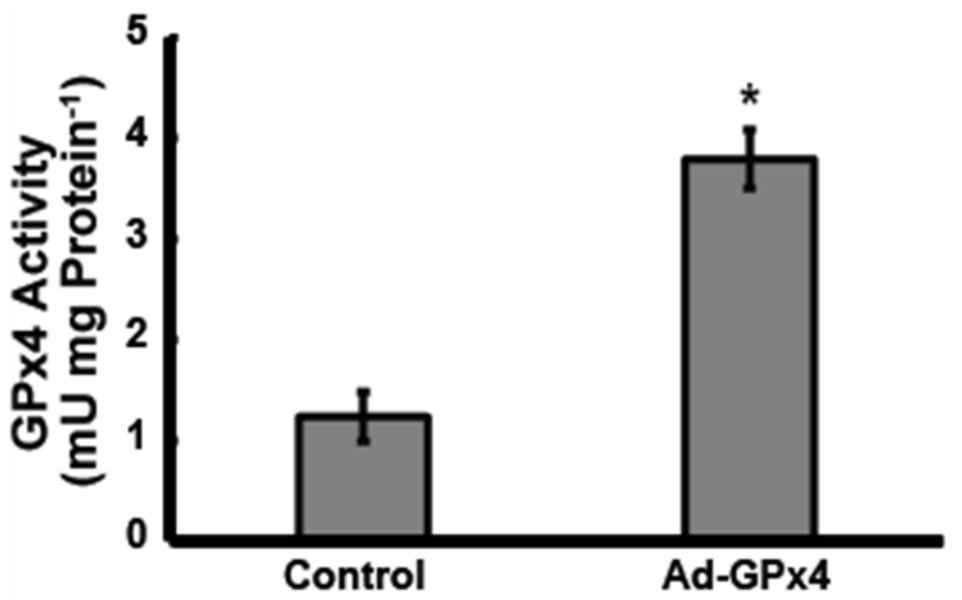


Figure II-18: Melanoma cells transfected with a GPx4 adenovirus exhibit high GPx4 activity.

A375 cells were plated in 60 mm tissue culture dishes and incubated for 48 h. Cells were then transfected with Ad-GPx4 for 24 h in serum free media. The adenovirus was then removed and full media replaced for 24 h. Cells were then analyzed for GPx4 activity by measuring the rate of NADPH oxidation by GSSG due to the oxidation of glutathione by lipid hydroperoxides and GPx4 spectrophotometrically. (* significant relative to control, $p < 0.05$, $N = 3$).

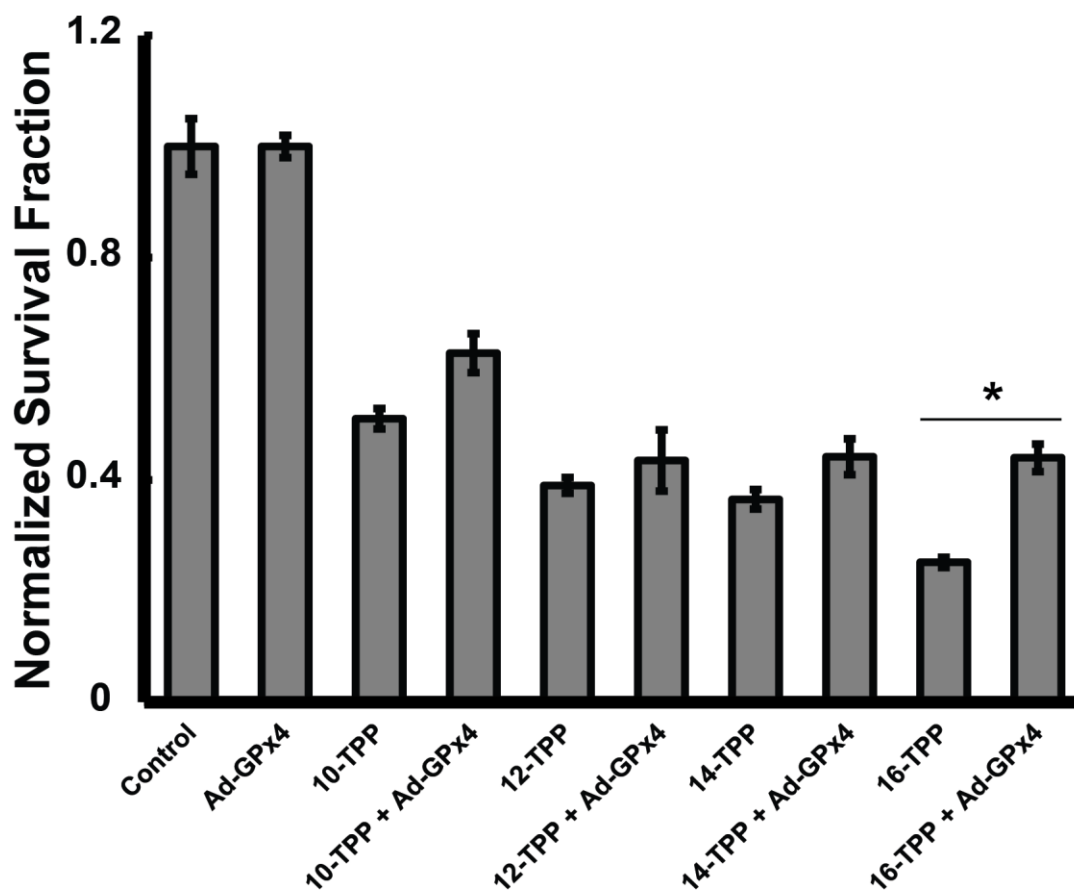


Figure II-19: GPx4 does not protect melanoma cells from TPP-mediated cytotoxicity.

A375 cells were plated in 60 mm tissue culture dishes and incubated for 48 h. Cells were then transfected with adenovirus (Ad-GPx4) for 24 h in serum free media. The adenovirus was then removed and full media replaced for 24 h. Cells were then treated with 1 μ M 10-, 12-, 14-, or 16-TPP for 24 h. Following drug treatment, cells were plated for a clonogenic survival assay. Results demonstrate that although there appears to be a trend towards improved clonogenic survival, only 16-TPP + GPx4 was significant compared to 16-TPP alone. Error bars represent the standard error of the mean (* significant relative to the same TPP drug treatment with Ad-GPx4, $p < 0.05$, $n = 3$ from 2 separate experiments, $N = 6$).

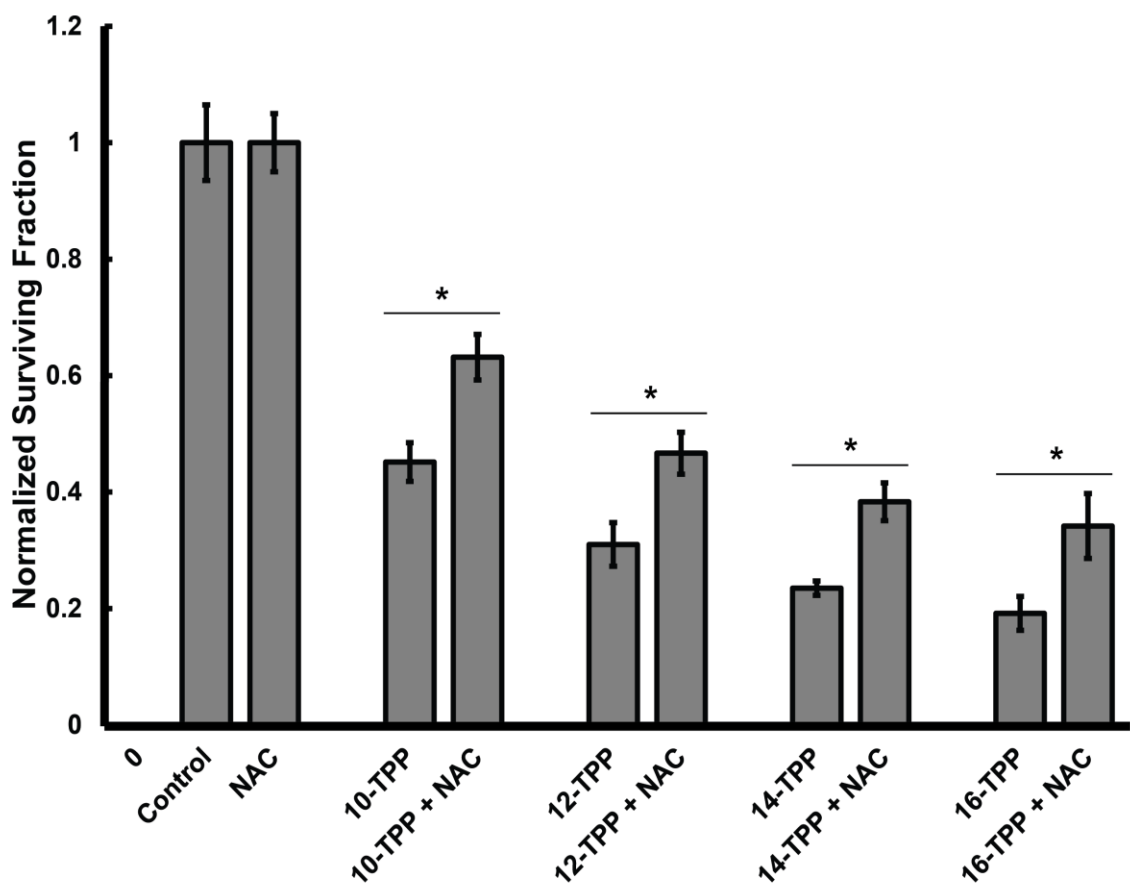


Figure II-20: NAC treatment partially protects melanoma cells from TPP mediated cytotoxicity.

A375 cells were plated in 60 mm tissue culture dishes and incubated for 48 h. Cells were then treated with 5-16 TPP alone or in combination with 20 mM N-acetylcysteine (NAC) for 24 h. Following treatment, cells were analysed for clonogenic survival. Error bars represent the standard error of the mean (* significant relative to the same TPP drug treatment with NAC, $p < 0.05$, $n = 3$ from 2 separate experiments; $N = 6$). Results demonstrate that NAC increased clonogenic survival by ~ 30% compared to cells treated with TPP alone. These results support that TPP inhibits the oxidative phosphorylation that results in increased ROS generation. Increased ROS oxidize GSH which ultimately results in melanoma cell death.

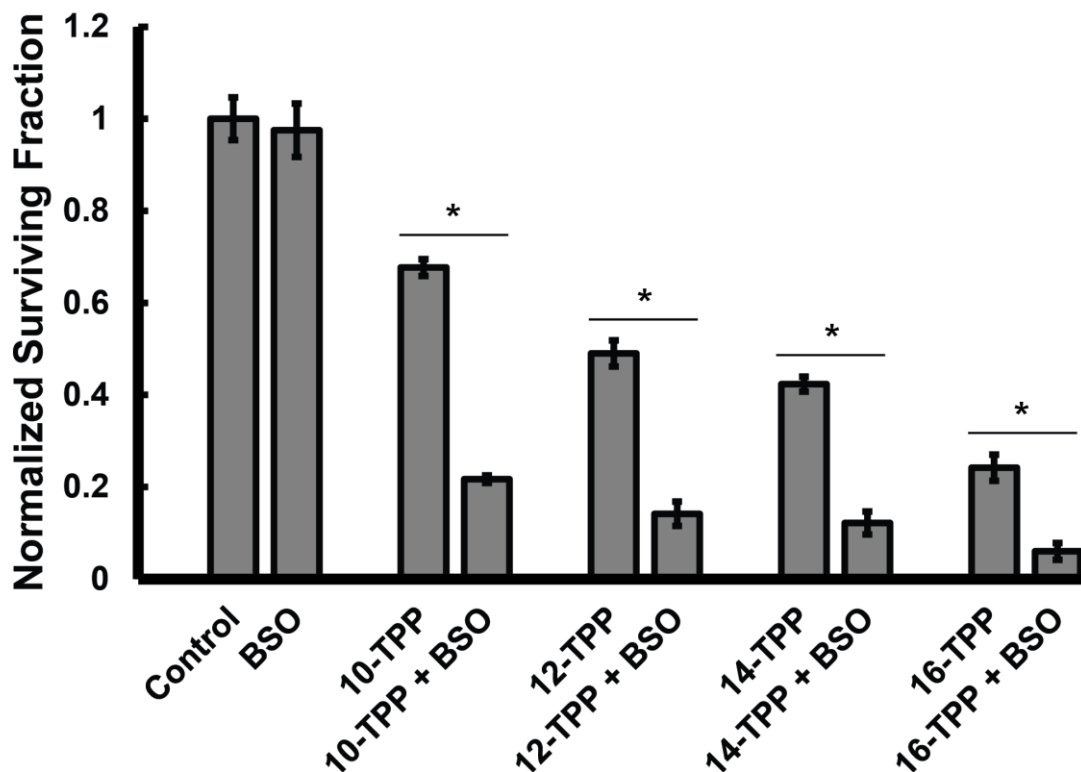


Figure II-21: Glutathione synthesis inhibition enhances the sensitivity of melanoma cells to TPP treatment.

A375 cells were plated in 60 mm tissue culture dishes and incubated for 48 h. Cells were then treated with 5-16 TPP alone or in combination with 100 μ M of the glutathione inhibitor l-buthionine-sulfoximine (BSO) for 24 h. Following treatment, cells were analyzed for clonogenic survival. Error bars represent the standard error of the mean (* significant relative to the same TPP drug treatment with BSO, $p < 0.05$, $n = 3$ from 2 separate experiments; $N = 6$). Results demonstrate BSO enhances the sensitivity of A375 melanoma cells to TPP treatment compared to TPP alone. These results support the development of a TPP and BSO combination therapy for metastatic melanoma.

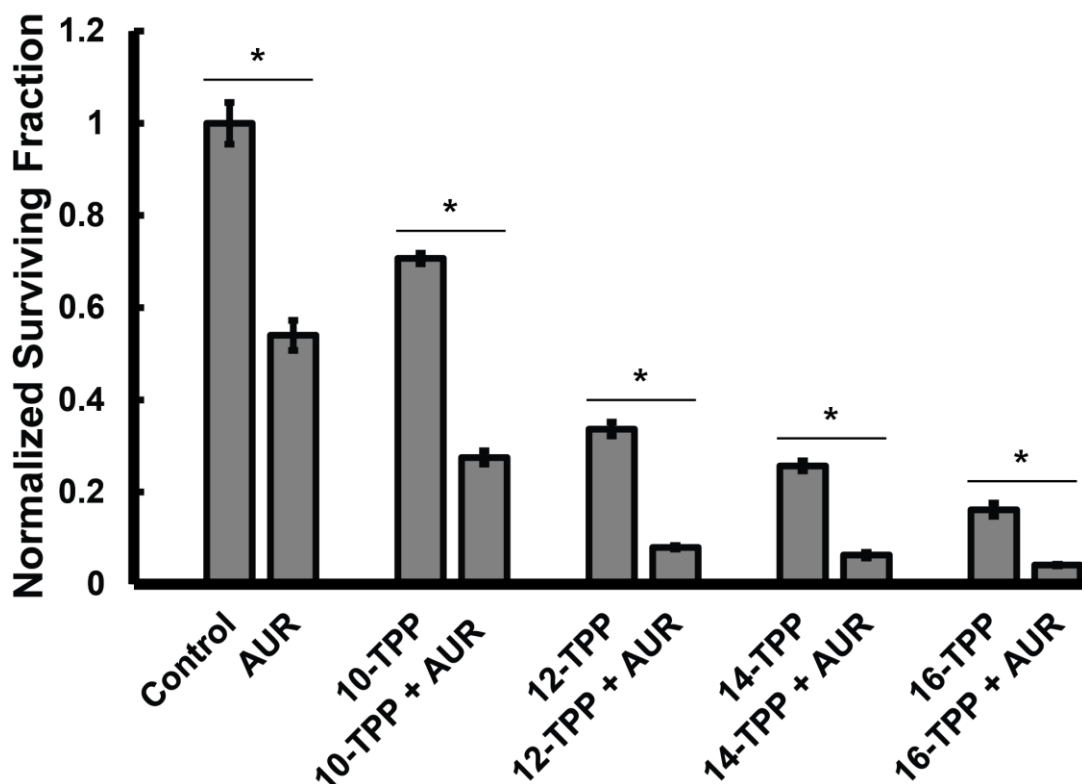


Figure II-22: Thioredoxin reductase inhibition enhances the sensitivity of melanoma cells to TPP treatment.

A375 cells were plated in 60 mm tissue culture dishes and incubated for 48 h. Cells were then treated with 5-16 TPP alone or in combination with 1.0 μ M of the thioredoxin reductase inhibitor auranofin (AUR) for 24 h. Following treatment, cells were analyzed for clonogenic survival. Error bars represent the standard error of the mean (*significant relative to the same TPP drug treatment with AUR, $p < 0.05$, $n = 3$ from 2 separate experiments; $N = 6$). Results demonstrate AUR enhances the sensitivity of A375 melanoma cells to TPP treatment compared to TPP alone. These results support the development of a TPP and AUR combination therapy for metastatic melanoma.

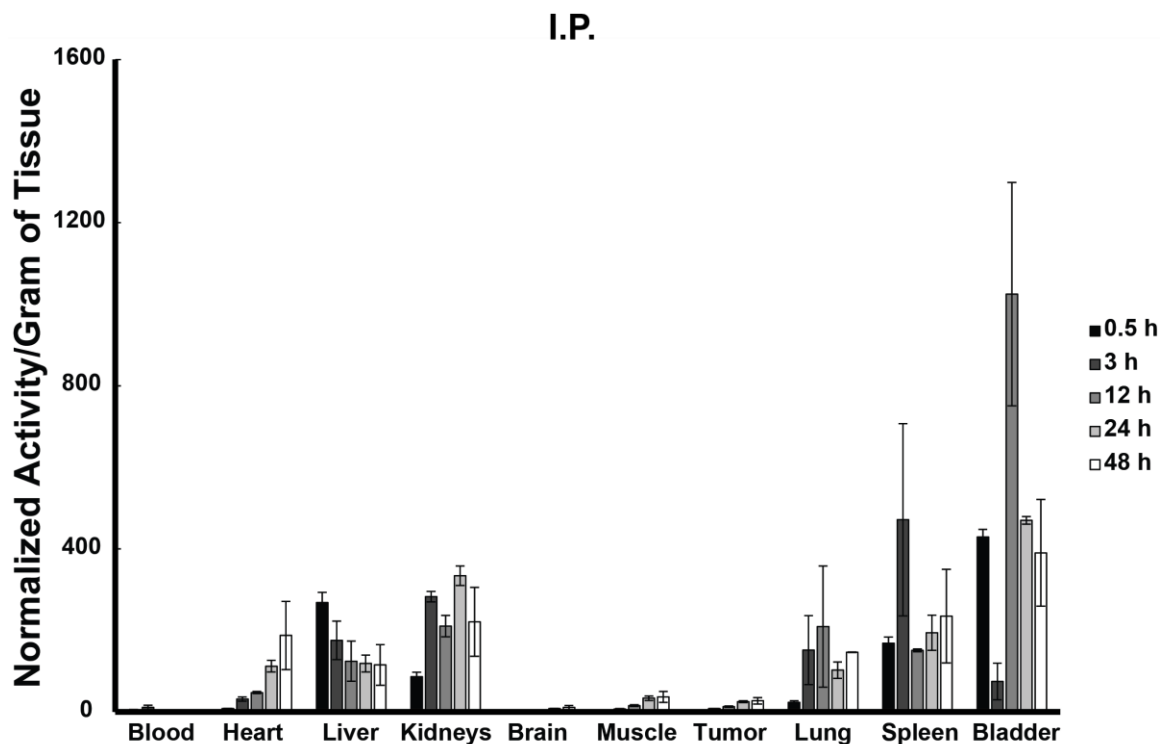


Figure II-23: TPP biodistribution following intraperitoneal injection.

Mice bearing A375 melanoma tumors were administered 2.5 μCi of carbon-14 labeled 12-TPP via I.P. injection. Animals were sacrificed 0.5 h, 3 h, 12 h, 24 h, or 48 h post-injection. Organs were harvested, dried, ground, and counted by liquid scintillation. Error bars represent standard error of the mean (N = 2 for each time point). Results demonstrate there was a time-dependent increase in 12-TPP accumulation in A375 melanoma tumors; although tumor accumulation was modest. There was off-target accumulation of 12-TPP in the heart, liver, kidneys, lung, spleen, and bladder.

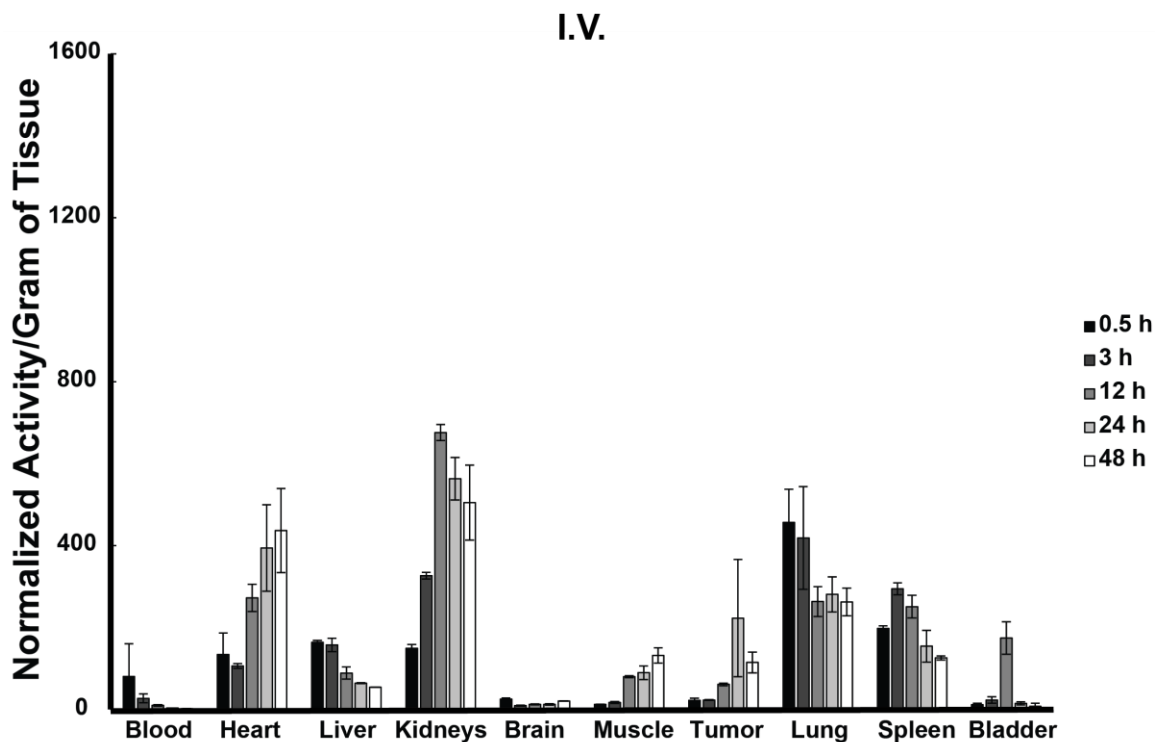


Figure II-24: TPP biodistribution following intravenous injection.

Mice bearing A375 melanoma tumors were administered 2.5 μCi of carbon-14 labeled 12-TPP via I.V. injection. Animals were sacrificed 0.5 h, 3 h, 12 h, 24 h, or 48 h post-injection. Organs were harvested, dried, ground, and counted by liquid scintillation. Error bars represent standard error of the mean (N = 2 for each time point). Results demonstrate there was a time-dependent increase in 12-TPP accumulation in A375 melanoma tumors. There was off-target accumulation of 12-TPP in the heart, liver, kidneys, lung, and spleen.

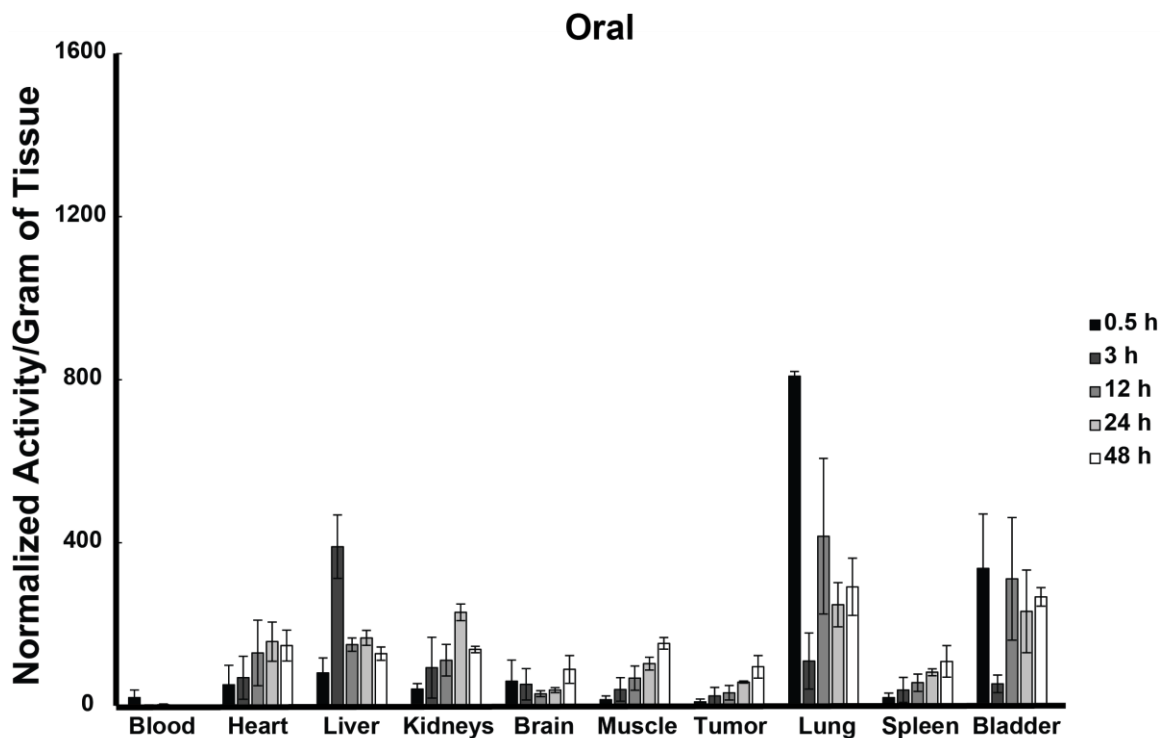


Figure II-25: TPP biodistribution following oral administration.

Mice bearing A375 melanoma tumors were administered 2.5 μCi of carbon-14 labeled 12-TPP via oral gavage. Animals were sacrificed 0.5 h, 3 h, 12 h, 24 h, or 48 h post-injection. Organs were harvested, dried, ground, and counted by liquid scintillation. Error bars represent standard error of the mean (N = 2 for each time point). Results demonstrate there was a time-dependent increase in 12-TPP accumulation in the A375 melanoma tumors. There was off-target accumulation of 12-TPP in all other organs analyzed as well.

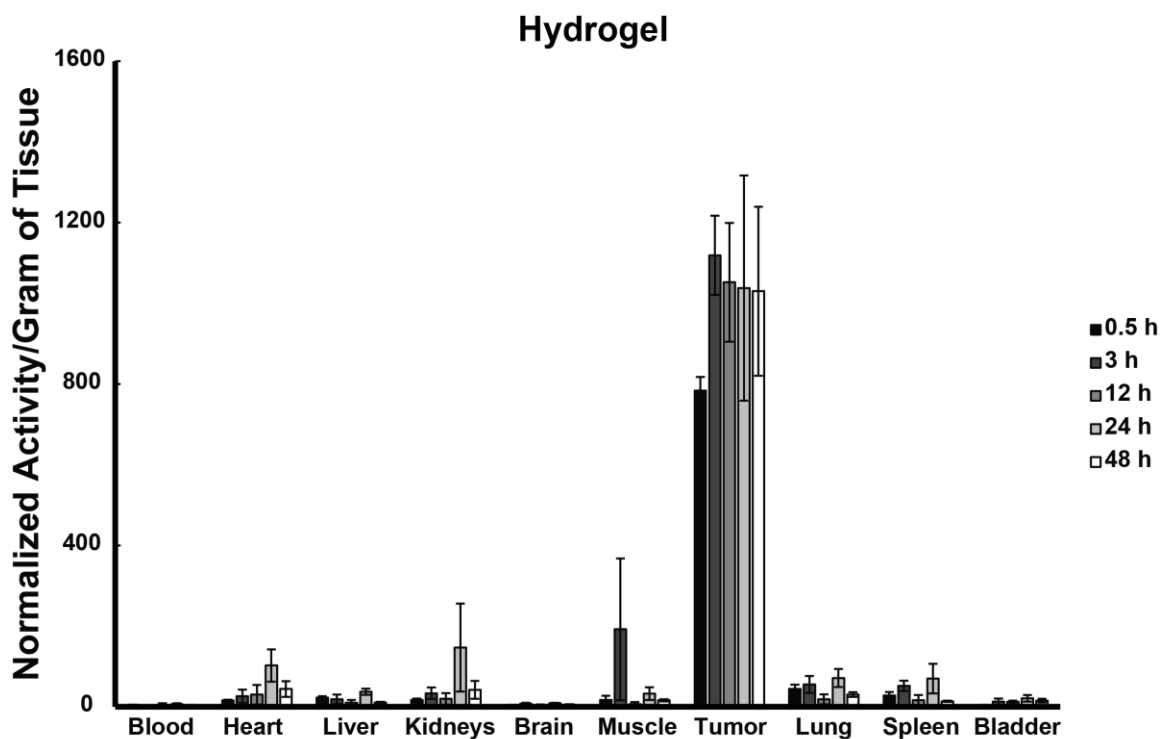


Figure II-26: TPP biodistribution following peritumoral administration via a thermosensitive hydrogel.

Mice bearing A375 melanoma tumors were administered 2.5 μCi of carbon-14 labeled 12-TPP peritumorally in a thermosensitive hydrogel. Animals were sacrificed 0.5 h, 3 h, 12 h, 24 h, or 48 h post-injection. Organs were harvested, dried, ground, and counted by liquid scintillation. Error bars represent standard error of the mean (N = 2 for each time point). Results demonstrate there was significant 12-TPP accumulation up to 48 h post-injection with minimal uptake in all other off-target organs analyzed. These findings support the use of a hydrogel delivery system for melanoma therapy.

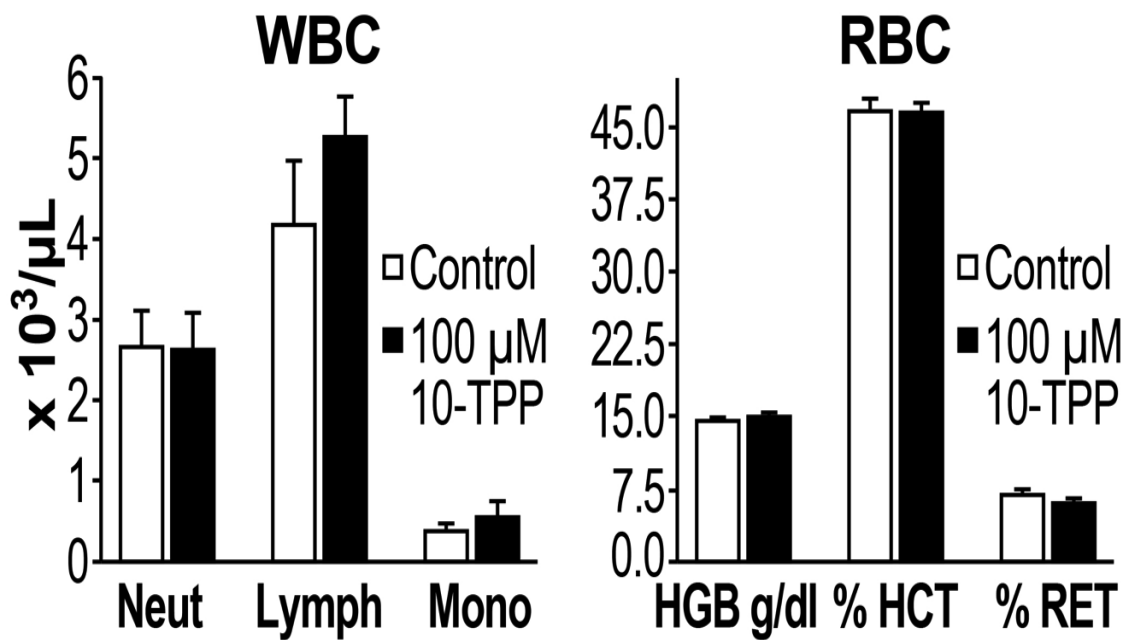


Figure II-27: TPP treatment does not cause bone marrow toxicity.

Mice were administered 100 μM 10-TPP via drinking water for 17 days (this administration route results in TPP accumulation in organs). Following treatment, animals were sacrificed and blood was drawn via cardiac puncture. White blood cell (WBC) counts and red blood cell (RBC) counts were determined by CBC analysis. Results indicate no significant differences in WBC parameters (HGB, HCT, RET) and RBC parameters (HGB, HCT, RET) between treatment and control mice. These results indicate that TPP treatment does not affect the bone marrow.

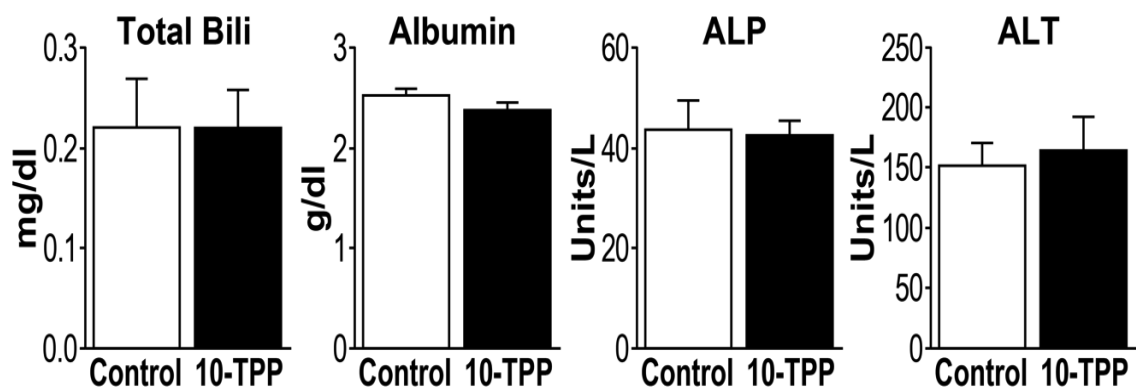


Figure II-28: TPP treatment does not cause liver toxicity.

Mice were administered 100 μ M 10-TPP via drinking water for 17 days (this administration route results in TPP accumulation in organs). Following treatment, animals were sacrificed and blood was drawn via cardiac puncture. Markers of liver function (Bili, albumin, ALP, ALT) were measured. There were no differences in bili, albumin, ALP, and ALT levels between treatment and control mice. These results indicate that TPP treatment does not cause liver toxicity.

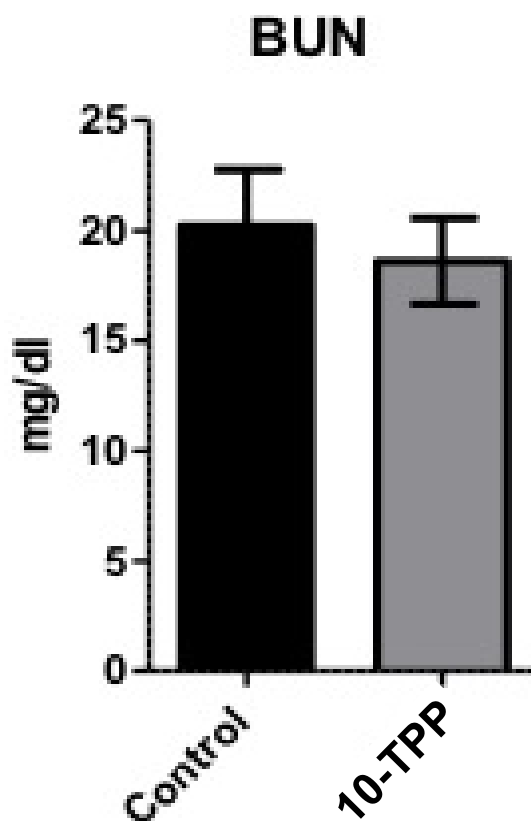


Figure II-29: TPP treatment does not affect blood urea nitrogen levels.

Mice were administered 100 μ M 10-TPP via drinking water for 17 days (this administration route results in TPP accumulation in organs). Following treatment, animals were sacrificed and blood was drawn via cardiac puncture. Blood urea nitrogen levels (BUN; an indicator of liver and kidney function) were measured. There were no differences in BUN levels between treatment and control mice. These results indicate that TPP treatment does not affect liver or kidney function.

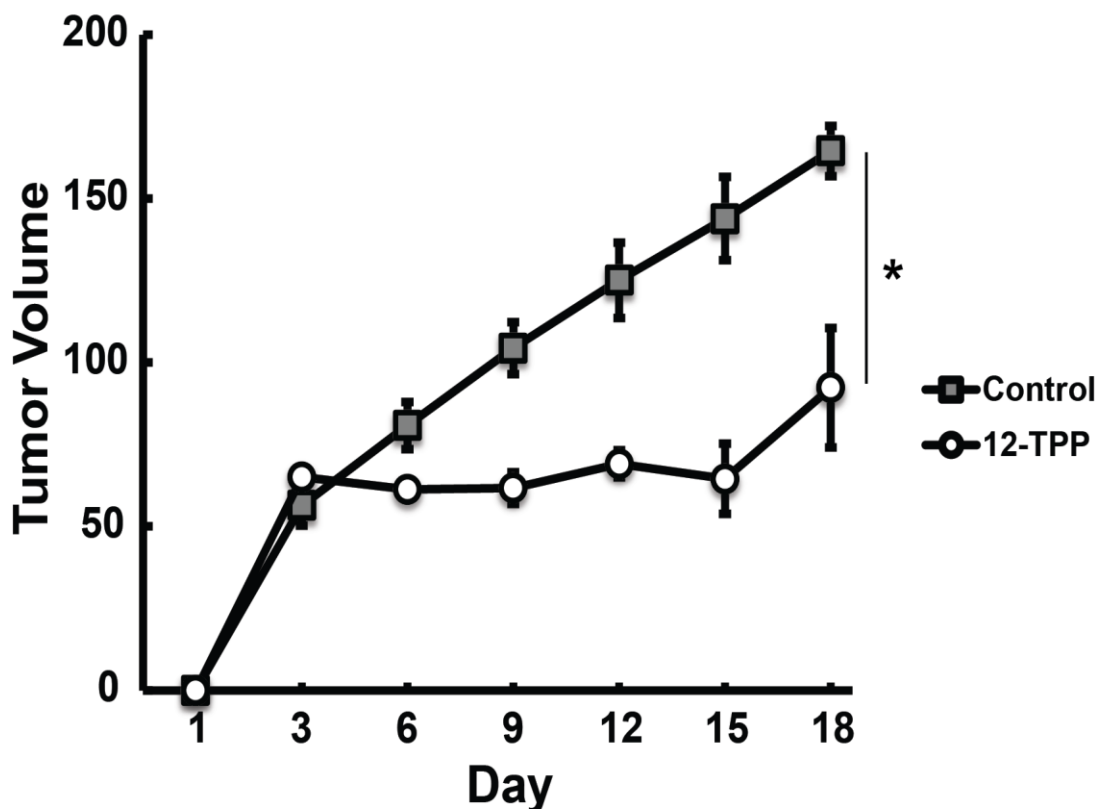


Figure II-30: TPP decreases melanoma tumor growth rate when administered via hydrogel.

Mice bearing A375 melanoma tumors were administered 10 μ M 12-TPP peritumorally via a hydrogel delivery system twice weekly for three weeks. Animal weight and tumor size were recorded twice weekly. Error bars represent standard error of the mean (N = 5 mice per group). Results show that 12-TPP administered peritumorally twice weekly significantly slowed A375 melanoma tumor growth weight compared to control mice. These results support the continued development of a TPP-hydrogel delivery system for the therapy of metastatic melanoma.

CHAPTER III: FUTURE DIRECTIONS – HYDROGEL-ADMINISTERED TPP BASED COMBINATION THERAPY FOR METASTATIC MELANOMA

Hypothesis and Specific Aims

Previous studies using a ^{14}C -12-TPP variant demonstrated that 12-TPP localizes to A375 melanoma tumors with minimal uptake in non-malignant tissues 48 h post injection when administered via a thermosensitive hydrogel delivery system. An efficacy study also demonstrated a significant delay in A375 tumor growth in mice treated for 3 weeks with 10 μM 12-TPP relative to untreated control mice. It is increasingly recognized that combination therapies versus single modalities result in more durable melanoma therapy due to the heterogeneity of melanoma tumors and melanoma therapeutic resistance [176-179]. Previous studies show that BSO and AUR enhance the sensitivity of melanoma tumors to TPP treatment. Importantly, a hydrogel delivery system can be loaded with many drugs with different targets and mechanisms of action that could potentially circumvent melanoma therapy resistance. Based on previous *in vivo* studies, the central hypothesis of future work is that an optimal concentration of TPP can be identified that results in the greatest reduction in melanoma tumor growth when delivered via hydrogel. Further, TPP can be combined with other chemotherapeutic drugs in order to enhance the sensitivity of melanoma tumors to TPP treatment.

Aim 1: Determine the concentration of TPP that can be delivered to melanoma tumors via hydrogel that results in the greatest reduction in melanoma tumor growth rate without systemic toxicity.

Aim 2: Identify TPP-based combination therapies that can be delivered via hydrogel that further slow melanoma tumor growth compared to TPP alone without causing systemic toxicity.

Significance

Melanoma is the most aggressive and lethal form of skin cancer [36, 180-183]. A major underlying reason for poor prognosis is that despite advances in chemotherapeutic, biological, and targeted therapies, durable treatments for metastatic melanoma remain elusive due to the resistance of melanoma tumors to therapy highlighting the need for novel treatment strategies [41, 176, 183, 184]. Previous studies demonstrate that TPP disrupts melanoma cell mitochondria metabolism, can be effectively delivered to melanoma tumors versus non-malignant tissues via hydrogel, and can slow melanoma tumor growth. Further, no current FDA approved drugs for melanoma target cellular metabolism. Since metabolism is essential for cell survival, a therapy that targets metabolism could circumvent melanoma resistance. Also, much melanoma research today focuses on combination therapies to improve therapeutic outcome for patients due to the heterogeneity of melanoma tumors and therapy resistance. The approach presented here allows for the use of many drugs with

different mechanisms of action that target multiple pathways as a way to combat melanoma resistance and improve prognosis for melanoma patients.

Aim 1

Background and Rationale

Previous biodistribution studies utilizing a ^{14}C -12-TPP demonstrated that a hydrogel delivery system effectively delivered 12-TPP to the tumor site with minimal uptake in non-malignant organs. These studies also showed that 12-TPP administered via I.P., I.V., and oral routes did not result in significant tumor accumulation relative to non-malignant organs. Further, a previous efficacy study showed that 10 μM 12-TPP significantly delayed A375 tumor growth when administered to mice peritumorally via hydrogel for three weeks. It remains unknown what maximum concentration of TPP can be administered via hydrogel to melanoma tumors without off-target toxicity that results in the greatest reduction in melanoma tumor growth. Collectively, biodistribution and efficacy studies support the continued development of a TPP-hydrogel system for the therapy of metastatic melanoma.

Experimental Design

Efficacy studies were performed with 10 μ M 12-TPP for three weeks. This dose appeared to be well tolerated by mice and mice maintained body weight throughout the course of the study. For future studies, mice (n = 6 per group) bearing A375 melanoma tumors will be injected with 20-100 μ M 12-TPP peritumorally in hydrogel. TPP will be administered twice weekly immediately after tumors are 5 x 5 mm in size. Tumor growth will be measured daily. Animals will be weighed daily and if mice lose >10 % of their body weight dosing will be adjusted accordingly. Mice will be sacrificed when tumors reach 1.5 cm in any direction. Following the completion of treatment and animal euthanasia, organs will be harvested and processed accordingly for pathological analysis. Blood will be collected and analyzed for liver, kidney, heart, bone marrow, and lung toxicity.

Anticipated Results

Results are expected to provide the dose of 12-TPP that leads to the greatest reduction in melanoma tumor growth while minimizing off-target toxicity in non-malignant tissues. Results will also provide insight into which non-malignant tissues are potentially affected by long term TPP treatment and allow for the development of new strategies that can minimize these off target effects.

Alternative Approach

If 12-TPP administered to mice bearing melanoma tumors peritumorally via hydrogel does not slow melanoma tumor growth rate for an extended period of time, alternative hydrogel formulations can be explored. Hydrogels can be designed to be more fluid or gel like. They can be designed to release TPP rapidly or more slowly depending on the formulation. This can allow for rapid TPP tumor accumulation or slow TPP tumor accumulation that can have an impact on melanoma tumor growth rate or potential off target effects in non-malignant tissue.

Aim 2

Background and Rationale

In vitro studies demonstrated that TPP disrupts melanoma mitochondria metabolism and results in increased ROS and decreased intracellular GSH that is essential for important cellular processes, maintaining cellular redox potential, and scavenging ROS species thereby protecting cells from cytotoxic oxidative stress. Additional studies utilizing the GSH inhibitor BSO and TRxR inhibitor AUR demonstrated that BSO and AUR enhance the sensitivity of melanoma cells to TPP treatment. Further, *in vivo* studies demonstrated that a TPP hydrogel delivery system is capable of delivering TPP directly at the tumor site and results

in delayed melanoma tumor growth. Importantly, hydrogels can be loaded with multiple drug combinations in order to target different pathways in order to induce melanoma cell cytotoxicity and potentially circumvent melanoma cell resistance.

Experimental Design

Mice bearing A375 melanoma tumors (n = 6 per group) will be injected peritumorally with hydrogel containing the concentration of 12-TPP found to best delay melanoma tumor growth while sparing non-malignant tissues identified under Aim 1. The hydrogel will also be loaded with BSO (100 μ M), AUR (5 μ M), and BSO and AUR both [83]. TPP will be administered twice weekly immediately after tumors are 5 x 5 mm in size. Tumor growth will be measured daily.

Animals will be weighed daily and if mice lose >10 % of their body weight dosing will be adjusted accordingly. Mice will be sacrificed when tumors reach 1.5 cm in any direction. Following the completion of treatment and euthanasia, mice will be sacrificed and organs will be harvested and processed accordingly for pathological analysis. Blood will be collected and analyzed for liver, kidney, heart, bone marrow, and lung toxicity.

Anticipated Results

Results are expected to demonstrate that inclusion of BSO or AUR in the TPP hydrogel formulation will significantly decrease melanoma tumor growth rate

compared to single agent TPP. A triple combination therapy with TPP, BSO, and AUR will result in the greatest reductions in melanoma tumor growth. Further, these studies will provide insight into potential off-target toxicity with these combination therapies for future experimental design.

Alternative Approach

A combination therapy could result in more systemic toxicity compared to single agent TPP. If combination therapies are not well tolerated by mice, the dose will be adjusted accordingly for future studies. If BSO and AUR combination therapies ultimately prove too toxic or do not affect melanoma tumor growth rate, a hydrogel containing TPP and a physiological relevant dose of mutant BRAF inhibitor vemurafenib (20 μ M) will be administered peritumorally in mice bearing BRAF A375 melanoma tumors [185, 186]. Interestingly, emerging evidence demonstrates that vemurafenib causes a shift from glycolysis to oxidative phosphorylation in melanoma cells [42, 50, 187-189]. This could potentially enhance the uptake of TPP into melanoma cell mitochondria and increase the cytotoxic effects of TPP in melanoma cells. A study was performed to determine if melanoma cells treated with vemurafenib for 5 or 60 days are more sensitive to TPP treatment compared to TPP treatment alone. In this study, BRAF mutant A375 melanoma cells were treated with 5-16 TPP for 24 h in cells not treated with vemurafenib and in A375 cells treated with 5 μ M vemurafenib for five days and sixty days (**Figure III-1**). Results demonstrate that

cells treated for 5 days with vemurafenib and TPP for 24 h exhibit no significant differences in clonogenic survival (taking into account the decrease in clonogenic survival attributed to vemurafenib alone). Results did show a significant decrease in clonogenic survival in cells treated with TPP plus 60 day vemurafenib compared to TPP alone. These results support that cells treated with vemurafenib for an extended period of time do have increased sensitivity to TPP treatment and provide rationale for a TPP and vemurafenib combination therapy.

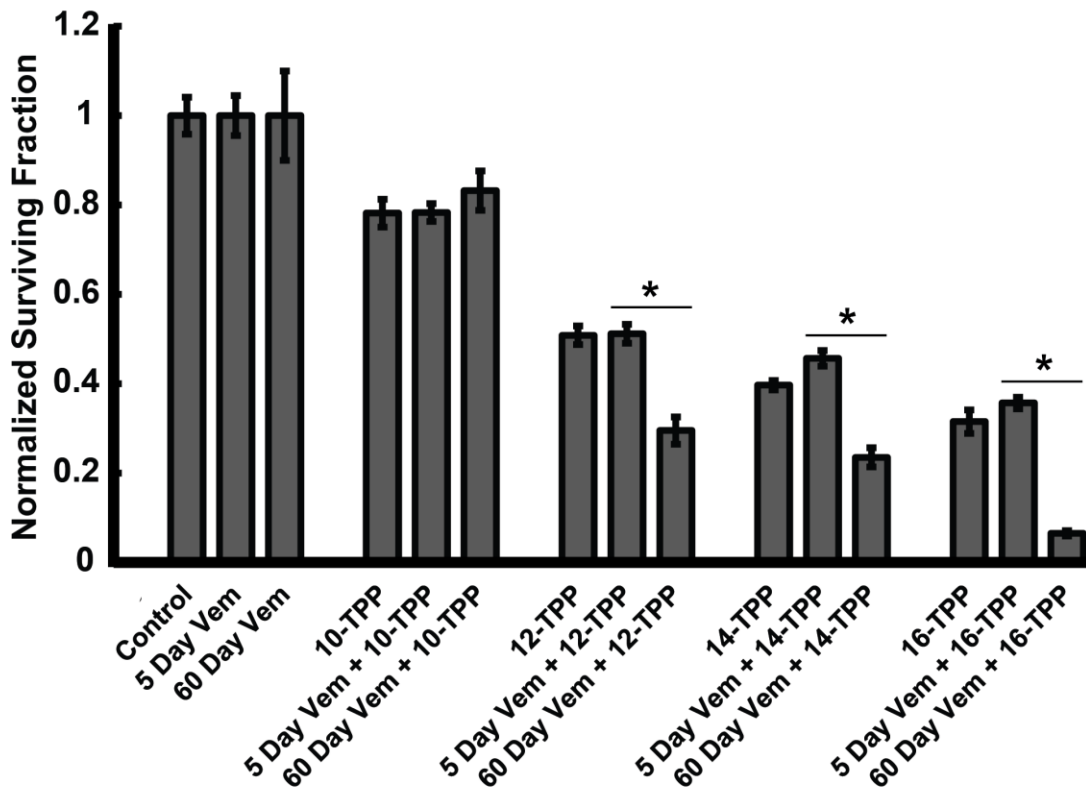


Figure III-1: Vemurafenib enhances the sensitivity of BRAF mutant melanoma cells to TPP treatment.

BRAF mutant A375 melanoma cells were treated with 5.0 μM of the BRAF inhibitor Vemurafenib (Vem) for five and sixty days. Cells were then treated with 0.5 μM 10-16 TPP for 24 h. Following treatment, cells were analyzed for clonogenic survival. Error bars represent the standard error of the mean (* significant relative to the same drug treatment between 5 and 60 day Vem, $p < 0.05$, $n = 3$ from 2 separate experiments; $N = 6$). Results demonstrate that there is no difference in clonogenic survival between TPP alone and TPP plus five day Vem treatment (taking into account the decrease in clonogenic survival attributed to Vem alone). Cells treated for sixty days with Vem and then for 24 h with TPP did show enhanced sensitivity to TPP treatment compared to TPP alone. These results support the development of a TPP and Vem combination therapy.

APPENDIX A: SUPPLEMENTARY DATA

Overview

Previous data demonstrate that TPP compounds modified with linear side chains disrupt mitochondria oxidative metabolism, increase DHE oxidation, decrease intracellular GSH and ATP, and lead to cytotoxicity in melanoma cells. Further, the TPP side chain is the reactive part of TPP derivatives responsible for these effects. Studies were also performed to understand the growth properties of melanoma cells. Experiments designed to support that the TPP side chain is the reactive part of TPP derivatives that induces melanoma cytotoxicity were also performed. In order to support that TPP derivatives disrupt the ETC and inhibit ATP-linked oxygen consumption, studies to determine specific ETC complexes affected by TPP treatment were conducted. In addition to mitochondria oxidative metabolism, studies were also performed to evaluate how TPP treatment affects melanoma cell glucose uptake and glycolytic activity. Finally, a metabolic gene array was performed to determine how TPP treatment affects the expression of genes associated with glycolysis, the TCA, and oxidative phosphorylation.

Consistent with previous findings, results demonstrate that a TPP derivative modified with a linear side chain decreases melanoma cell clonogenic survival, whereas a TPP derivative without a side chain does not. Also consistent with previous findings, a 10-TPP compound inhibits ETC activity, specifically at complexes I and III. Interestingly, metabolic flux analysis

demonstrates that in addition to ETC inhibition, 12-TPP treatment causes an increase in glycolytic activity and increases melanoma cell glucose uptake. Lastly, metabolic gene array data demonstrates that 12-TPP decreases the expression of multiple genes associated with glycolysis, the TCA, and oxidative phosphorylation following 24 h treatment. Collectively, these results support that TPP derivatives alter melanoma cell metabolism and the TPP side chain is responsible for these effects.

Materials and methods

Cell Culture

A375 human melanoma cells were obtained from American Type Culture Collection (catalog no. CRL-1619; Manassas, VA). MDA-MB-231 human breast cancer cells were compliments of Dr. Douglas Spitz at the University of Iowa. A375 cells were cultured in DMEM (Gibco, Life Technologies, Carlsbad, CA) containing 10% fetal bovine serum (Gibco) and 1% penicillin/streptomycin (Gibco). MDA-MB-231 cells were cultured in RPMI media supplemented with 10% FBS and 1% penicillin/streptomycin. Cells were maintained at 37 °C in a humidified 5% CO₂ incubator and detached with 0.25% trypsin-EDTA (Gibco). Experiments were performed with cells at or below passage twenty.

Chemicals and Reagents

The structures of the compounds used for experiments in Appendix A can be found in **Figure A-1**. Azide-TPP and bis-TPP were synthesized in house at the University of Iowa. 10-TPP and 12-TPP were purchased from Alpha Aesar (Ward Hill, MA).

Cell Growth Curves

A375 and MeWo human melanoma cells were plated in 60 mm tissue culture dishes at a density of 150,000 cells/dish. Cells were then trypsinized and counted daily for 6-7 days. Cells were counted using a Beckman Z1 particle counter (Beckman Coulter, Fullerton, CA). The cell population doubling time (T_d) was calculated from the exponential portion of the growth curve using the equation $T_d = (0.693 * t) / (\ln(N_t / N_0))$, where t is time in days, N_t is the cell number at time t , and N_0 is the initial cell number.

Clonogenic Cell Survival Assay

MDA-MB-231 cells were plated in 60 mm tissue culture dishes at a density of 125,000 cells/dish and incubated for 48 h. Cells were then treated with 0.25-2.0 μ M TPP for 24 h. Following drug treatment, cells were trypsinized and plated at a density of 500 cells/dish and incubated for 2 weeks. Colonies were then fixed with 70% ethanol, stained with Coomassie blue G250 (Sigma) in 45% methanol and 10% acetic acid, and counted. Only colonies ≥ 50 cells were

counted. Surviving fraction (SF) was calculated using the following formula: SF = (number of colonies counted)/(number of cells seeded x plating efficiency).

Metabolic Flux Measurements

A375 cells were plated in a 96 well XF96 cell culture plate at a density of 10,000 cells/well for 48 h. Media was then replaced with Seahorse MEM media (pH 7.4) supplemented with 25 mM glucose and 1.0 mM sodium pyruvate. The extracellular acidification rate (ECAR) measured using a Seahorse Bioscience XF96 extracellular flux analyzer (Seahorse Bioscience). Measurements were made every 10 min over the course of 1.5 h. At the 20 min mark, 1.0 μ M 12-TPP was added to treatment cells only followed by the sequential addition of oligomycin (2.5 μ M; Sigma) at the 55 min mark, FCCP (0.3 μ M; Sigma) at the 85 min mark, and antimycin A/rotenone (5 μ M; Sigma) at the 115 min mark in both control and treatment cells.

Enrichment of Mouse Liver Mitochondria

Livers were harvested from mice and placed in cold homogenizing medium [0.25 M sucrose, 5 mM hepes, 0.1 mM EDTA, 0.1% fatty acid free bovine serum albumin (BSA); pH 7.25]. Samples were homogenized on ice using a glass dounce homogenizer and centrifuged at 1000 x g for 10 min at 4 °C. Supernatants were transferred to high-speed centrifuge tubes, while pellets

were resuspended in cold homogenizing medium and reprocessed as described above. Supernatants were centrifuged at 10,000 x g for 10 min at 4 °C. Supernatants were discarded and mitochondrial fractions were resuspended in cold potassium phosphate buffer (pH 7.25).

Electron Transport Chain Complex Activity Assays

All assays were performed as previously described at 30 °C in a 1.0 mL total volume using a Beckman Coulter DU 800 Spectrophotometer [190, 191]. The mitochondrial samples receiving treatment were incubated for 10 min in a high concentration of 10-TPP (500 µM to simulate the concentration of the compound in active, respiring mitochondria); however, the final 10-TPP concentration in all complex activity assays was approximately 10 µM following sample dilution after the initial incubation. Total protein content was determined by Bradford assay (Biorad) and all electron transport chain enzyme activities were normalized to the total protein content [192].

The complex I activity assay measured the rate of absorbance change due to rotenone-inhibitable NADH oxidation ($\epsilon=6.81 \text{ mM}^{-1} \text{ cm}^{-1}$). Mitochondria (resuspended in 20 mM potassium phosphate buffer; pH 7.0) were lysed due to freeze thawing and divided into four samples. Sample one contained complex I working buffer [25 mM potassium phosphate buffer (pH 7.2), 5 mM magnesium chloride, 2 mM potassium cyanide, 2.5 mg/mL BSA, 0.13 mM NADH], antimycin A (200 µg/mL), coenzyme Q₁ (7.5 mM), and mitochondria (0.37 µg/µL). Sample

two contained complex I working buffer, antimycin A, coenzyme Q₁, rotenone (200 µg/mL), and mitochondria (0.37 µg/µL). Sample three contained complex I working buffer, antimycin A, coenzyme Q₁, 10-TPP, and mitochondria (0.36 µg/µL). Sample 4 contained complex I working buffer, antimycin A, coenzyme Q₁, rotenone, 10-TPP, and mitochondria (0.36 µg/µL). Samples were mixed and incubated for 1 min at 30 °C. Absorbance was read every 20 s for 3 min at 30 °C and the rate of absorbance change at 340 nm (reference wavelength = 425 nm) was measured. Activity was calculated using the following formula: $(\Delta\text{Abs}_{340} - \Delta\text{Abs}_{340 \text{ Rot}})/6.81/\text{mg protein} = \mu\text{mol}/\text{min}/\text{mg protein}$.

The Complex II activity assay measured the rate of absorbance change due to the reduction of 2,6-dichloroindophenol (DCIP; $\epsilon=19.1 \text{ mM}^{-1} \text{ cm}^{-1}$) by coenzyme Q in the presence and absence of succinate. Mitochondria (resuspended in 20 mM potassium phosphate buffer; pH 7.0) were lysed due to freeze thawing and divided into four samples. Sample one contained complex II working buffer [25 mM potassium phosphate buffer (pH 7.2), 5 mM magnesium chloride, 2 mM potassium cyanide, 2.5 mg/mL BSA], 25 mM potassium phosphate buffer, and mitochondria (0.37 µg/µL). Sample two contained complex II working buffer, 0.2 M succinate, and mitochondria (0.37 µg/µL). Sample three contained complex II working buffer, 25 mM potassium phosphate buffer, 10-TPP, and mitochondria (0.36 µg/µL). Sample four contained complex II working buffer, succinate, 10-TPP, and mitochondria (0.36 µg/µL). Samples were mixed and incubated for 10 min at 30 °C. Following incubation, antimycin A (200 µg/mL), rotenone (200 µg/mL), 5 mM DCIP, and 7.5 mM coenzyme Q₁ were

added to each cuvette and incubated for 1 min. The absorbance was read every 20 s for 3 min at 30 °C and the rate of absorbance change at 600 nm was measured. Activity was calculated using the following formula: $(\Delta\text{Abs}_{600 \text{ Succinate}} - \Delta\text{Abs}_{600 \text{ No Succinate}})/19.1/\text{mg protein} = \mu\text{mol}/\text{min}/\text{mg protein}$.

The complex III activity assay measured the rate of absorbance change due to cytochrome c reduction ($\epsilon=19.6 \text{ mM}^{-1} \text{ cm}^{-1}$) by coenzyme Q₂. Coenzyme Q₂ was reduced by adding 1 N HCl and potassium borohydride to 35 mM coenzyme Q₂ until the reaction mixture turned from bright yellow to clear. The clear solution was transferred to a new tube and HCl was added to keep coenzyme Q₂ reduced. Fresh mitochondria (resuspended in 20 mM potassium phosphate buffer; pH 7.0) were divided into four samples. Sample one contained complex III working buffer [25 mM potassium phosphate buffer (pH 7.2), 5 mM magnesium chloride, 2 mM potassium cyanide, 2.5 mg/ml BSA, 0.5 mM n-dodecyl β -maltoside], rotenone (200 $\mu\text{g}/\text{mL}$), 1.5 mM cytochrome c, and 3.5 mM coenzyme Q₂. Sample two contained complex III working buffer, rotenone, cytochrome c, coenzyme Q₂, and mitochondria (2.97 $\mu\text{g}/\mu\text{L}$). Sample three contained complex III working buffer, rotenone, cytochrome c, coenzyme Q₂, and 10-TPP. Sample four contained complex III working buffer, rotenone, cytochrome c, coenzyme Q₂, 10-TPP, and mitochondria (2.84 $\mu\text{g}/\mu\text{L}$). Samples were mixed and absorbance was read every 5 s for 1 min at 30 °C and the rate of absorbance change at 550 nm (reference wavelength = 580 nm) was measured. Activity was calculated using the following formula: $(\Delta\text{Abs}_{550\text{mit}} - \Delta\text{Abs}_{550})/19.6/\text{mg protein} = \mu\text{mol}/\text{min}/\text{mg protein}$.

The complex IV activity assay measured the rate of cytochrome c oxidation ($\epsilon=19.6 \text{ mM}^{-1} \text{ cm}^{-1}$). Cytochrome c was reduced by adding 0.1 M dithiothreitol to cytochrome c. The reaction mixture was incubated on ice for 15 min until the reaction color changed from dark red to orange red. Mitochondria (resuspended in 20 mM potassium phosphate buffer; pH 7.0) were lysed due to freeze thawing and divided into two samples. Sample one contained complex IV working buffer [20 mM potassium phosphate buffer (pH 7.0), 0.5 mM n-dodecyl β -maltoside, 1.5 mM reduced cytochrome c, and mitochondria (0.37 $\mu\text{g}/\mu\text{L}$)]. Sample two contained complex IV working buffer, reduced cytochrome c, 10-TPP, and mitochondria (0.36 $\mu\text{g}/\mu\text{L}$). Absorbance was read every 20 s for 2 min at 30 °C and the rate of absorbance change at 550 nm (reference wavelength = 580 nm) was measured. Activity was calculated using the following formula: $\Delta\text{Abs}_{550}/19.6/\text{mg protein} = \mu\text{mol}/\text{min}/\text{mg protein}$.

Glucose Uptake Measurements

A375 cells were plated in 60 mm tissue culture dishes at a density of 150,000 cells/dish and incubated for 48 h. Cells were then treated with 1.0 μM TPP for 1 h. Following treatment, cells were washed twice with low glucose DMEM. Cells were then incubated with low glucose DMEM containing 20 μM 2-deoxy-2-[(7-nitro-2,1,3-benzoxadiazol-4-yl)amino]-D-glucose (2-NBDG; Life Technologies) for 2 h. Following incubation, cells were washed twice with PBS, trypsinized, and analyzed using a Becton Dickinson LSR UV flow cytometer at

540 nm. Data from 10,000 events were collected and mean fluorescence intensity was analyzed using Flowjo software. Background fluorescence was corrected to the auto-fluorescence of unlabeled cells.

Metabolic Gene Array

A375 cells were plated in 60 mm tissue culture dishes at a density of 150,000 cells/dish and incubated for 48 h. Cells were treated with 1.0 μ M TPP for 24 h. Cells were then pelleted and total RNA was isolated using a PerfectPure RNA purification kit (5 Prime). RNA concentration and purity was measured with a nonospectrophotometer (Implen, Westlake Village, CA). Isolated RNA was reversed transcribed into cDNA with a high capacity cDNA reverse transcription kit (Applied Biosystems). The products of the cDNA reaction were loaded into a metabolic gene array containing primers for 26 genes associated with glycolysis, TCA, or oxidative phosphorylation synthesized by Dr. Ehab Sarsour, University of Iowa. A reverse transcriptase-polymerase chain reaction (PCR) reaction was performed using Power SYBR[®] Green PCR Master Mix (Applied Biosystems) and a StepOnePlus[™] system. Primer sequence information for the metabolic genes analyzed can be found in **Table II-1**.

Statistical Analysis

Statistical significance for *in vitro* studies with more than three groups was determined using one-way analysis of variance (ANOVA) with post hoc analyses

using the Tukey's honestly significant difference test for multiple comparisons. Statistical significance for *in vitro* studies with less than three groups was done using a Student's t test. Homogeneity of variance was assumed at 95 % confidence interval. Results with $p < 0.05$ were considered significant. Statistical analysis was performed using SPSS Statistics Version 21 (IBM).

Table A-1: The PCR primers used in this study.

Gene (Home Sapien)	Gene Bank No.	Sequence (5' → 3')		Amplicon size (bp)
18S	NM_001101.3	Forward:	TCACCATTGGCAATGAGCGGTT	89
		Reverse:	AGTTTCGTGGATGCCACAGGACT	
beta-actin	NM_001101.3	Forward:	TCACCATTGGCAATGAGCGGTT	89
		Reverse:	AGTTTCGTGGATGCCACAGGACT	
G6PD	NM_000402.3	Forward:	CCCGGAAACGGTCGTACACT	72
		Reverse:	CATGACGCTGTCTGCGCTTC	
PKM1	NM_182471.2	Forward:	CAGCACCTGATAGCTCGTGA	76
		Reverse:	TTGAGGCTCGCACAAGTTCT	
PKM2	NM_002654.4	Forward:	GGTTTCGGAGGTTTGATG	415
		Reverse:	ACGGCCGTGGCTTCTGT	
HK2	NM_000189.4	Forward:	TTGAGAGCACCTGTGACGAC	156
		Reverse:	CCACACCCACTGTCACTTTG	
HK3	NM_002115.2	Forward:	TGCTGAGAGATGCCATTCCGG	138
		Reverse:	TGCCCGTGTCTACAAC TAGC	
PFK1	NM_001166686.1	Forward:	TCCGACACAGTCTCCTGGAC	187
		Reverse:	GCTGCCTCCTAGCGACTCTT	
PDHB	NM_000925.1	Forward:	CTCCGGAAGCTCAGTCAA	130
		Reverse:	AGCACTGCTGCAGCTTCTAA	
SDHA	NM_004168.2	Forward:	TTGATGCAGTGGTGGTAGGC	139
		Reverse:	TTGATTCCTCCCTGTGCTGC	
SDHB	NM_003000.2	Forward:	GCAGCAGTATCTGCAGTCCA	153
		Reverse:	CAGCGATAGGCCTGCATAAGA	
SDHC	NM_003001.3	Forward:	GGAACCACGGCCAAAGAAGA	159
		Reverse:	AGAGACCCCTGCACTCAAAG	
SDHD	NM_003002.3	Forward:	ATACACTTGTACCCGAGCCAC	177
		Reverse:	AAGGCCCCAGTGACCATGAAG	
ACO2	NM_001098.2	Forward:	TGACTCGGCTGCAGAAAGCTC	100
		Reverse:	TCGTTGGGCTCAAAGTGCC	
ACO1	NM_001278352.1	Forward:	CCTGGAGTGTGGTAGGAACA	188
		Reverse:	CACAATTCCGAATGGCTGCTT	
PGC-1 α	NM_013261.3	Forward:	GCATGAGTGTGTGCTCTGT	133
		Reverse:	CAGCACTCGATGTCACTC	
PGC-1 β	NM_133263.3	Forward:	CTATCTCGCTGACACGCAGG	200
		Reverse:	TGTCAATCTGGAAGAGCTCGG	
NRF-1	NM_005011.3	Forward:	AGCCGCTCTGAGAACTTCAT	153
		Reverse:	AGGCGAGTCTTCATCAGCAC	
NRF-2	NM_006164.4	Forward:	GTCCCAGCAGGACATGGATT	107
		Reverse:	GTCATACTCTTTCCGTGCG	
TFAM	NM_003201.2	Forward:	CCAAAAAGACCTCGTTCAGCTT	87
		Reverse:	CTTCAGCTTTTCTGCGGTG	
COX5A	NM_004255.3	Forward:	AAGGACAAAGCAGGACCTCA	133
		Reverse:	AGCCCATCCATGCGGTTTAC	
ATP5g1	NM_005175.2	Forward:	CAGGGGTTGCAGGGTAGTAG	92
		Reverse:	TGGTACAACAGCGGATCAGAG	
Cyt C	NM_018947.5	Forward:	CCGTTGAAAAGGGAGGCAAG	123
		Reverse:	CCCAGATGATGCCTTTGTTCT	
NDUFS3	NM_004551.2	Forward:	AGTTCAGGTGTCCTGCTTCA	131
		Reverse:	CGTCCACTGCTGTCAAGTCA	
COX4	NM_001861.3	Forward:	GGAGTCTTCTCGATCCCGT	109
		Reverse:	CAACATTCTGCCGCCACTG	

Results

Melanoma Cell Growth Curves

In order to generate cellular growth curves and to calculate the population doubling time of A375 and MeWo human melanoma cells, A375 and MeWo cells were plated in 60 mm tissue culture dishes at a density of 150,000 cells/dish. Cells were then trypsinized and counted daily for 6-7 days (**Figures A-2 and A-3**). Results demonstrate that A375 cells have a population doubling time of 24 h, while MeWo cells have a population doubling time of 34 h.

TPP Linear Side Chains Induce Cytotoxicity

Data suggest that TPP derivatives modified with side chains embed in the mitochondria inner membrane, disrupt mitochondria metabolism, and induce cytotoxicity in cancer cells. Studies were performed to determine whether the mitochondria targeting TPP moiety or TPP side chain cause disruption in cancer cell metabolism and survival. Clonogenic survival assays were conducted in MDA-MB-231 human breast cancer cells using two TPP derivatives. The first TPP derivative was comprised of a TPP moiety connected to an azide functional group through a ten-carbon linker (azide-TPP). The second molecule studied was comprised of a TPP moiety connected to a second TPP moiety through a ten-carbon linker (bis-TPP). Cells were treated with 0.5 μ M, 1.0 μ M, or 2.0 μ M azide-TPP or bis-TPP for 24 h. Results demonstrate that bis-TPP had no effect

on MDA-MB-231 clonogenic survival at all concentrations tested (**Figure A-4**). Azide-TPP resulted in a ~40% decrease in clonogenic survival at a 0.5 μM concentration. Cells treated with 1.0 μM azide-TPP exhibited ~20% clonogenic survival and cells treated with 2.0 μM azide-TPP exhibited <10% clonogenic survival. These results provide strong support that the TPP side chain is the reactive part of TPP derivatives that inserts into the inner mitochondria membrane and induces cytotoxicity in breast cancer cells.

TPP Decreases Mitochondria Electron Transport Chain Complex Activity

Oxygen consumption studies demonstrate that TPP derivatives disrupt ATP-linked oxygen consumption in melanoma cells and suggest that specific ETC complexes can be identified as the site of the inhibitory mechanism. In order to gain a more detailed understanding of TPP ETC complex interactions, the activity of ETC complexes I-IV was measured in isolated mouse liver mitochondria to determine specifically where TPP derivatives inhibit oxidative phosphorylation (**Figure A-5**) [190, 191, 193]. Active respiring mitochondria receiving treatment were incubated for 10 min with 10 μM 10-TPP. The complex I activity assay measured the rate of absorbance change due to rotenone-inhibitable NADH oxidation. The Complex II activity assay measured the rate of absorbance change due to the reduction of DCIP by coenzyme Q in the presence and absence of succinate. The complex III activity assay measured the rate of absorbance change due to cytochrome C reduction by coenzyme Q₂,

while the complex IV activity assay measured the rate of cytochrome C oxidation. Results demonstrate that 10-TPP strongly inhibits complex I activity and significantly decreases complex III activity, while complex II and IV activity appears to be largely unaffected. These results provide support for metabolic flux results that TPP compounds act as inhibitors of oxidative phosphorylation via inhibition of specific ETC complexes.

TPP Increases Melanoma Cell Glycolytic Activity

Previous experiments demonstrate that TPP compounds decrease melanoma cell mitochondria ATP-linked oxygen consumption and inhibit the activity of ETC complexes I and III. In order to determine if the TPP-induced decreases in ATP-linked oxygen consumption forces melanoma cells into glycolysis as a compensatory mechanism for ETC inhibition, extracellular acidification rates (ECAR) via lactate production was measured as an indicator of glycolytic activity. For these experiments, A375 human melanoma cells were treated with or without 12-TPP (1.0 μM) followed by the sequential addition of oligomycin, FCCP, and antimycin A/rotenone. Changes in glycolytic activity in the presence of 12-TPP and subsequent addition of oligomycin, FCCP, and antimycin A/rotenone were analyzed (**Figure A-6**). Following addition of 12-TPP, there was an increase in the ECAR due to lactate production in treated cells compared to untreated cells. This argues that 12-TPP is inhibiting the ETC as observed in the OCR measurements and forcing cells into glycolysis in order to

compensate for the decrease in ATP-linked oxygen consumption. The addition of oligomycin resulted in an increase in glycolysis in untreated cells in order to compensate for the decrease in ATP-linked oxygen consumption and subsequent ATP synthesis. Cells treated with 12-TPP did not exhibit increases in glycolytic rate following addition of oligomycin. No changes in ECAR were observed in both treated and untreated cells when FCCP and antimycin A/rotenone were added either. These results demonstrate that TPP disrupts mitochondria metabolism via ETC inhibition (specifically ATP-linked oxygen consumption) and force cells into glycolysis as a compensatory mechanism for decreased ATP-linked oxygen consumption.

TPP Increases Melanoma Cell Glucose Uptake

Metabolic flux experiments demonstrated that a 12-TPP compound inhibited oxygen consumption and increased the glycolytic rate in melanoma cells. To determine how A375 melanoma cell glucose uptake changes following treatment with 12-TPP, a fluorescent 2-NBDG glucose analog was utilized. For this experiment, A375 cells were treated with 1.0 μM 12-TPP for 1 h. Following treatment, cells were incubated with 20 μM 2-NBDG for 2 h and analyzed by flow cytometry (**Figure A-7**). Results demonstrate that cells treated with 12-TPP increased glucose uptake by ~ 40% compared to untreated control cells. These results support that 12-TPP inhibits the ETC and forces cells into glycolysis as a compensatory mechanism for decreased ATP-linked oxygen consumption.

TPP Decreases Melanoma Cell Metabolic Gene Expression

Metabolic flux analysis demonstrated that 12-TPP decreases ETC activity and specifically inhibits ATP-linked oxygen consumption in melanoma cells immediately upon addition to cells. Further, 12-TPP treatment forced cells into glycolysis presumably to compensate for decreased ETC activity. In order to determine how a longer TPP treatment affects the expression of genes associated with glycolysis, the TCA, and oxidative phosphorylation, a metabolic gene array was performed. For this experiment, A375 human melanoma cells were treated for 24 h with 1.0 μ M 12-TPP. Following treatment, RNA was isolated and used to generate cDNA. Products of the cDNA reaction were then loaded into a gene array containing 26 primers for genes associated with glycolysis, TCA, or oxidative phosphorylation. Results demonstrated that six genes (GLUT4, G6PD, PFK1, PKM2, PKM1, and LDHA) associated with glycolysis exhibited a >2 fold decreases in gene expression compared to untreated cells (**Figure A-8**). Two genes associated with the TCA were also found to have decreased expression compared to control cells (PDHB and ACO2). Lastly, three genes associated with oxidative phosphorylation (NDUFS3, SDHB, and ATP5 β) had decreased expression compared to control cells. These results demonstrate that expression of genes associated with glycolysis, TCA, and ETC are decreased following 24 h treatment with 1.0 μ M 12-TPP and support that TPP disrupts mitochondria metabolism which eventually results in

decreased glycolysis and cytotoxicity in melanoma cells following a 24 h treatment.

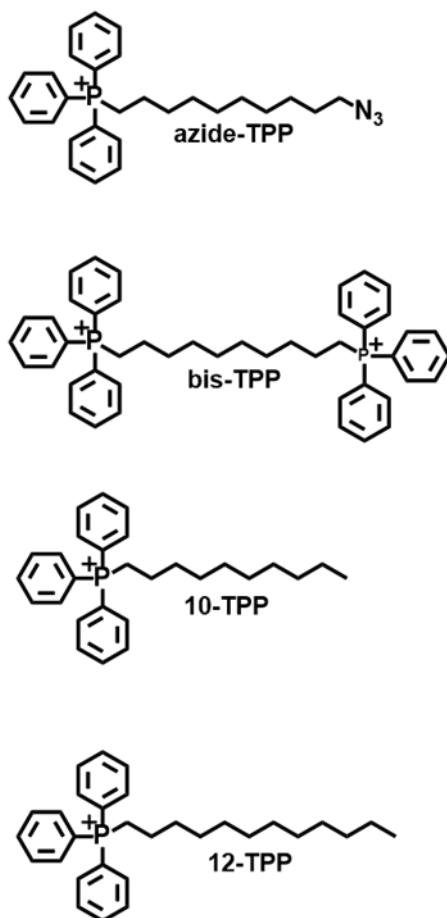


Figure A-1: The TPP structures examined in supplementary experiments.

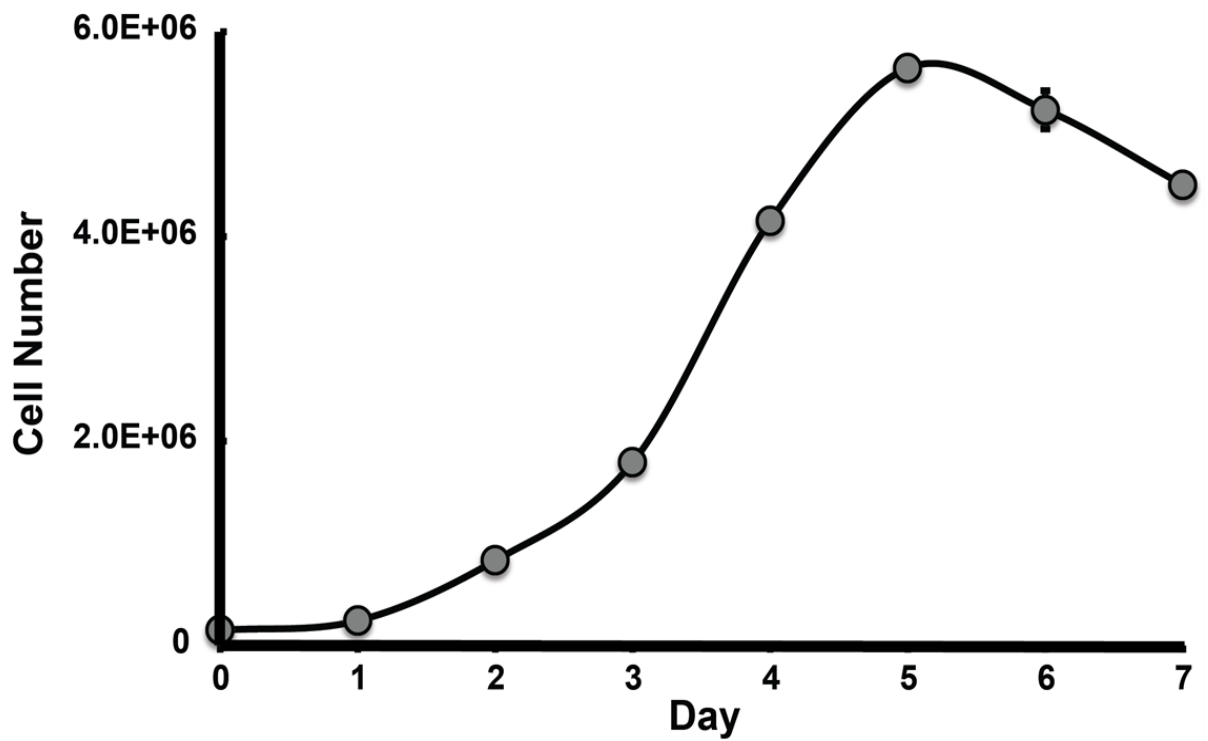


Figure A-2: A375 melanoma cell growth curve.

In order to generate cellular growth curves and to calculate the population doubling time of A375 cells, A375 cells were plated in 60 mm tissue culture dishes at a density of 150,000 cells/dish. Cells were then trypsinized and counted daily for 6-7 days. Population doubling time calculations demonstrate that A375 cells have a population doubling time of 24 h.

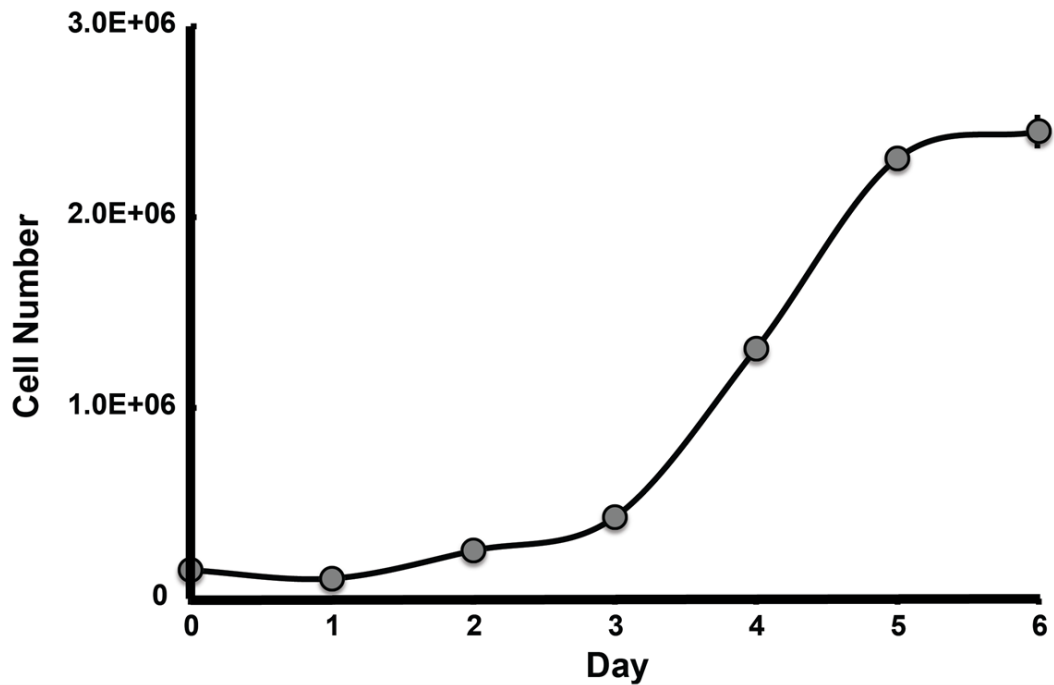


Figure A-3: MeWo melanoma cell growth curve.

In order to generate cellular growth curves and to calculate the population doubling time of MeWo cells, MeWo cells were plated in 60 mm tissue culture dishes at a density of 150,000 cells/dish. Cells were then trypsinized and counted daily for 6-7 days. Population doubling time calculations demonstrate that MeWo cells have a population doubling time of 34 h.

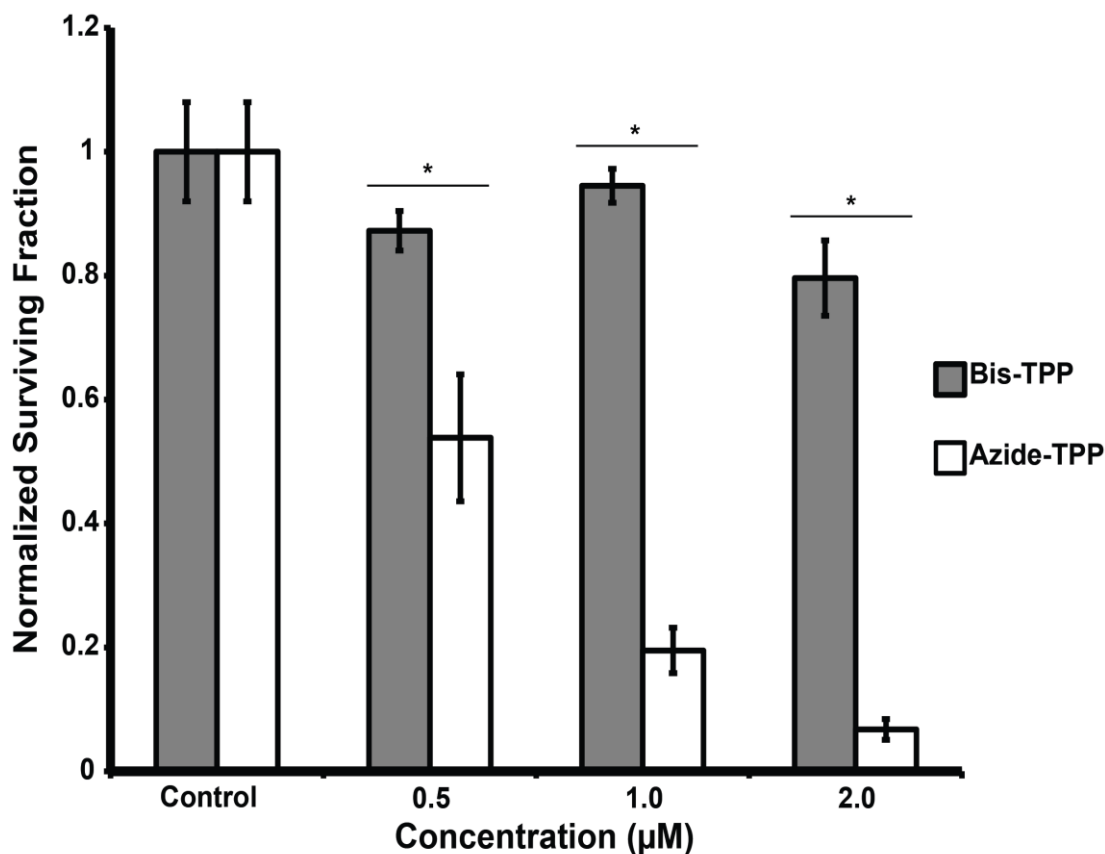


Figure A-4. TPP linear side-chains induce cytotoxicity.

MDA-MB-231 cells were treated with 0.5 µM, 1.0, or 2.0 µM µM azide-TPP or bis-TPP for 24 h and analyzed for clonogenic survival. Error bars represent the standard error of the mean (* significant relative to azide-TPP versus bis-TPP treatment at the given concentration, $p < 0.05$, $N = 4-8$). Results demonstrate that a TPP derivative modified with a linear side chain reduces breast cancer cell clonogenic survival, while a TPP derivative modified with two TPP moieties does not. These results suggest that the TPP side chain is the reactive part of TPP derivatives that induces cytotoxicity, not the TPP mitochondria-targeting moiety.

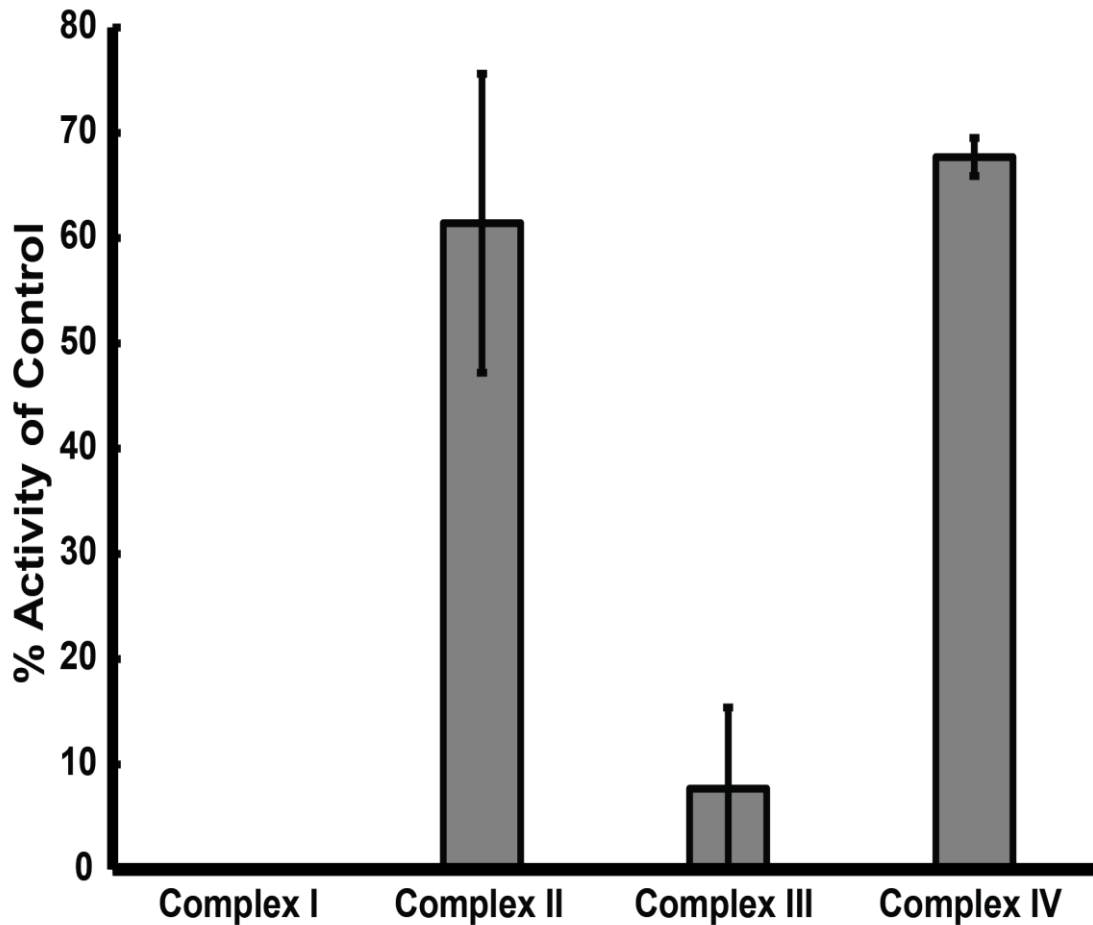


Figure A-5: TPP inhibits mitochondria electron transport chain activity.

The activity of electron transport chain complexes I-IV was measured spectrophotometrically in enriched mitochondria treated with 10 μ M 10-TPP. Error bars represent the standard error of the mean (N = 2). These results indicate that 10-TPP selectively inhibits electron transport chain complexes I and III activity relative to untreated controls and supports the hypothesis that TPP compounds disrupt mitochondria oxidative metabolism.

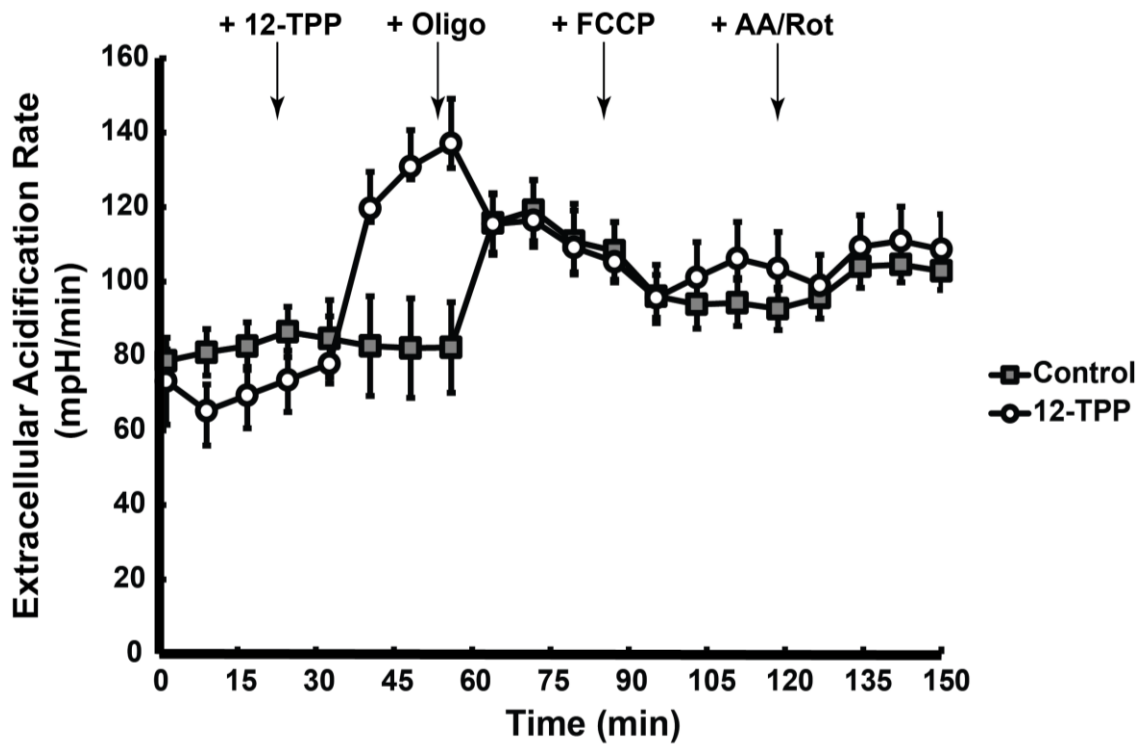


Figure A-6. TPP increases melanoma cell glycolytic activity.

A375 melanoma cells were plated in XF96 plates and incubated for 48 h. Extracellular acidification rate (ECAR) measurements were made using a Seahorse Bioscience XF96 extracellular flux analyzer in 15 min increments for 150 min. (1) 12-TPP was injected at the 20 min mark followed by the sequential addition of (2) oligomycin, (3) FCCP, and (3) antimycin A and rotenone. Results show that 12-TPP treatment immediately increases the ECAR in A375 melanoma cells. Error bars represent the standard error of the mean (N = 4). These results support the hypothesis that TPP interferes with mitochondria oxidative metabolism via ATP-linked oxygen consumption, which forces cells into glycolysis as a compensatory mechanism to meet metabolic requirements.

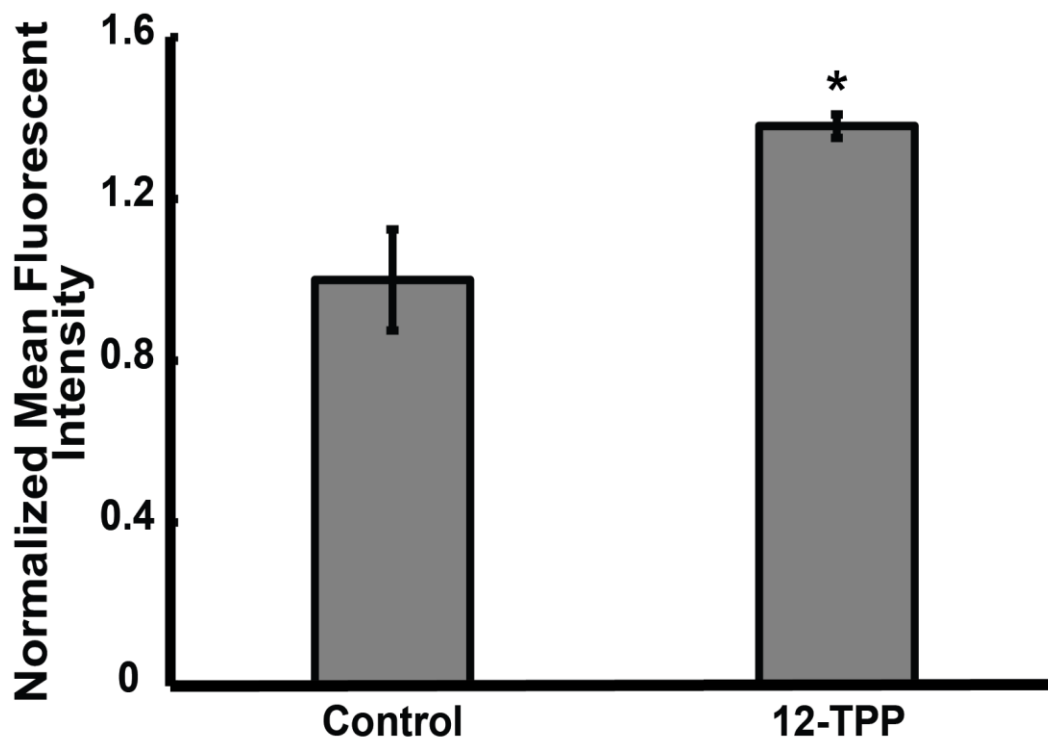


Figure A-7. TPP increases melanoma cell glucose uptake.

A375 human melanoma cells were plated in 60 mm tissue culture dishes and incubated for 48 h. After incubation, cells were treated with 12-TPP for 1 h. Cells were then incubated with the fluorescent glucose analog 2-NBDG for 2 h. Following labeling, cells were analyzed by flow cytometry. Error bars represent the standard error of the mean (* significant relative to control, $p < 0.05$, $N = 3$). Results suggest that TPP derivatives increase glucose uptake presumably as a compensatory mechanism to oxidative phosphorylation inhibition.

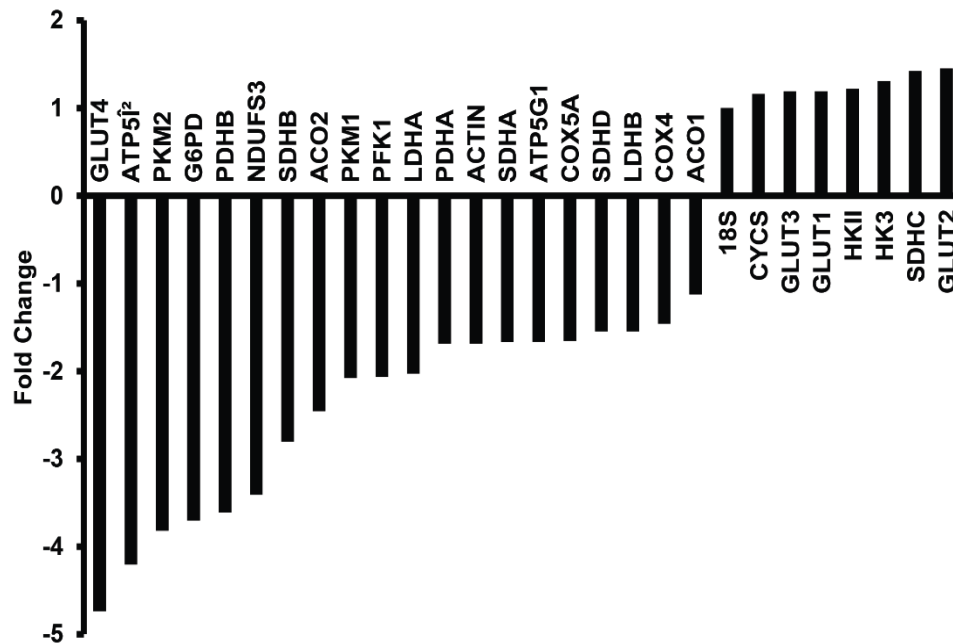


Figure A-8: TPP decreases melanoma cell metabolic gene expression.

A375 cells were treated with 1.0 μ M 12-TPP for 24 h. Following treatment, RNA was isolated and reversed transcribed into cDNA. The products from the cDNA reaction were loaded into a gene array containing the primer sequences for 26 genes associated with glycolysis, the citric acid cycle (TCA), or oxidative phosphorylation and a RT-PCR reaction was ran (N = 3). Data is presented as the fold change in PCR amplification compared to 18s control. Results demonstrate that 12-TPP leads to a roughly > 2 fold decrease in six genes associated with glycolysis (GLUT4, G6PD, PFK1, PKM2, LDHA), two genes associated with the TCA (PDHB, ACO2) and three genes associated with oxidative phosphorylation (NDUFS3, SDHB, ATP5Î²) and support the hypothesis that TPP disrupts mitochondria metabolism which in turn eventually leads to a decrease in TCA and glycolysis and cytotoxicity.

Discussion

Our data demonstrate that TPP compounds disrupt mitochondria oxidative metabolism, increase DHE oxidation, decrease intracellular GSH and ATP, and lead to cytotoxicity in melanoma cells. Further, there is a structure-activity relationship between TPP side chain length and metabolic disruption and cytotoxicity in melanoma cells, with longer side-chains imparting greater effects than shorter chains. In the data presented in Appendix A, experiments designed to support that the TPP side chain is the reactive part of TPP derivatives that induces melanoma cytotoxicity were performed. Studies designed to elucidate that specific ETC complexes are disrupted and lead to decreased OCR were also performed. Studies were also conducted to determine how TPP treatment affects melanoma cell glucose uptake and glycolytic activity. Finally, a metabolic gene array was performed to evaluate how TPP treatment affects the expression of genes associated with glycolysis, the TCA, and oxidative phosphorylation.

Consistent with previous findings, results demonstrate that a TPP derivative modified with linear side chain (azide-TPP) decreases melanoma clonogenic survival, whereas a TPP derivative without a side chain (bis-TPP) does not. This finding argues that the TPP side chain is the reactive part of TPP derivatives that affects melanoma cell metabolism and cytotoxicity, not the TPP moiety itself. We further find that a 10-TPP compound specifically inhibits ETC complex I and III activity, while complex II and IV activity is largely unaffected. This supports previous studies that show TPP compounds disrupt mitochondria

oxidative metabolism and decreases ATP-linked oxygen consumption, presumably through complex I and III inhibition. Metabolic flux analysis demonstrates that in addition to ETC inhibition, 12-TPP causes an immediate increase in melanoma cell ECAR, an indicator of glycolytic activity, and increases melanoma cell glucose uptake. The increase in glucose uptake and glycolytic activity is likely a compensatory mechanism due to TPP oxidative phosphorylation inhibition. Finally, previous studies (e.g., JC-1, DHE, metabolic flux measurements, glucose uptake) were done using short TPP incubation times. In order to see how longer TPP treatment times affect melanoma cell metabolism, a metabolic gene array was performed to determine how 24 h 12-TPP treatment affects the expression of genes associated with glycolysis, the TCA, and oxidative phosphorylation. Results demonstrate that 12-TPP decreases the expression of multiple genes associated with glycolysis, the TCA, and oxidative phosphorylation following 24 h treatment. These decreases in glycolysis, the TCA, and oxidative phosphorylation gene expression are likely attributed to TPP ETC inhibition, which is resulting in total decreases in metabolism and subsequent cell death. Collectively, these results demonstrate that TPP derivatives disrupt melanoma cellular metabolism, and the side chain of TPP derivatives cause these disruptions in melanoma cellular metabolism.

APPENDIX B: SYNTHESIS AND CHARACTERIZATION OF TRIPHENYLPHOSPHONIUM DERIVATIVES

Overview

Evidence demonstrates that TPP side chains can be modified to facilitate their uptake in cellular mitochondria and induce cytotoxicity. Further, TPP derivatives can be used as organic synthesis building blocks or as tools for the delivery of bioactive molecules to cellular mitochondria for a host of applications. Therefore I synthesized a small library of TPP variants with side chains of varying chemical compositions. These compounds were synthesized for the potential use as anticancer agents or organic synthesis building blocks to link to various bioactive moieties to TPP.

Materials and Methods

General Considerations

All solvents and reagents were used as received unless otherwise noted. Unless described otherwise, solutions were prepared using ultrahigh-purity water and chemicals with metal concentrations certified to <20 parts per trillion (Baseline, Seastar Chemicals, British Columbia, Canada). Alternatively, a 0.22 μm filtered deionized 18 MX milliQ Advantage purification system (Millipore,

Billerica, MA, USA) was used to obtain highly pure water. Analytical and semi-preparatory high performance liquid chromatography (HPLC) was carried out by reverse phase methods using an Agilent 1200 series HPLC (Agilent Technologies, Santa Clara, CA), equipped with Clarity 5 μm Oligo-RP C18 50 x 4.6 mm columns. The identity of reaction products was confirmed by comparison of the theoretical mass to that observed by electrospray ionization mass spectrometry (ESI-MS).

Azide-TPP Synthesis

(10-azidodecyl)triphenylphosphonium was synthesized by refluxing triphenylphosphine (0.5 g, 2.0 mmol) (Alpha Aesar, Ward Hill, Ma) with a 25-fold excess of 1, 10-dibromodecane (10.5 g, 50.0 mmol) (Alpha Aesar) in 10 mL benzene (Sigma, St. Louis, MO) for 24 h at 80 °C yielding a (10-bromodecyl)triphenylphosphonium intermediate. The intermediate (0.77 g, 1.6 mmol) was refluxed with a 5- fold excess of sodium azide (NaN_3) (0.52 g, 8.0 mmol) (Sigma) in a 30 mL 1:1 mixture of EtOH and water for 24 h at 80 °C yielding (10-azidodecyl)triphenylphosphonium. The final product was purified by silica gel chromatography using the following solvents: (50% hexanes / 50% ethyl acetate; 100% ethyl acetate; 10% methanol / 90% ethyl acetate; 50% methanol / 50% ethyl acetate; and 100% methanol). Fractions collected were analyzed using thin layer chromatography. ESI-MS confirmed final product mass (observed 444.3, calculated 444.57).

Bis-TPP Synthesis

Decane-1,10-diylbis(triphenylphosphonium) was synthesized by refluxing triphenylphosphine (0.8 g, 2.0 mmol) (Alpha Aesar) with a 10-fold excess of 1,10-dibromodecane (1.0 g, 20.0 mmol) (Alpha Aesar) in 10 mL benzene for 72 h at 80 °C. The final product was purified by silica gel chromatography using the following solvents: (50% hexanes / 50% ethyl acetate; 100% ethyl acetate; 10% methanol / 90% ethyl acetate; 50% methanol / 50% ethyl acetate; and 100% methanol). Fractions collected were analyzed using thin layer chromatography. ESI-MS confirmed final product mass (observed 663.36, calculated 664.84).

17-TPP Synthesis

(10-(4-butyl-1H-1,2,3-triazol-1-yl)decyl)triphenylphosphonium was synthesized by reacting 1-hexyne (15.0 μmol) (Alfa Aesar) in a 10-fold excess to (10-azidodecyl)triphenylphosphonium (1.5 μmol). 0.1 M Copper sulfate (CuSO_4) (Sigma) was added to the reaction mixture in a 5-fold excess (7.5 μmol) to (10-azidodecyl)triphenylphosphonium while sodium L-ascorbate (NaAsc) (Sigma) was added to the reaction mixture in a 15-fold excess (22.5 μmol) to (10-azidodecyl)triphenylphosphonium to provide catalytic Cu^{1+} for cycloaddition of the azide and terminal alkyne. The reaction mixture was incubated at room temperature for 24 h with gentle agitation in 500.0 μL of 1:1 NaCl/DMSO. The final product was purified by HPLC using 0.1 v/v % TFA with a 5-100 % (v/v)

acetonitrile gradient at 1 mL/m over 30 m while monitoring absorbance (Abs 280 nm). The major peak was collected and pooled from multiple runs, lyophilized, and stored at -80 °C. ESI-MS confirmed final product mass (observed 526.3, calculated 527.72).

21-TPP Synthesis

(10-(4-octyl-1H-1,2,3-triazol-1-yl)decyl)triphenylphosphonium was synthesized by reacting 1-decyne (15.0 μmol) (Alfa Aesar) in a 10-fold excess to (10-azidodecyl)triphenylphosphonium (1.5 μmol). 0.1 M CuSO_4 was added to the reaction mixture in a 5-fold excess (7.5 μmol) to (10-azidodecyl)triphenylphosphonium while NaAsc was added to the reaction mixture in a 15-fold excess (22.5 μmol) to (10-azidodecyl)triphenylphosphonium to provide catalytic Cu^{1+} for cycloaddition of the azide and terminal alkyne. The reaction mixture was incubated at room temperature for 24 h with gentle agitation in 500.0 μL of 1:1 NaCl/DMSO. The final product was purified by HPLC using 0.1 v/v % TFA with a 5-100 % (v/v) acetonitrile gradient at 1 mL/m over 30 m while monitoring absorbance (Abs 280 nm). The major peak was collected and pooled from multiple runs, lyophilized, and stored at -80 °C. ESI-MS confirmed final product mass (observed 582.4, calculated 583.83).

TPP-OH Synthesis

(10-(4-(hydroxymethyl)-1H-1,2,3-triazol-1-yl)decyl)triphenylphosphonium was synthesized by reacting propargyl alcohol (30 μ L, 500 nmol) (Sigma) with a with a 1.5- fold excess of (10-azidodecyl)triphenylphosphonium (750.0 nmol) to propargyl alcohol. CuSO_4 was added to the reaction mixture in a 5 fold excess (2500 nmol) to propargyl alcohol. NaAsc was added to the reaction mixture in a 14-fold excess (7000 nmol) to propargyl alcohol. The reaction mixture was incubated at room temperature for 24 h with gentle agitation in 500 μ L of 1:1 $\text{H}_2\text{O}/\text{DMSO}$. The final product was purified by HPLC using 0.1 v/v % TFA with a 5-90 % (v/v) acetonitrile gradient at 1 mL/m over 30 m while monitoring absorbance (Abs 280 nm). The major peak was collected and pooled from multiple runs, lyophilized, and stored at -80°C . ESI-MS confirmed final product mass (observed 500.3, calculated 501.29).

TPP-COOH Synthesis

(10-(4-(hydroxymethyl)-1H-1,2,3-triazol-1-yl)decyl)triphenylphosphonium was synthesized reacting 10-undecynoic acid (100 μ L, 500 nmol) (Alpha Aesar) with a with a 1.5- fold excess of (10-azidodecyl)triphenylphosphonium (750 nmol). CuSO_4 was added to the reaction mixture in a 5-fold excess (2500 nmol) to 10-undecynoic acid. NaAsc was added to the reaction mixture in a 14-fold excess (7000 nmol) to 10-undecynoic acid. The reaction mixture was incubated

at room temperature for 24 h with gentle agitation in 500 μL of 1:1 $\text{H}_2\text{O}/\text{DMSO}$. The final product was purified by HPLC using 0.1 v/v % TFA with a 5-90 % (v/v) acetonitrile gradient at 1 mL/m over 30 m while monitoring absorbance (Abs 280 nm). The major peak was collected and pooled from multiple runs, lyophilized, and stored at $-80\text{ }^\circ\text{C}$. ESI-MS confirmed final product mass (observed 626.4, calculated 627.84).

Results

Azide-TPP Synthesis

Click chemistry involves the reaction of an azide functional group with an alkyne functional group to form a stable triazole linkage [194-196]. The click reaction is characterized by its selectivity, rapid kinetics, high yields, and mild reaction conditions that makes it a powerful tool in synthetic chemistry for the conjugation of bioactive molecules to agents that target cancer cells [194]. Based on these reasons, TPP was modified with a ten-carbon chain containing a terminal azide functional group. This allows for the conjugation of TPP to other bioactive molecules modified with an alkyne functional group by click chemistry. ESI-MS confirmation of the product can be found in **Figure B-1**.

Bis-TPP Synthesis

Evidence demonstrates that the TPP moiety of TPP derivatives targets mitochondria. Evidence also demonstrates that linear side chains attached to a mitochondria targeting TPP moiety embed in the mitochondria membrane and disrupt mitochondria metabolism that results in cell death. To support the evidence that TPP targets mitochondria and the TPP side chain inserts into the mitochondria membrane, a bis-TPP compound containing two TPP moieties connected by a ten-carbon linker was synthesized. A bis-TPP compound was synthesized under the premise that the two TPP mitochondria targeting moieties of the bis-TPP compound will locate to the inner mitochondria membrane, but the carbon linker would not insert in the mitochondria membrane and disrupt mitochondria metabolism and cause cancer cell cytotoxicity. ESI-MS confirmation of the product can be found in **Figure B-2**.

17-TPP Synthesis

TPP derivatives modified with linear side chains preferentially accumulate in cellular mitochondria where the side chain inserts into the inner mitochondria membrane. Further, evidence demonstrated that inclusion of longer TPP side chains improve TPP mitochondria accumulation. Evidence also shows that inclusion of longer side chains enhances the effects of TPP derivatives on cellular mitochondria metabolism and cytotoxicity. Based on this knowledge,

TPP derivatives with increasing side chain lengths were synthesized. A 17-TPP compound was the first TPP compound synthesized to study how TPP side chain length affects melanoma cell mitochondrial uptake and cytotoxicity. ESI-MS confirmation of the product can be found in **Figure B-3**.

21-TPP Synthesis

To further interrogate the effects of TPP side chain length on melanoma cell mitochondria and cytotoxicity, a 21-TPP compound was synthesized in addition to a 17-TPP compound. ESI-MS confirmation of the product can be found in **Figure B-4**.

TPP-COOH Synthesis

Compounds modified with a carboxylic acid group can react with hydroxyl-modified compounds to form an ester linkage between the two compounds and can be used for the organic synthesis of bioactive drugs [197-200]. Further, this ester linkage can be hydrolyzed in mitochondria to reform the individual carboxylic acid and hydroxyl-modified compounds [200]. This can be a potential avenue for TPP delivery and cleavage of a bioreactive molecule to the mitochondria. Based on this knowledge, a TPP-COOH compound was synthesized for use in esterification reactions. This allows for the attachment of a bioactive moiety modified with a hydroxyl functional group to be conjugated to the

mitochondria-targeting TPP group [198, 199]. ESI-MS confirmation of the product can be found in **Figure B-5**.

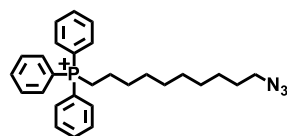
TPP-OH Synthesis

Compounds modified with a carboxylic acid group can react with hydroxyl-modified compounds to form an ester linkage between the two compounds and can be used for the organic synthesis of bioactive drugs [197-200]. Further, this ester linkage can be hydrolyzed to reform the individual carboxylic acid and hydroxyl-modified compounds [200]. This can be a potential avenue for TPP delivery and cleavage of a bioactive molecule to the mitochondria. Based on this knowledge, a TPP-OH compound was synthesized for use in esterification reactions. This allows for the attachment of a bioactive moiety modified with a carboxylic acid functional group to be conjugated to the mitochondria-targeting TPP group [198, 199]. Further, mitochondria esterases can cleave the TPP from the bioactive moiety resulting in the delivery of two drugs. ESI-MS confirmation of the product can be found in **Figure B-6**.

Discussion

Previous data and literature show that TPP derivatives modified with linear side chains accumulate in TPP where the side chain inserts into the mitochondria membrane and disrupts mitochondria metabolism that can ultimately result in cell

death. For this reason, TPP compounds modified with a second TPP targeting moiety and a 17 and 21 carbon chain were synthesized in order to study how the side chain length and mitochondria membrane insertion affects mitochondria function that can result in cell death. Lastly, triphenylphosphonium derivatives are widely used for their ability to target and localize in cellular mitochondria. This makes them useful tools in research for the attachment and delivery of various bioactive molecules to mitochondria for a host of applications. For this reason, in this study an azide modified TPP variant was synthesized so that it can participate in a click reaction with other alkyne containing moieties. This allows for the attachment of bioactive molecules to TPP that then localize to mitochondria. TPP variants modified with hydroxyl and carboxylic acids were also synthesized. This allows for their use in esterification reactions as another tool to conjugate bioactive molecules to TPP derivatives that localizes attached bioactive molecules to the mitochondria. The addition of azide, carboxylic, and hydroxyl groups to TPP simplifies the conjugation of TPP to other molecules and expands the potential applications of TPP conjugates.



Azide-TPP
MW: 444.57

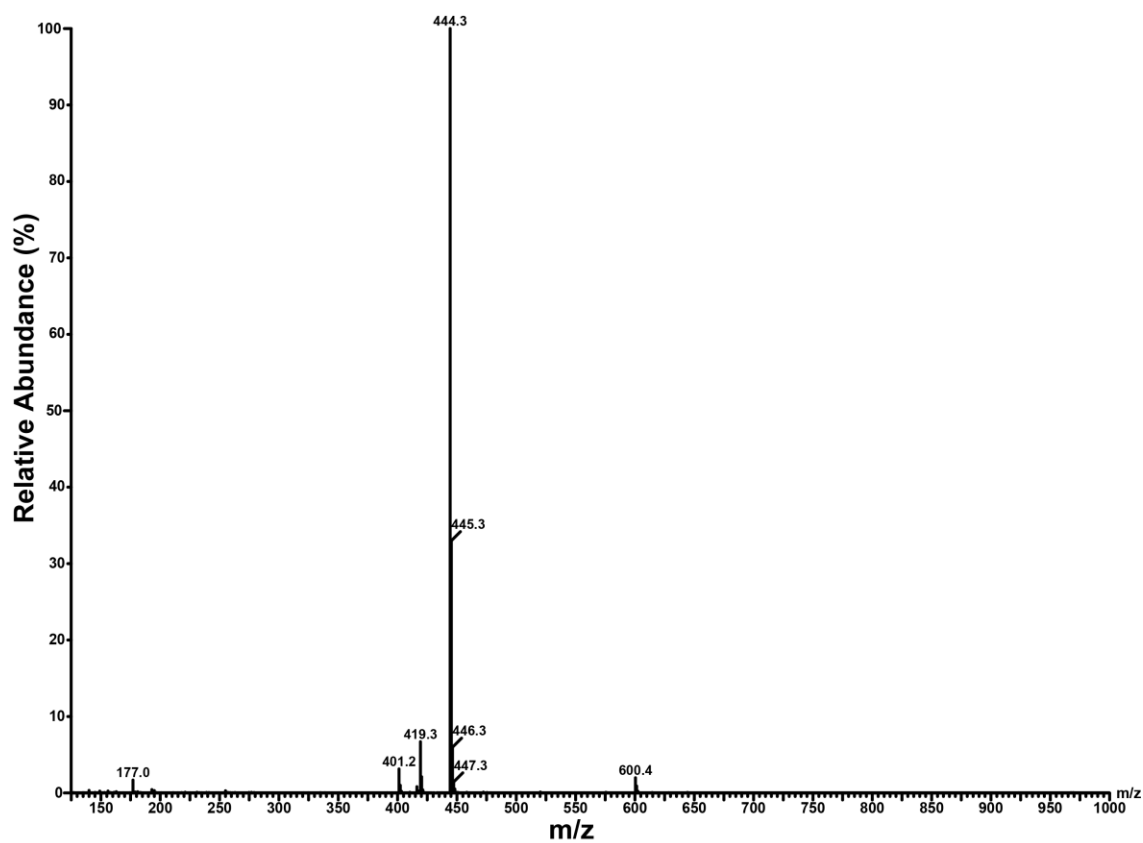
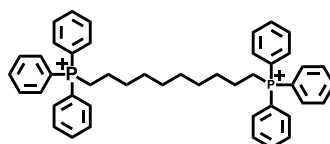


Figure B-1: Azide-TPP mass spectroscopy confirmation of the product.

ESI-MS of purified azide-TPP (observed 444.3, calculated 444.57).



Bis-TPP
MW: 664.84

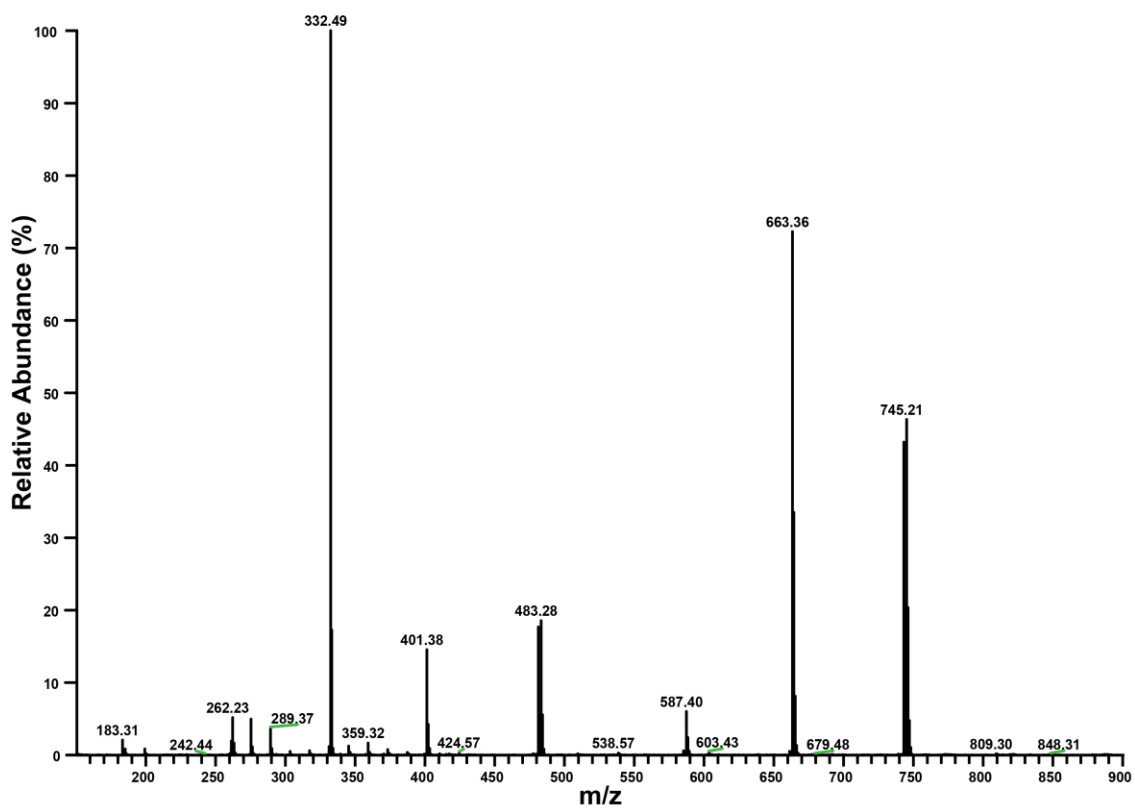
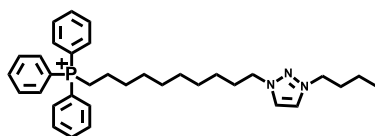


Figure B-2: bis-TPP mass spectroscopy confirmation of the product.

ESI-MS of purified bis-TPP (observed 663.36, calculated 664.84).



17-TPP
MW: 527.72

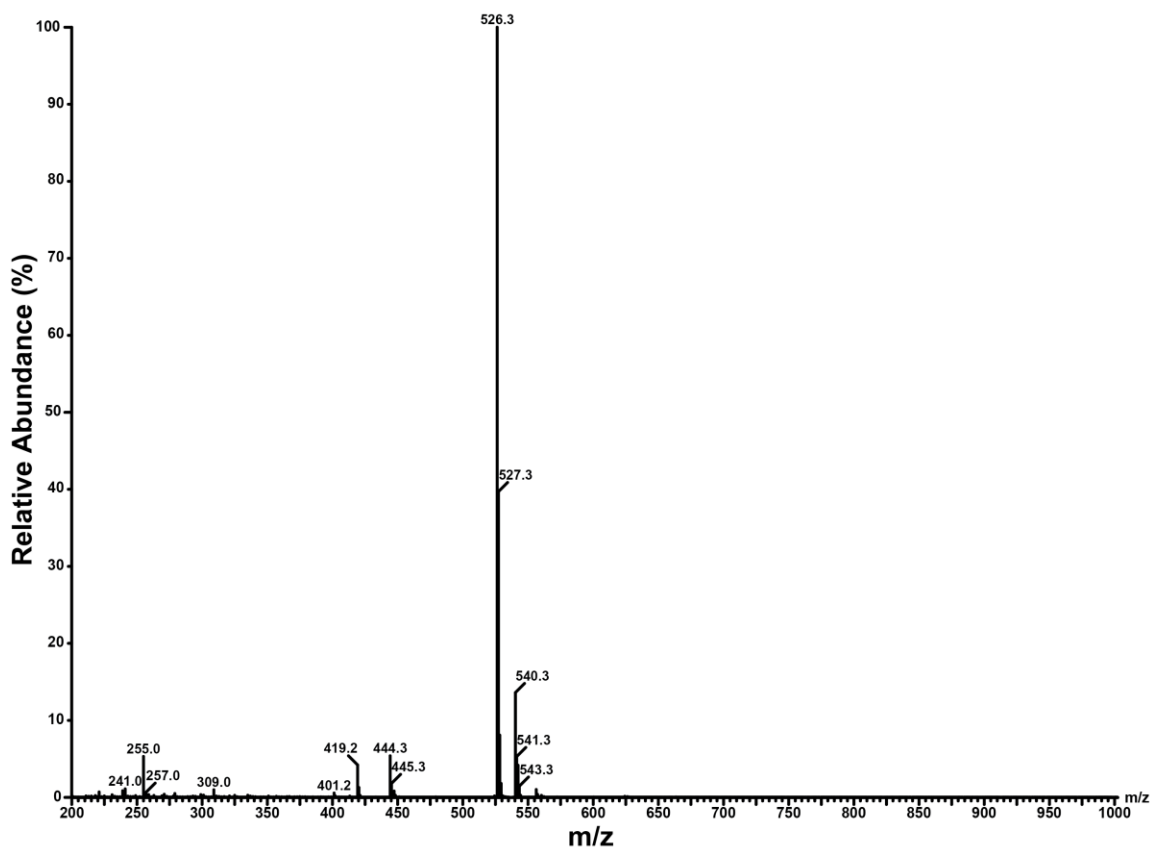
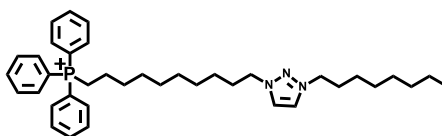


Figure B-3: 17-TPP mass spectroscopy confirmation of the product.

ESI-MS of purified 17-TPP (observed 527.3, calculated 527.72).



21-TPP
MW: 583.83

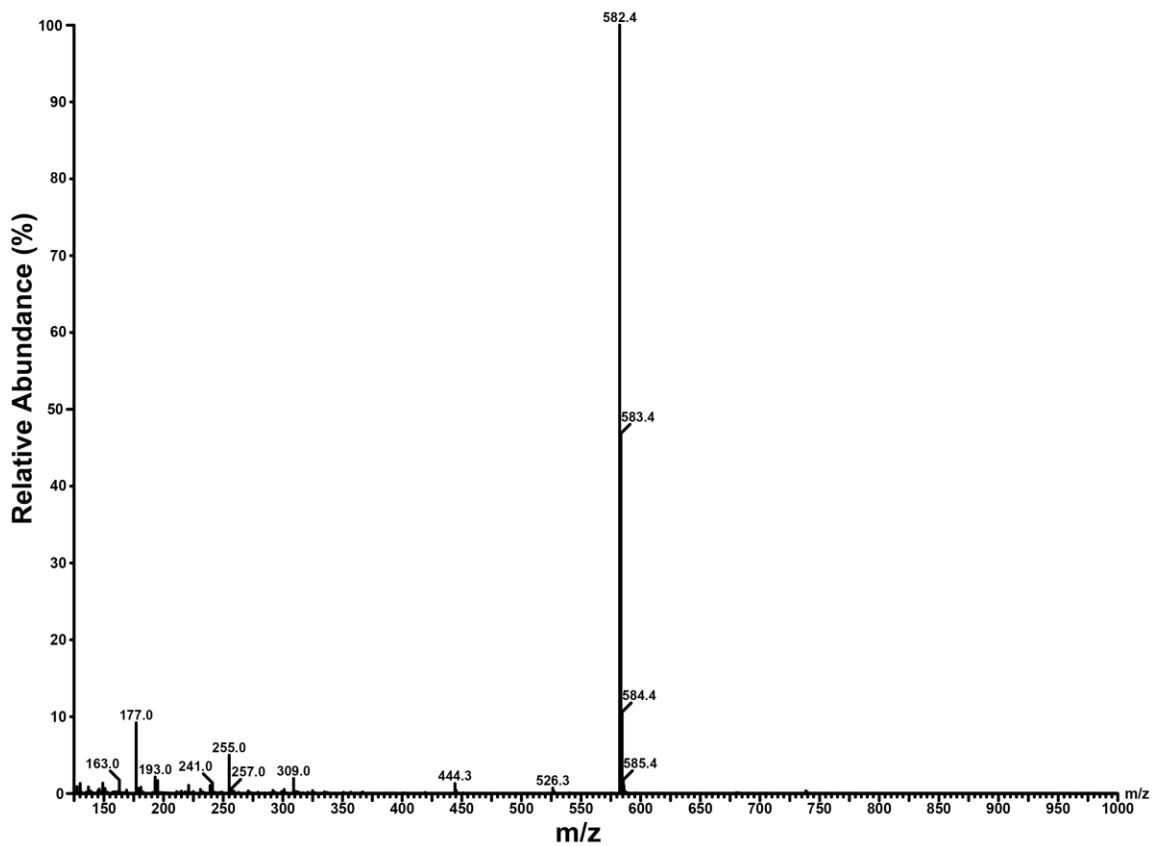
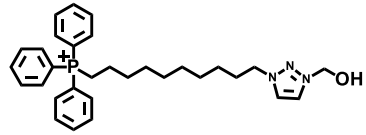


Figure B-4: 21-TPP mass spectroscopy confirmation of the product.

ESI-MS of purified 21-TPP (observed 583.4, calculated 583.83).



TPP-OH
MW: 501.29

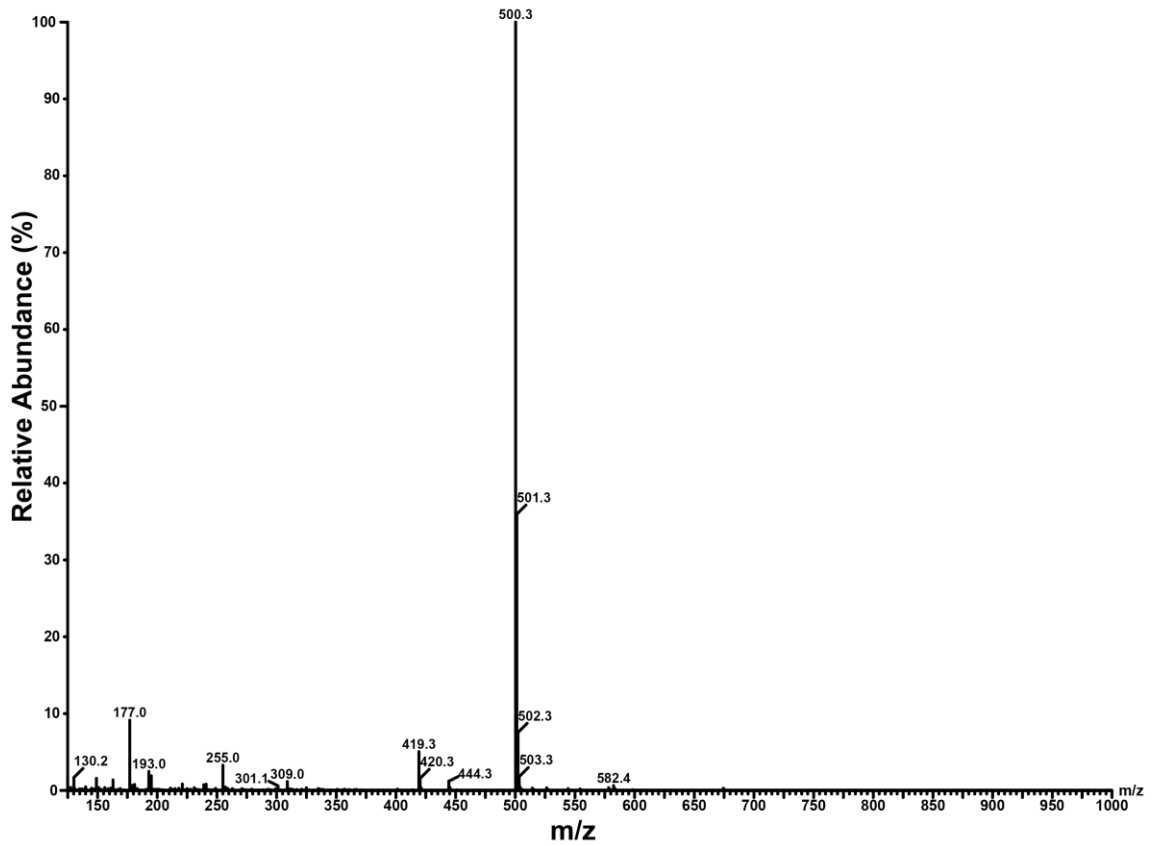
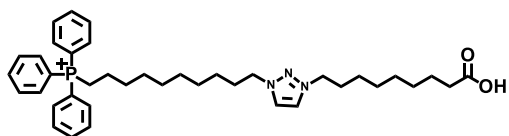


Figure B-5: TPP-OH mass spectroscopy confirmation of the product.

ESI-MS of purified TPP-OH (observed 501.3, calculated 501.29).



TPP-COOH
MW: 627.84

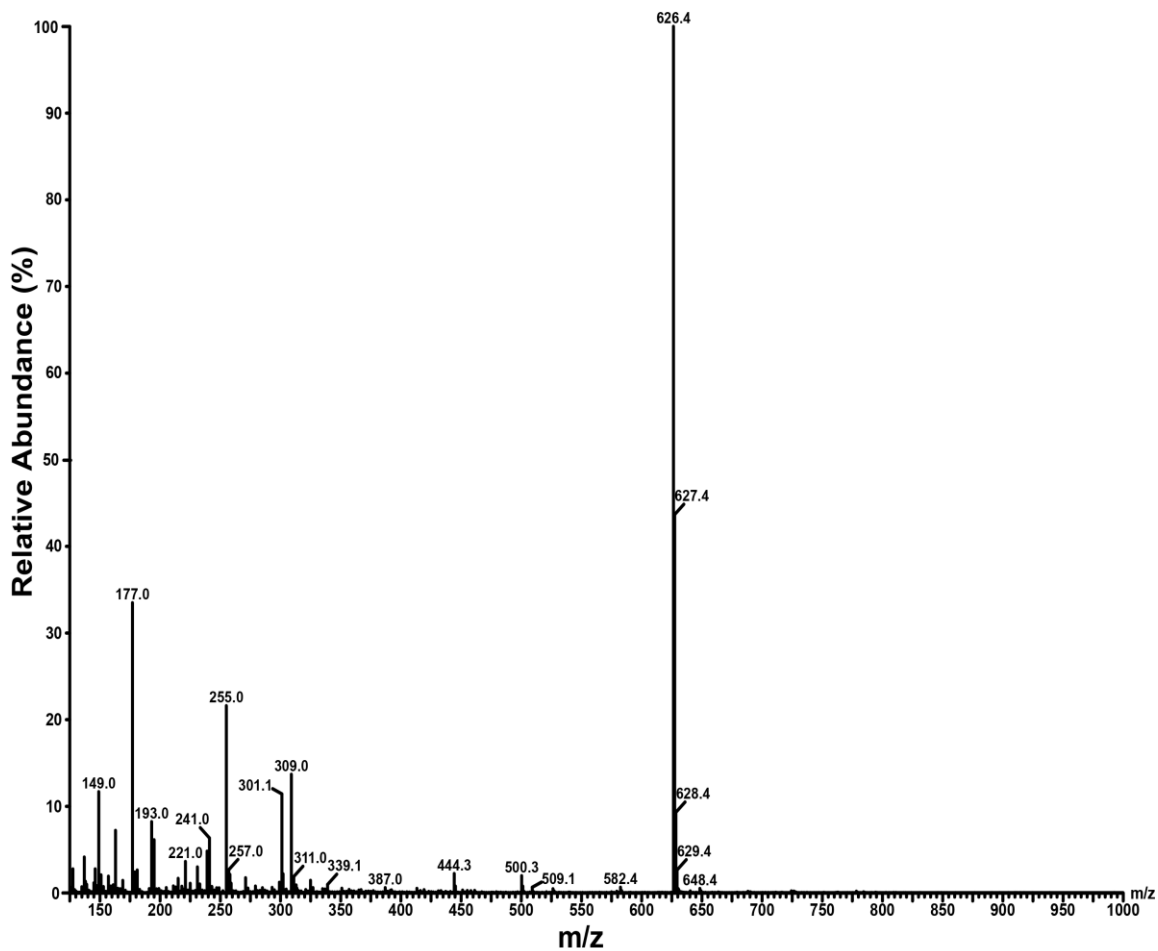


Figure B-6: TPP-COOH mass spectroscopy confirmation of the product.

ESI-MS of purified TPP-COOH (observed 627.4, calculated 627.84).

APPENDIX C: TRIPHENYLPHOSPHONIUM DERIVATIVE HIGH THROUGHPUT SCREENS

Overview

Previous experiments demonstrate that TPP molecular side chains can be rationally designed to inhibit melanoma cell mitochondria metabolism that ultimately results in melanoma cell cytotoxicity. In order to sample a large range of space in terms of TPP side chain chemical compositions, a chemical library containing 45 commercially available TPP derivatives, each differing in side chain molecular composition, was purchased. MTT cell viability screens were performed utilizing High-throughput technology at the University of Iowa High-Throughput Screening Facility in order to identify structure-activity relationships between side chain composition and decreased cell viability in A375 melanoma cells relative to non-malignant melanocytes. The overall goal was to identify specific compositions of matter of the TPP side chain that decrease A375 cell viability relative to non-malignant melanocytes. The identified compositions of matter can then be used to improve TPP drug design.

Materials and Methods

TPP Compound Library

A compound library containing 45 TPP derivatives each modified with different linear side chains was purchased from Specs (Cumberland, MD). The compound library was 10 mM TPP in 350 μ L DMSO.

MTT HTS Assay

A375 (50 k cells/well) and melanocyte (90 k cells/well) cells were plated in 96 well plates and incubated for 24 h. Cells were then treated with TPP (2.0 μ M) for 24 h. Following treatment, media was aspirated and MTT (Sigma) (5 mg/mL dissolved in 1X PBS (Gibco) was added to each well and incubated for 1 h. MTT was then aspirated and DMSO was added to each well to dissolve the formazan salt. The absorbance of the formazan solution was measured at 590 nm using a Hamilton (Reno, NV) MicroLab Star automated liquid handling instrument at the University of Iowa High Throughput Facility.

Results

TPP High Throughput Screens

In order to identify specific compositions of matter of TPP drugs that result in the highest differential cytotoxicity between A375 melanoma cells and non-malignant melanocyte cells, a high throughput MTT viability screen was performed in the University of Iowa College of Pharmacy High Throughput Screening Facility. A375 melanoma cells and non-malignant melanocytes were treated with 2.0 μ M TPP for 24 h with 45 different TPP derivatives each modified with different molecular side chains (**Figure C-1**). Results identified six lead compounds that result in the highest decrease in A375 cell viability relative to non-malignant melanocytes (A1-A3; B1-B3) (**Figure C-2**). The compounds identified have specific side chain structural similarities that impart melanoma cell specific cytotoxicity. Structural features include vinyl chloride groups and amide bond linkages to terminal halo substituted benzyl groups. These results demonstrate that there is a structure-activity relationship between side chain molecular composition and cell viability; and specific compositions of matter can be identified that result in the highest decrease in A375 cell viability relative to non-malignant melanocytes. The specific compositions of matter identified can be used to improve TPP drug design that will result in greater cytotoxicity to melanoma cells versus non-malignant cells.

Discussion

Previous data suggest that TPP side chains can be manipulated in order to improve their cytotoxic effects on melanoma cells. In order to sample a large range of chemical space in terms of TPP side chain composition, a compound library containing 45 commercially available TPP derivative each modified with different molecular side chains was purchased and high throughput viability screens were performed in A375 melanoma and non-malignant melanocyte cells. Results identified six lead compounds have specific side chain structural similarities that result in the highest decrease in A375 cell viability relative to non-malignant melanocytes. Structural similarities include vinyl chloride groups and amide bond linkages to terminal halo substituted benzyl groups. These specific chemical groups can be used to design novel melanoma drugs that can potentially improve the cytotoxic effect of TPP drugs in melanoma cells while sparing off target toxicity in non-malignant cells.

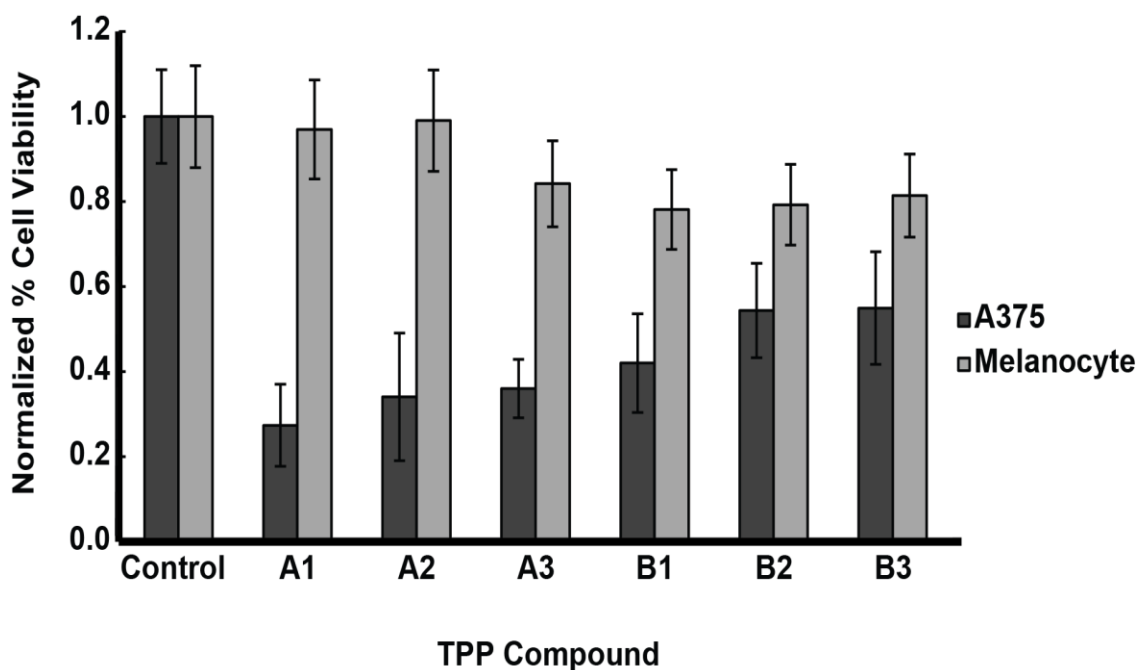


Figure C-1: TPP high throughput melanoma versus non-malignant cell viability assay.

A375 melanoma cells and non-malignant melanocytes were treated for 24 h with 45 TPP compounds, each containing molecular side chains comprised of different compositions of matter. Following treatment, MTT cell viability assays were performed. Results identified six lead compounds that result in the highest decrease in A375 cell viability relative to non-malignant melanocytes (A1-A3; B1-B3). Error bars represent standard deviation of the mean (N = 2 for A375 cells; N = 1 for melanocyte cells). Error bars for melanocytes were calculated based on a fixed percentage. Results support that specific compositions of matter of TPP side chains can be identified that result in the highest differential cytotoxicity in melanoma versus non-malignant cells.

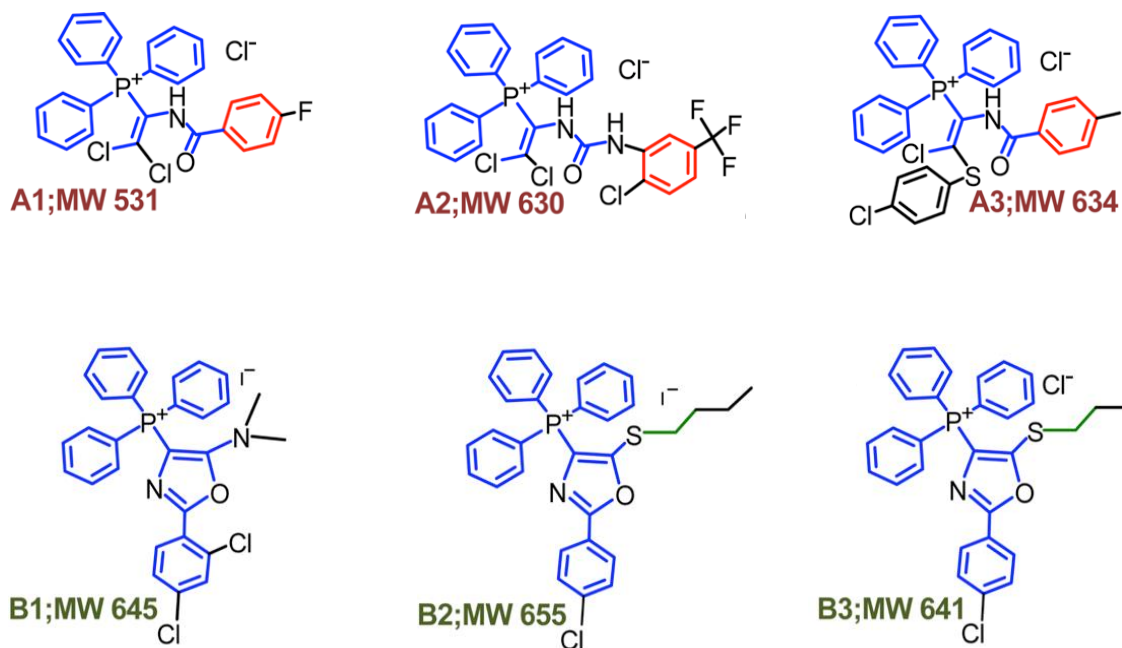


Figure C-2: The chemical structures of lead TPP compounds identified in high throughput screens that result in the greatest differential cytotoxicity in melanoma versus non-malignant cells.

High throughput MTT cell viability screens were performed in A375 melanoma cells and non-malignant melanocytes. Results identified six lead compounds that result in the highest differential cytotoxicity in melanoma cells versus non-malignant cells. The compounds identified have structural features including vinyl chloride groups and amide bond linkages to terminal halo substituted benzyl groups that can be used to develop novel TPP drugs that are cytotoxic to melanoma versus non-malignant cells.

APPENDIX D: CHELATOR-MODIFIED TRIPHENYLPHOSPHONIUM DERIVATIVES FOR PET IMAGING

Overview

TPP compounds have gained recent attention as imaging agents due to their ability to accumulate in mitochondria rich tissues such as the heart and tumors *in vivo* [95-97, 144, 201-203]. It has been suggested that TPP compounds can be used to image tumors due to the high negative voltage potential of cancer cells relative to non-malignant tissues [95-97, 204]. However, success is limited due to the lack of tumor accumulation relative to non-malignant organs and much work needs to be done to improve TPP biodistribution if traditional administration routes are employed. TPP compounds have also been evaluated for use in cardiac perfusion imaging (CPI); a non-invasive diagnostic tool used to assess patient risk for heart attack from coronary artery disease and course of treatment [144, 202, 203]. Commonly employed radiotracers for cardiac perfusion imaging have been [^{99m}Tc]-sestamibi, [^{99m}Tc]-tetrofosmin, and ²⁰¹Thallium by single-photon emission computed tomography (SPECT), but technical limitations (*e.g.*, low spatial resolution and tracer inhomogeneity due to tissue attenuation or scatter) may affect the accuracy of SPECT [97, 144, 201, 202]. Positron emission tomography (PET) imaging agents have been employed for CPI as well since PET offers higher resolution and a method for attenuation correction compared to SPECT [144, 201, 205, 206]. The PET radionuclides

⁸²Rubidium (1.27 minute half life), [¹³N]-ammonia (9.97 minute half life), [¹⁵O]-water (2.04 minute half life) have been evaluated for CPI [144, 201]. However, the short half-life of these PET radiotracers limits their clinical utility for cardiac and imaging [144, 201, 207]. Recently [⁶⁴Cu]-labeled TPP and [¹⁸F]-labeled TPP derivatives have been evaluated for use in CPI and tumor imaging [96, 97, 144, 201, 203]. Although ⁶⁴Cu and ¹⁸F have a longer half-life (12.7 hours and 109.8 minutes) relative to traditional CPI PET imaging agents; this approach requires the installation of an on-site cyclotron for clinical feasibility [96, 97, 144, 201, 205, 207, 208].

A potential alternative radioisotope that could be used to label TPP for imaging is ⁶⁸Ga. Gallium-68 has a 68-minute half-life and is easily produced using a generator, thus circumventing the need for an on-site cyclotron [207, 209-211]. In order to evaluate the potential of TPP derivatives for PET imaging, I conjugated alkyne-modified DOTA, NOTA, and PCTA ⁶⁸Ga chelators synthesized in house to an azide-modified decylTPP variant via click chemistry [206]. Investigations demonstrate that these constructs can be labeled with ⁶⁸Ga and achieve high specific activity and radiochemical purity. Collectively, these results highlight the potential to produce a ⁶⁸Ga labeled TPP derivative for PET imaging applications.

Materials and Methods

TPP-DOTA Synthesis

DOTA-TPP was synthesized by reacting (10-azidodecyl)triphenylphosphonium (1.5 μmol) in a 3-fold excess to DOTA-MFCO (0.5 μmol). The reaction mixture was incubated at room temperature for 24 h with gentle agitation. The final product was purified by HPLC using 0.1 v/v % TFA with a 5-90 % (v/v) acetonitrile gradient at 1 mL/m over 30 m while monitoring absorbance (Abs 280 nm). The major peak was collected and pooled from multiple runs, lyophilized, and stored at $-80\text{ }^{\circ}\text{C}$. LC-MS confirmed final product mass (observed 1071.20; calculated 1071.29).

TPP-NOTA Synthesis

NOTA-TPP was synthesized by reacting (10-azidodecyl)triphenylphosphonium (1.5 μmol) in a 3-fold excess to NOTA-MFCO (0.5 μmol). The reaction mixture was incubated at room temperature for 24 h with gentle agitation. The final product was purified by HPLC using 0.1 v/v % TFA with a 5-90 % (v/v) acetonitrile gradient at 1 mL/m over 30 m while monitoring absorbance (Abs 280 nm). The major peak was collected and pooled

from multiple runs, lyophilized, and stored at -80 °C. LC-MS confirmed final product mass (observed 970.10; calculated 970.18).

TPP-PCTA Synthesis

PCTA-TPP was synthesized by reacting (10-azidodecyl)triphenylphosphonium (1.5 µmol) in a 3-fold excess to PCTA-MFCO (0.5 µmol). The reaction mixture was incubated at room temperature for 24 h with gentle agitation. The final product was purified by HPLC using 0.1 v/v % TFA with a 5-90 % (v/v) acetonitrile gradient at 1 mL/min over 30 min while monitoring absorbance (Abs 280 nm). The major peak was collected and pooled from multiple runs, lyophilized, and stored at -80 °C. LC-MS confirmed final product mass (observed 1212.30; calculated 1212.48).

TPP-Chelator Radiolabeling

⁶⁸Ga was prepared using a ⁶⁸Ga/⁶⁸Ge generator system (Model IGG100, Eckert-Ziegler, Berlin, Germany). Briefly, ⁶⁸Ga was eluted from the generator with 10 mL 0.1 M HCl directly onto a cation-exchange resin bed (Phenomenex, Strata-X-C). Pure ⁶⁸Ga was eluted from the resin bed with 400 µL of 98% acetone/0.05 M aq. HCl directly into a solution containing 3 mL of H₂O and 5-10 nmol of chelator modified TPP and incubated at 100 °C for 15 min. Following the radiolabeling period, a final purification step using a disposable C-18 cartridge

(Phenomenex, Strata-X) was necessary to achieve suitable radiochemical purity. The C-18 cartridge was rinsed with 1 mL of 95% EtOH followed by 2 mL of water. The radiolabeling mixture was drawn onto and off the cartridge twice. Unbound ^{68}Ga was eluted with 2 mL of water while radiolabeled TPP conjugates were eluted with 500 μL of 1:1 NaCl and 95% ethanol. Aliquots were extracted from the purified radiolabeling reaction mixture and directly assayed by radio-HPLC analysis.

Results

TPP-DOTA, TPP-NOTA, and TPP-PCTA Synthesis

In order to radiolabel TPP, TPP first had to be modified with ^{68}Ga chelators. An azide-modified TPP was connected to alkyne-modified DOTA, NOTA, and PCTA ^{68}Ga chelators via click chemistry. The relatively short half-life of ^{68}Ga requires chelators that incorporate ^{68}Ga rapidly under mild reaction conditions [206, 207]. Further, a chelator-modified TPP derivative must achieve a high specific activity that is stable *in vivo* [206, 207]. The chelates DOTA, NOTA, and PCTA were chosen because data shows these chelates efficiently radiolabel under mild conditions and have good biodistribution properties [206, 207]. Results demonstrate that TPP can successfully be conjugated to DOTA, NOTA, and PCTA chelates. LC-MS of the products can be found in **Figures D-1, D-2, and D-3**.

TPP-DOTA and TPP-NOTA Radiolabeling

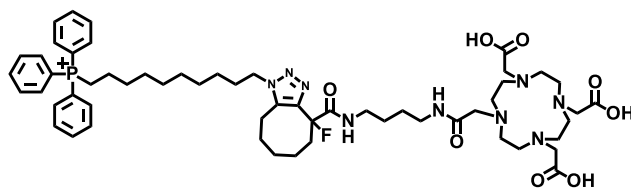
In order to determine if a TPP-chelator conjugate can be successfully radiolabeled with ^{68}Ga and achieve high radiochemical purity, TPP-DOTA and TPP-NOTA were incubated with 165 MBq ^{68}Ga eluted from in-house generators for 15 minutes. Following incubation, the TPP-chelate conjugates were purified and analyzed by radio-HPLC. Results demonstrate that TPP-DOTA and TPP-NOTA achieve > 97% radiochemical purity following radiolabeling and purification. Radio-HPLC traces can be found in **Figures D-4 and D-5**.

Discussion

TPP compounds have been investigated for use in CPI and tumor imaging due to their ability to accumulate in mitochondria rich tissues such as the heart and tumors [95-97, 144, 201-204]. SPECT is one technique that has been employed for CPI and tumor imaging, but technical limitations such as low resolution and photon attenuation in soft tissues has limited the accuracy of SPECT imaging [97, 144, 201, 202]. PET imaging agents offer higher resolution offers a higher resolution and a method for attenuation correction compared to SPECT, but problems with the short half lives of the radionuclides investigated and the need for an on-site cyclotron have limited the clinical feasibility of using PET radionuclide for imaging [144, 201, 205-207]. The PET radionuclides ^{82}Rb (1.27 minute half life), ^{13}N -ammonia (9.97 minute half life), ^{15}O -

water (2.04 minute half life) have been evaluated for CPI [144, 201]. However, the short half-life of these PET radiotracers limits their clinical utility for cardiac and imaging [144, 201, 207].

An alternative approach to PET imaging takes advantage of ^{68}Ga , a radionuclide that has a half life of 68 minutes and is easily produced by a generator [207, 209-211]. To investigate the potential of radiolabeling TPP derivatives with ^{68}Ga for PET imaging, an azide-modified TPP compound was conjugated to alkyne-modified DOTA, NOTA, and PCTA ^{68}Ga chelators [206]. Further, to determine if TPP-chelator conjugates can be radiolabeled with ^{68}Ga and what radiochemical purity is achievable, TPP-chelator compounds were radiolabeled with ^{68}Ga and analyzed by radio-HPLC. Results demonstrate that TPP compounds can be successfully conjugated to ^{68}Ga chelators and TPP-DOTA and TPP-NOTA achieve > 97% radiochemical purification following radiolabeling and purification. Collectively, these results highlight the potential to produce a ^{68}Ga labeled TPP derivative for application in PET imaging.



DOTA-TPP
MW: 1071.29

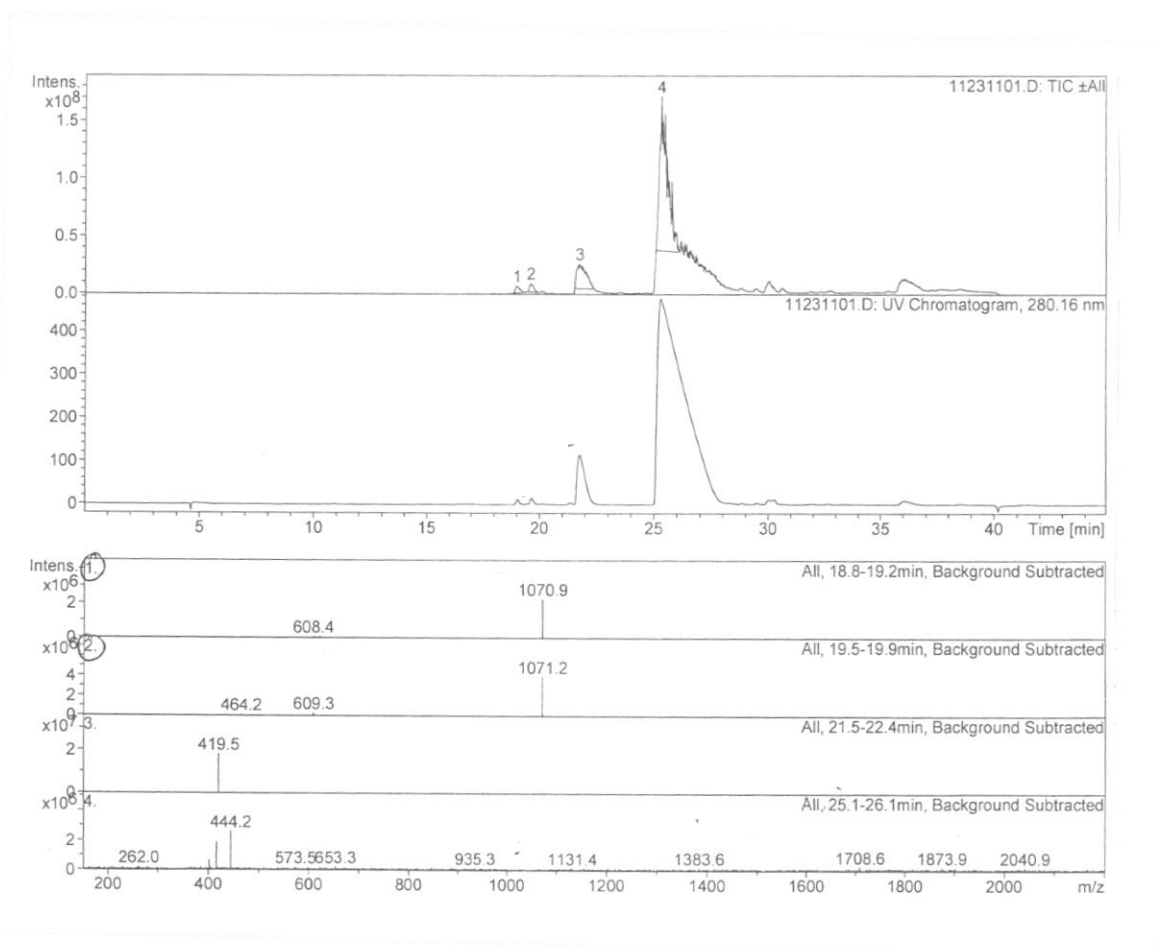


Figure D-1: TPP-DOTA mass spectroscopy confirmation of the product.

LC-MS of purified TPP-DOTA (observed 1071.2, calculated 1071.29).

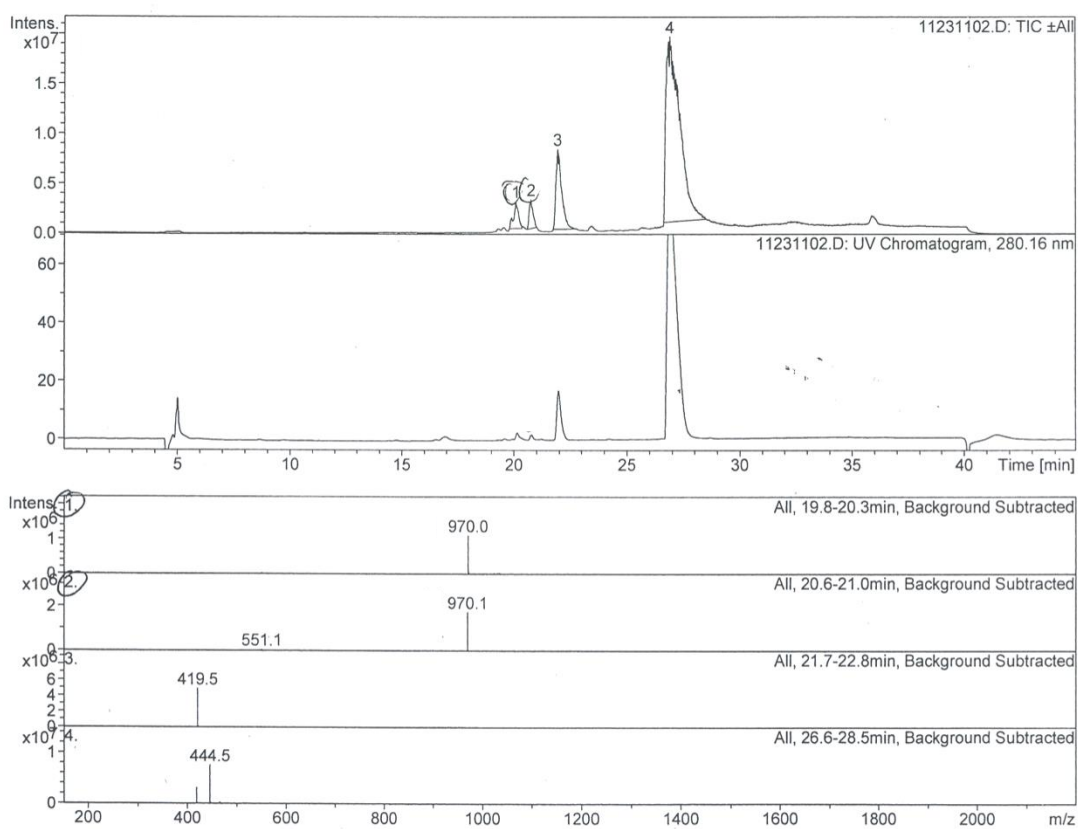
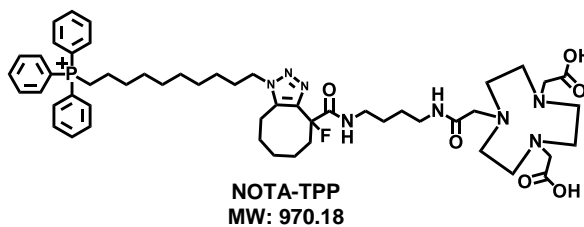


Figure D-2: TPP-NOTA mass spectroscopy confirmation of the product.

ESI-MS of purified TPP-NOTA (observed 970.10; calculated 970.18)

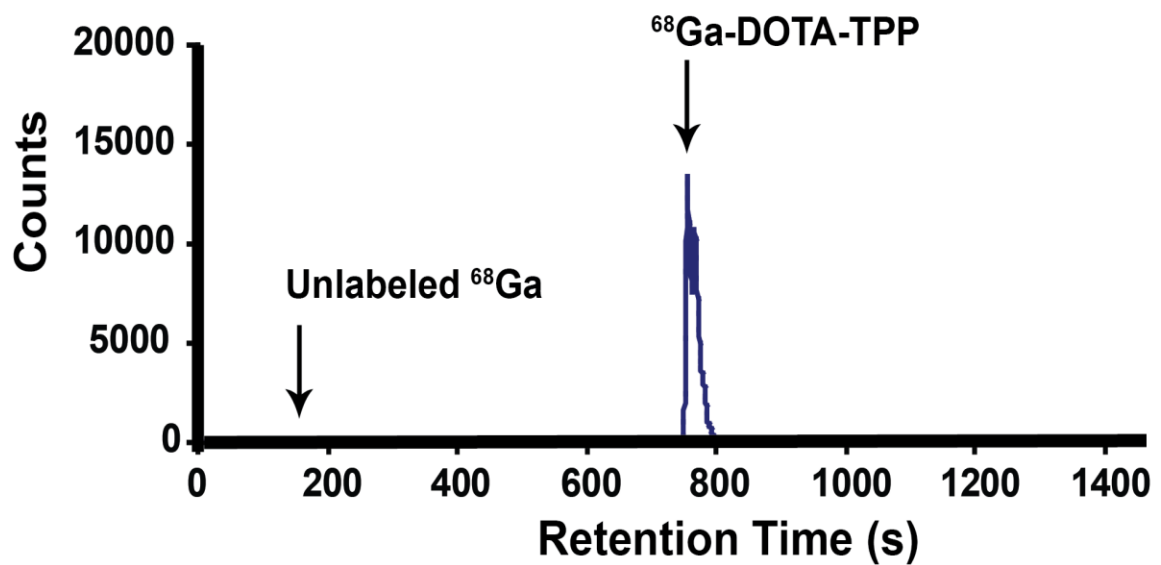


Figure D-4: TPP-DOTA radio-HPLC trace.

Radiochemical purity was assessed on TPP-DOTA by radio-HPLC. TPP-DOTA (10 nmol) was incubated with 165 MBq ⁶⁸Ga at 100° C for 15 min. Following incubation, TPP-DOTA was purified using a C-18 column to remove unlabeled ⁶⁸Ga in order to achieve < 97% radiochemical purity.

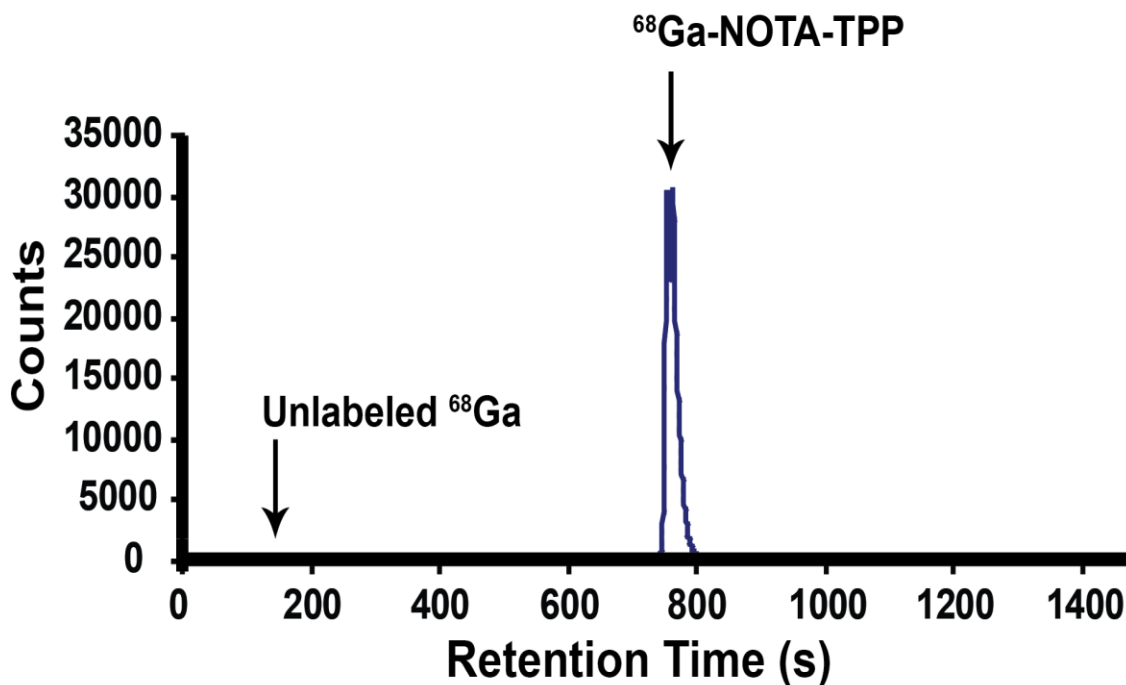


Figure D-5: TPP-NOTA radio-HPLC trace.

Radiochemical purity was assessed on TPP-NOTA by radio-HPLC. TPP-NOTA (5 nmol) was incubated with 191 MBq ⁶⁸Ga at 100° C for 15 min. Following incubation, TPP-DOTA was purified using a C-18 column to remove unlabeled ⁶⁸Ga in order to achieve < 97% radiochemical purity.

REFERENCES

1. Meierjohann, S., *Oxidative stress in melanocyte senescence and melanoma transformation*. Eur J Cell Biol, 2014. **93**(1-2): p. 36-41.
2. Gray-Schopfer, V., C. Wellbrock, and R. Marais, *Melanoma biology and new targeted therapy*. Nature, 2007. **445**(7130): p. 851-7.
3. Spagnolo, F., et al., *BRAF-mutant melanoma: treatment approaches, resistance mechanisms, and diagnostic strategies*. Onco Targets Ther, 2015. **8**: p. 157-68.
4. Miller, A.J. and M.C. Mihm, Jr., *Melanoma*. N Engl J Med, 2006. **355**(1): p. 51-65.
5. Lo, J.A. and D.E. Fisher, *The melanoma revolution: from UV carcinogenesis to a new era in therapeutics*. Science, 2014. **346**(6212): p. 945-9.
6. Shirley, S.H., et al., *Melanocyte and melanoma cell activation by calprotectin*. J Skin Cancer, 2014. **2014**: p. 846249.
7. Eding, C.B., et al., *Melanoma Growth and Progression After Ultraviolet A Irradiation: Impact of Lysosomal Exocytosis and Cathepsin Proteases*. Acta Derm Venereol, 2015. **95**(7): p. 792-7.
8. Weder, G., et al., *Increased plasticity of the stiffness of melanoma cells correlates with their acquisition of metastatic properties*. Nanomedicine, 2014. **10**(1): p. 141-8.
9. Lopez, S., et al., *Comparison of the Transcriptional Profiles of Melanocytes from Dark and Light Skinned Individuals under Basal Conditions and Following Ultraviolet-B Irradiation*. PLoS One, 2015. **10**(8): p. e0134911.
10. Maresca, V., E. Flori, and M. Picardo, *Skin phototype: a new perspective*. Pigment Cell Melanoma Res, 2015. **28**(4): p. 378-89.

11. Zaidi, M.R., C.P. Day, and G. Merlino, *From UVs to metastases: modeling melanoma initiation and progression in the mouse*. J Invest Dermatol, 2008. **128**(10): p. 2381-91.
12. Braeuer, R.R., et al., *Why is melanoma so metastatic?* Pigment Cell Melanoma Res, 2014. **27**(1): p. 19-36.
13. Heilmann, S., et al., *A Quantitative System for Studying Metastasis Using Transparent Zebrafish*. Cancer Res, 2015.
14. Dou, J., et al., *Effect of downregulation of ZEB1 on vimentin expression, tumour migration and tumourigenicity of melanoma B16F10 cells and CSCs*. Cell Biol Int, 2014. **38**(4): p. 452-61.
15. Cheng, G.C., et al., *Oxidative stress and thioredoxin-interacting protein promote intravasation of melanoma cells*. Experimental cell research, 2004. **300**(2): p. 297-307.
16. Mirkina, I., et al., *Phenotyping of human melanoma cells reveals a unique composition of receptor targets and a subpopulation co-expressing ErbB4, EPO-R and NGF-R*. PLoS One, 2014. **9**(1): p. e84417.
17. Tung, J.C., et al., *Tumor mechanics and metabolic dysfunction*. Free Radic Biol Med, 2015. **79**: p. 269-80.
18. Zhang, P., et al., *Sequential binding of alphaVbeta3 and ICAM-1 determines fibrin-mediated melanoma capture and stable adhesion to CD11b/CD18 on neutrophils*. J Immunol, 2011. **186**(1): p. 242-54.
19. Haier, J. and G.L. Nicolson, *Tumor cell adhesion under hydrodynamic conditions of fluid flow*. APMIS, 2001. **109**(4): p. 241-62.
20. Zbytek, B., et al., *Current concepts of metastasis in melanoma*. Expert Rev Dermatol, 2008. **3**(5): p. 569-585.
21. Mills, L., et al., *Fully human antibodies to MCAM/MUC18 inhibit tumor growth and metastasis of human melanoma*. Cancer Res, 2002. **62**(17): p. 5106-14.

22. Park, E.S., et al., *Cross-species hybridization of microarrays for studying tumor transcriptome of brain metastasis*. Proc Natl Acad Sci U S A, 2011. **108**(42): p. 17456-61.
23. Bailey, C.M., J.A. Morrison, and P.M. Kulesa, *Melanoma revives an embryonic migration program to promote plasticity and invasion*. Pigment Cell Melanoma Res, 2012. **25**(5): p. 573-83.
24. Yang, X., et al., *VEGF-B promotes cancer metastasis through a VEGF-A-independent mechanism and serves as a marker of poor prognosis for cancer patients*. Proc Natl Acad Sci U S A, 2015. **112**(22): p. E2900-9.
25. Heinz, M., et al., *Activin A is anti-lymphangiogenic in a melanoma mouse model*. J Invest Dermatol, 2015. **135**(1): p. 212-21.
26. Spiric, Z., Z. Eri, and M. Eric, *Significance of Vascular Endothelial Growth Factor (VEGF)-C and VEGF-D in the Progression of Cutaneous Melanoma*. Int J Surg Pathol, 2015.
27. Zimna, A. and M. Kurpisz, *Hypoxia-Inducible Factor-1 in Physiological and Pathophysiological Angiogenesis: Applications and Therapies*. Biomed Res Int, 2015. **2015**: p. 549412.
28. Filippi, I., et al., *Different Expression of Hypoxic and Angiogenic Factors in Human Endometriotic Lesions*. Reprod Sci, 2015.
29. Khammari, A., et al., *Adoptive T cell therapy combined with intralesional administrations of TG1042 (adenovirus expressing interferon-gamma) in metastatic melanoma patients*. Cancer Immunol Immunother, 2015. **64**(7): p. 805-15.
30. Sanlorenzo, M., et al., *Melanoma immunotherapy*. Cancer Biol Ther, 2014. **15**(6): p. 665-74.
31. Lok, E., et al., *Melanoma brain metastasis globally reconfigures chemokine and cytokine profiles in patient cerebrospinal fluid*. Melanoma Res, 2014. **24**(2): p. 120-30.

32. Schlosser, H.A., et al., *Overcoming tumor-mediated immunosuppression*. Immunotherapy, 2014. **6**(9): p. 973-88.
33. Blank, C.U. and A. Enk, *Therapeutic use of anti-CTLA-4 antibodies*. Int Immunol, 2015. **27**(1): p. 3-10.
34. Siegel, R.L., K.D. Miller, and A. Jemal, *Cancer statistics, 2015*. CA Cancer J Clin, 2015. **65**(1): p. 5-29.
35. Guy, G.P., Jr., et al., *Vital signs: melanoma incidence and mortality trends and projections - United States, 1982-2030*. MMWR Morb Mortal Wkly Rep, 2015. **64**(21): p. 591-6.
36. Finn, L., S.N. Markovic, and R.W. Joseph, *Therapy for metastatic melanoma: the past, present, and future*. BMC medicine, 2012. **10**: p. 23.
37. Marzuka, A., et al., *Melanoma Treatments: Advances and Mechanisms*. J Cell Physiol, 2015. **230**(11): p. 2626-33.
38. Michielin, O. and C. Hoeller, *Gaining momentum: New options and opportunities for the treatment of advanced melanoma*. Cancer Treat Rev, 2015.
39. Lindsay, C.R., P. Spiliopoulou, and A. Waterston, *Blinded by the light: why the treatment of metastatic melanoma has created a new paradigm for the management of cancer*. Ther Adv Med Oncol, 2015. **7**(2): p. 107-21.
40. Niezgoda, A., P. Niezgoda, and R. Czajkowski, *Novel Approaches to Treatment of Advanced Melanoma: A Review on Targeted Therapy and Immunotherapy*. Biomed Res Int, 2015. **2015**: p. 851387.
41. Amaria, R.N., K.D. Lewis, and R. Gonzalez, *Therapeutic options in cutaneous melanoma: latest developments*. Therapeutic advances in medical oncology, 2011. **3**(5): p. 245-51.
42. Roesch, A., et al., *Overcoming intrinsic multidrug resistance in melanoma by blocking the mitochondrial respiratory chain of slow-cycling JARID1B(high) cells*. Cancer Cell, 2013. **23**(6): p. 811-25.

43. Sullivan, R.J. and K.T. Flaherty, *New strategies in melanoma: entering the era of combinatorial therapy*. Clin Cancer Res, 2015. **21**(11): p. 2424-35.
44. Bhatia, S., S.S. Tykodi, and J.A. Thompson, *Treatment of metastatic melanoma: an overview*. Oncology (Williston Park), 2009. **23**(6): p. 488-96.
45. Palathinkal, D.M., et al., *Current systemic therapies for melanoma*. Dermatol Surg, 2014. **40**(9): p. 948-63.
46. Delyon, J., M. Maio, and C. Lebbe, *The ipilimumab lesson in melanoma: achieving long-term survival*. Semin Oncol, 2015. **42**(3): p. 387-401.
47. Hoos, A., et al., *Development of ipilimumab: contribution to a new paradigm for cancer immunotherapy*. Semin Oncol, 2010. **37**(5): p. 533-46.
48. Tarhini, A.A. and F. Iqbal, *CTLA-4 blockade: therapeutic potential in cancer treatments*. Onco Targets Ther, 2010. **3**: p. 15-25.
49. Camacho, L.H., *CTLA-4 blockade with ipilimumab: biology, safety, efficacy, and future considerations*. Cancer Med, 2015. **4**(5): p. 661-72.
50. Theodosakis, N., et al., *Mitochondrial function in melanoma*. Arch Biochem Biophys, 2014. **563**: p. 56-9.
51. Philips, G.K. and M. Atkins, *Therapeutic uses of anti-PD-1 and anti-PD-L1 antibodies*. Int Immunol, 2015. **27**(1): p. 39-46.
52. Homet Moreno, B., et al., *Anti-PD-1 therapy in melanoma*. Semin Oncol, 2015. **42**(3): p. 466-73.
53. Wolchok, J.D., *PD-1 Blockers*. Cell, 2015. **162**(5): p. 937.
54. Lunt, S.Y. and M.G. Vander Heiden, *Aerobic glycolysis: meeting the metabolic requirements of cell proliferation*. Annu Rev Cell Dev Biol, 2011. **27**: p. 441-64.

55. Nelson, D.L., A.L. Lehninger, and M.M. Cox, *Lehninger principles of biochemistry*. 5th ed 2008, New York: W.H. Freeman.
56. Vander Heiden, M.G., L.C. Cantley, and C.B. Thompson, *Understanding the Warburg effect: the metabolic requirements of cell proliferation*. *Science*, 2009. **324**(5930): p. 1029-33.
57. Heller, A., G. Brockhoff, and A. Goepferich, *Targeting drugs to mitochondria*. *Eur J Pharm Biopharm*, 2012. **82**(1): p. 1-18.
58. Lu, J., M. Tan, and Q. Cai, *The Warburg effect in tumor progression: mitochondrial oxidative metabolism as an anti-metastasis mechanism*. *Cancer Lett*, 2015. **356**(2 Pt A): p. 156-64.
59. Liemburg-Apers, D.C., et al., *Mitoenergetic Dysfunction Triggers a Rapid Compensatory Increase in Steady-State Glucose Flux*. *Biophys J*, 2015. **109**(7): p. 1372-86.
60. Pelicano, H., et al., *Glycolysis inhibition for anticancer treatment*. *Oncogene*, 2006. **25**(34): p. 4633-46.
61. Kathagen, A., et al., *Hypoxia and oxygenation induce a metabolic switch between pentose phosphate pathway and glycolysis in glioma stem-like cells*. *Acta Neuropathol*, 2013. **126**(5): p. 763-80.
62. Li, X.B., J.D. Gu, and Q.H. Zhou, *Review of aerobic glycolysis and its key enzymes - new targets for lung cancer therapy*. *Thorac Cancer*, 2015. **6**(1): p. 17-24.
63. Wamelink, M.M., E.A. Struys, and C. Jakobs, *The biochemistry, metabolism and inherited defects of the pentose phosphate pathway: a review*. *J Inher Metab Dis*, 2008. **31**(6): p. 703-17.
64. Gillies, R.J., I. Robey, and R.A. Gatenby, *Causes and consequences of increased glucose metabolism of cancers*. *J Nucl Med*, 2008. **49 Suppl 2**: p. 24S-42S.
65. Chen, X., Y. Qian, and S. Wu, *The Warburg effect: evolving interpretations of an established concept*. *Free Radic Biol Med*, 2015. **79**: p. 253-63.

66. Annibaldi, A. and C. Widmann, *Glucose metabolism in cancer cells*. Curr Opin Clin Nutr Metab Care, 2010. **13**(4): p. 466-70.
67. Wittig, I. and H. Schagger, *Supramolecular organization of ATP synthase and respiratory chain in mitochondrial membranes*. Biochim Biophys Acta, 2009. **1787**(6): p. 672-80.
68. Lenaz, G. and M.L. Genova, *Structure and organization of mitochondrial respiratory complexes: a new understanding of an old subject*. Antioxid Redox Signal, 2010. **12**(8): p. 961-1008.
69. Obre, E. and R. Rossignol, *Emerging concepts in bioenergetics and cancer research: metabolic flexibility, coupling, symbiosis, switch, oxidative tumors, metabolic remodeling, signaling and bioenergetic therapy*. Int J Biochem Cell Biol, 2015. **59**: p. 167-81.
70. Jastroch, M., et al., *Mitochondrial proton and electron leaks*. Essays Biochem, 2010. **47**: p. 53-67.
71. Hammoudi, N., et al., *Metabolic alterations in cancer cells and therapeutic implications*. Chinese journal of cancer, 2011. **30**(8): p. 508-25.
72. Asgari, Y., et al., *Alterations in cancer cell metabolism: the Warburg effect and metabolic adaptation*. Genomics, 2015. **105**(5-6): p. 275-81.
73. Coleman, M.C., et al., *Superoxide mediates acute liver injury in irradiated mice lacking sirtuin 3*. Antioxid Redox Signal, 2014. **20**(9): p. 1423-35.
74. Hrycay, E.G. and S.M. Bandiera, *Involvement of Cytochrome P450 in Reactive Oxygen Species Formation and Cancer*. Adv Pharmacol, 2015. **74**: p. 35-84.
75. Sullivan, L.B. and N.S. Chandel, *Mitochondrial reactive oxygen species and cancer*. Cancer Metab, 2014. **2**: p. 17.
76. Murphy, M.P., *How mitochondria produce reactive oxygen species*. Biochem J, 2009. **417**(1): p. 1-13.

77. Liu-Smith, F., R. Dellinger, and F.L. Meyskens, Jr., *Updates of reactive oxygen species in melanoma etiology and progression*. Arch Biochem Biophys, 2014. **563**: p. 51-5.
78. Lanciano, P., et al., *Molecular mechanisms of superoxide production by complex III: a bacterial versus human mitochondrial comparative case study*. Biochim Biophys Acta, 2013. **1827**(11-12): p. 1332-9.
79. Fath, M.A., et al., *Mitochondrial electron transport chain blockers enhance 2-deoxy-D-glucose induced oxidative stress and cell killing in human colon carcinoma cells*. Cancer biology & therapy, 2009. **8**(13): p. 1228-36.
80. Dayal, D., et al., *Mitochondrial complex II dysfunction can contribute significantly to genomic instability after exposure to ionizing radiation*. Radiation research, 2009. **172**(6): p. 737-45.
81. Aykin-Burns, N., et al., *Increased levels of superoxide and H₂O₂ mediate the differential susceptibility of cancer cells versus normal cells to glucose deprivation*. The Biochemical journal, 2009. **418**(1): p. 29-37.
82. Ahmad, I.M., et al., *Mitochondrial O₂⁻ and H₂O₂ mediate glucose deprivation-induced stress in human cancer cells*. J Biol Chem, 2005. **280**(6): p. 4254-63.
83. Fath, M.A., et al., *Enhancement of Carboplatin-mediated lung cancer cell killing by simultaneous disruption of glutathione and thioredoxin metabolism*. Clinical cancer research : an official journal of the American Association for Cancer Research, 2011. **17**(19): p. 6206-17.
84. Scarbrough, P.M., et al., *Simultaneous inhibition of glutathione- and thioredoxin-dependent metabolism is necessary to potentiate 17AAG-induced cancer cell killing via oxidative stress*. Free radical biology & medicine, 2012. **52**(2): p. 436-43.
85. Coleman, M.C., et al., *2-deoxy-D-glucose causes cytotoxicity, oxidative stress, and radiosensitization in pancreatic cancer*. Free radical biology & medicine, 2008. **44**(3): p. 322-31.

86. Tennant, D.A., R.V. Duran, and E. Gottlieb, *Targeting metabolic transformation for cancer therapy*. Nat Rev Cancer, 2010. **10**(4): p. 267-77.
87. Schafer, F.Q. and G.R. Buettner, *Redox environment of the cell as viewed through the redox state of the glutathione disulfide/glutathione couple*. Free radical biology & medicine, 2001. **30**(11): p. 1191-212.
88. Vander Heiden, M.G., *Targeting cancer metabolism: a therapeutic window opens*. Nat Rev Drug Discov, 2011. **10**(9): p. 671-84.
89. Zhao, Y., E.B. Butler, and M. Tan, *Targeting cellular metabolism to improve cancer therapeutics*. Cell Death Dis, 2013. **4**: p. e532.
90. Xu, K., et al., *A Comparative Study of Gene-Expression Data of Basal Cell Carcinoma and Melanoma Reveals New Insights about the Two Cancers*. PLoS one, 2012. **7**(1): p. e30750.
91. Scott, D.A., et al., *Comparative metabolic flux profiling of melanoma cell lines: beyond the Warburg effect*. J Biol Chem, 2011. **286**(49): p. 42626-34.
92. Venza, M., et al., *Cellular Mechanisms of Oxidative Stress and Action in Melanoma*. Oxid Med Cell Longev, 2015. **2015**: p. 481782.
93. Vayalil, P.K., et al., *A novel class of mitochondria-targeted soft electrophiles modifies mitochondrial proteins and inhibits mitochondrial metabolism in breast cancer cells through redox mechanisms*. PLoS One, 2015. **10**(3): p. e0120460.
94. Rohlena, J., et al., *Anticancer drugs targeting the mitochondrial electron transport chain*. Antioxid Redox Signal, 2011. **15**(12): p. 2951-74.
95. Min, J.J., et al., *Tetraphenylphosphonium as a novel molecular probe for imaging tumors*. J Nucl Med, 2004. **45**(4): p. 636-43.

96. Yang, C.T., et al., *⁶⁴Cu-labeled 2-(diphenylphosphoryl)ethyldiphenylphosphonium cations as highly selective tumor imaging agents: effects of linkers and chelates on radiotracer biodistribution characteristics*. *Bioconjug Chem*, 2008. **19**(10): p. 2008-22.
97. Wang, J., et al., *⁶⁴Cu-Labeled triphenylphosphonium and triphenylarsonium cations as highly tumor-selective imaging agents*. *J Med Chem*, 2007. **50**(21): p. 5057-69.
98. Tong, L., et al., *Reactive oxygen species in redox cancer therapy*. *Cancer Lett*, 2015. **367**(1): p. 18-25.
99. O'Leary, B.R., et al., *Loss of SOD3 (EcSOD) Expression Promotes an Aggressive Phenotype in Human Pancreatic Ductal Adenocarcinoma*. *Clin Cancer Res*, 2015. **21**(7): p. 1741-51.
100. Cumming, R.C., et al., *Protein disulfide bond formation in the cytoplasm during oxidative stress*. *J Biol Chem*, 2004. **279**(21): p. 21749-58.
101. Zhang, H., et al., *Glutaredoxin 2 Reduces Both Thioredoxin 2 and Thioredoxin 1 and Protects Cells from Apoptosis Induced by Auranofin and 4-Hydroxynonenal*. *Antioxid Redox Signal*, 2014.
102. Hamilton, D., J.H. Wu, and G. Batist, *Structure-based identification of novel human gamma-glutamylcysteine synthetase inhibitors*. *Molecular pharmacology*, 2007. **71**(4): p. 1140-7.
103. Mandal, P.K., et al., *System x(c)- and thioredoxin reductase 1 cooperatively rescue glutathione deficiency*. *J Biol Chem*, 2010. **285**(29): p. 22244-53.
104. Li, L., et al., *Combined inhibition of glycolysis, the pentose cycle, and thioredoxin metabolism selectively increases cytotoxicity and oxidative stress in human breast and prostate cancer*. *Redox Biol*, 2015. **4**: p. 127-35.
105. Brigelius-Flohe, R., A. Banning, and K. Schnurr, *Selenium-dependent enzymes in endothelial cell function*. *Antioxid Redox Signal*, 2003. **5**(2): p. 205-15.

106. Wang, G., et al., *Mitochondria thioredoxin's backup role in oxidative stress resistance in Trichoderma reesei*. Microbiol Res, 2015. **171**: p. 32-8.
107. Arner, E.S., et al., *Analysis of the inhibition of mammalian thioredoxin, thioredoxin reductase, and glutaredoxin by cis-diamminedichloroplatinum (II) and its major metabolite, the glutathione-platinum complex*. Free radical biology & medicine, 2001. **31**(10): p. 1170-8.
108. Morris, G., et al., *The glutathione system: a new drug target in neuroimmune disorders*. Mol Neurobiol, 2014. **50**(3): p. 1059-84.
109. Godwin, A.K., et al., *High resistance to cisplatin in human ovarian cancer cell lines is associated with marked increase of glutathione synthesis*. Proceedings of the National Academy of Sciences of the United States of America, 1992. **89**(7): p. 3070-4.
110. Sarsour, E.H., A.L. Kalen, and P.C. Goswami, *Manganese superoxide dismutase regulates a redox cycle within the cell cycle*. Antioxid Redox Signal, 2014. **20**(10): p. 1618-27.
111. Buettner, G.R., et al., *A new paradigm: manganese superoxide dismutase influences the production of H₂O₂ in cells and thereby their biological state*. Free radical biology & medicine, 2006. **41**(8): p. 1338-50.
112. Salem, K., et al., *Copper-zinc superoxide dismutase-mediated redox regulation of bortezomib resistance in multiple myeloma*. Redox Biol, 2015. **4**: p. 23-33.
113. Janowiak, B.E., et al., *Gamma-glutamylcysteine synthetase-glutathione synthetase: domain structure and identification of residues important in substrate and glutathione binding*. Biochemistry, 2006. **45**(35): p. 10461-73.
114. Schmitt, B., et al., *Effects of N-acetylcysteine, oral glutathione (GSH) and a novel sublingual form of GSH on oxidative stress markers: A comparative crossover study*. Redox Biol, 2015. **6**: p. 198-205.
115. Deponte, M., *Glutathione catalysis and the reaction mechanisms of glutathione-dependent enzymes*. Biochim Biophys Acta, 2013. **1830**(5): p. 3217-66.

116. Anderson, M.E., *Glutathione: an overview of biosynthesis and modulation*. Chem Biol Interact, 1998. **111-112**: p. 1-14.
117. Sies, H., *Glutathione and its role in cellular functions*. Free Radic Biol Med, 1999. **27**(9-10): p. 916-21.
118. Anderson, C.P. and C.P. Reynolds, *Synergistic cytotoxicity of buthionine sulfoximine (BSO) and intensive melphalan (L-PAM) for neuroblastoma cell lines established at relapse after myeloablative therapy*. Bone marrow transplantation, 2002. **30**(3): p. 135-40.
119. Cox, A.G., et al., *The thioredoxin reductase inhibitor auranofin triggers apoptosis through a Bax/Bak-dependent process that involves peroxiredoxin 3 oxidation*. Biochem Pharmacol, 2008. **76**(9): p. 1097-109.
120. Fan, C., et al., *Enhancement of auranofin-induced lung cancer cell apoptosis by selenocystine, a natural inhibitor of TrxR1 in vitro and in vivo*. Cell Death Dis, 2014. **5**: p. e1191.
121. Gandin, V., et al., *Cancer cell death induced by phosphine gold(I) compounds targeting thioredoxin reductase*. Biochem Pharmacol, 2010. **79**(2): p. 90-101.
122. Hrabe, J.E., et al., *Disruption of thioredoxin metabolism enhances the toxicity of transforming growth factor beta-activated kinase 1 (TAK1) inhibition in KRAS-mutated colon cancer cells*. Redox Biol, 2015. **5**: p. 319-327.
123. Milagros Rocha, M. and V.M. Victor, *Targeting antioxidants to mitochondria and cardiovascular diseases: the effects of mitoquinone*. Med Sci Monit, 2007. **13**(7): p. RA132-45.
124. Murphy, M.P. and R.A. Smith, *Drug delivery to mitochondria: the key to mitochondrial medicine*. Adv Drug Deliv Rev, 2000. **41**(2): p. 235-50.
125. Ross, M.F., et al., *Lipophilic triphenylphosphonium cations as tools in mitochondrial bioenergetics and free radical biology*. Biochemistry (Mosc), 2005. **70**(2): p. 222-30.

126. Ross, M.F., et al., *Rapid and extensive uptake and activation of hydrophobic triphenylphosphonium cations within cells*. *Biochem J*, 2008. **411**(3): p. 633-45.
127. Millard, M., et al., *Preclinical evaluation of novel triphenylphosphonium salts with broad-spectrum activity*. *PLoS One*, 2010. **5**(10).
128. Smith, R.A., et al., *Delivery of bioactive molecules to mitochondria in vivo*. *Proc Natl Acad Sci U S A*, 2003. **100**(9): p. 5407-12.
129. Murphy, M.P., *Targeting lipophilic cations to mitochondria*. *Biochim Biophys Acta*, 2008. **1777**(7-8): p. 1028-31.
130. Smith, R.A. and M.P. Murphy, *Animal and human studies with the mitochondria-targeted antioxidant MitoQ*. *Ann N Y Acad Sci*, 2010. **1201**: p. 96-103.
131. Snow, B.J., et al., *A double-blind, placebo-controlled study to assess the mitochondria-targeted antioxidant MitoQ as a disease-modifying therapy in Parkinson's disease*. *Mov Disord*, 2010. **25**(11): p. 1670-4.
132. Gane, E.J., et al., *The mitochondria-targeted anti-oxidant mitoquinone decreases liver damage in a phase II study of hepatitis C patients*. *Liver Int*, 2010. **30**(7): p. 1019-26.
133. Reily, C., et al., *Mitochondrially targeted compounds and their impact on cellular bioenergetics*. *Redox Biol*, 2013. **1**(1): p. 86-93.
134. Trendeleva, T.A., et al., *Role of charge screening and delocalization for lipophilic cation permeability of model and mitochondrial membranes*. *Mitochondrion*, 2013. **13**(5): p. 500-6.
135. Ross, M.F., et al., *Accumulation of lipophilic dications by mitochondria and cells*. *Biochem J*, 2006. **400**(1): p. 199-208.
136. Honig, B.H., W.L. Hubbell, and R.F. Flewelling, *Electrostatic interactions in membranes and proteins*. *Annu Rev Biophys Biophys Chem*, 1986. **15**: p. 163-93.

137. Porteous, C.M., et al., *Rapid uptake of lipophilic triphenylphosphonium cations by mitochondria in vivo following intravenous injection: implications for mitochondria-specific therapies and probes*. *Biochim Biophys Acta*, 2010. **1800**(9): p. 1009-17.
138. Ganapathy-Kanniappan, S., *Targeting tumor glycolysis by a mitotropic agent*. *Expert Opin Ther Targets*, 2015: p. 1-5.
139. Trnka, J., M. Elkalaf, and M. Andel, *Lipophilic triphenylphosphonium cations inhibit mitochondrial electron transport chain and induce mitochondrial proton leak*. *PLoS One*, 2015. **10**(4): p. e0121837.
140. Bielski, E.R., et al., *Effect of the Conjugation Density of Triphenylphosphonium Cation on the Mitochondrial Targeting of Poly(amidoamine) Dendrimers*. *Mol Pharm*, 2015. **12**(8): p. 3043-53.
141. Apostolova, N. and V.M. Victor, *Molecular strategies for targeting antioxidants to mitochondria: therapeutic implications*. *Antioxid Redox Signal*, 2015. **22**(8): p. 686-729.
142. Smith, R.A., R.C. Hartley, and M.P. Murphy, *Mitochondria-targeted small molecule therapeutics and probes*. *Antioxid Redox Signal*, 2011. **15**(12): p. 3021-38.
143. Benedetti, M.S., et al., *Drug metabolism and pharmacokinetics*. *Drug Metab Rev*, 2009. **41**(3): p. 344-90.
144. Kim, D.Y., et al., *Synthesis of [(1)(8)F]-labeled (2-(2-fluoroethoxy)ethyl)triphenylphosphonium cation as a potential agent for myocardial imaging using positron emission tomography*. *Bioorg Med Chem Lett*, 2012. **22**(1): p. 319-22.
145. Zhao, G., et al., *Membrane potential-dependent uptake of 18F-triphenylphosphonium--a new voltage sensor as an imaging agent for detecting burn-induced apoptosis*. *J Surg Res*, 2014. **188**(2): p. 473-9.
146. Kwak, M.K., et al., *Suppression of in vivo tumor growth by using a biodegradable thermosensitive hydrogel polymer containing chemotherapeutic agent*. *Invest New Drugs*, 2010. **28**(3): p. 284-90.

147. Kim, Y., et al., *Locally targeted delivery of a micron-size radiation therapy source using temperature-sensitive hydrogel*. Int J Radiat Oncol Biol Phys, 2014. **88**(5): p. 1142-7.
148. Cho, J.K., H.J. Kuh, and S.C. Song, *Injectable poly(organophosphazene) hydrogel system for effective paclitaxel and doxorubicin combination therapy*. J Drug Target, 2014. **22**(8): p. 761-7.
149. Heilmann, S., et al., *A thermosensitive morphine-containing hydrogel for the treatment of large-scale skin wounds*. Int J Pharm, 2013. **444**(1-2): p. 96-102.
150. Frith, J.E., et al., *An injectable hydrogel incorporating mesenchymal precursor cells and pentosan polysulphate for intervertebral disc regeneration*. Biomaterials, 2013. **34**(37): p. 9430-40.
151. Peng, Q., et al., *Injectable and biodegradable thermosensitive hydrogels loaded with PHBHHx nanoparticles for the sustained and controlled release of insulin*. Acta Biomater, 2013. **9**(2): p. 5063-9.
152. Liu, Y., et al., *[Controlled release of functional proteins IGF-1, aFGF and VEGF through self-assembling peptide nanofiber hydrogel]*. Sheng Wu Yi Xue Gong Cheng Xue Za Zhi, 2011. **28**(2): p. 310-3.
153. Wu, J., et al., *A thermosensitive hydrogel based on quaternized chitosan and poly(ethylene glycol) for nasal drug delivery system*. Biomaterials, 2007. **28**(13): p. 2220-32.
154. Cheng, G., et al., *Mitochondria-Targeted Drugs Synergize with 2-Deoxyglucose to Trigger Breast Cancer Cell Death*. Cancer Research, 2012. **72**(10): p. 2634-2644.
155. Carmichael, J., et al., *Evaluation of a tetrazolium-based semiautomated colorimetric assay: assessment of chemosensitivity testing*. Cancer research, 1987. **47**(4): p. 936-42.
156. Griffith, O.W., *Determination of glutathione and glutathione disulfide using glutathione reductase and 2-vinylpyridine*. Anal Biochem, 1980. **106**(1): p. 207-12.

157. Anderson, M.E., *Determination of glutathione and glutathione disulfide in biological samples*. Methods Enzymol, 1985. **113**: p. 548-55.
158. Spitz, D.R. and L.W. Oberley, *An assay for superoxide dismutase activity in mammalian tissue homogenates*. Anal Biochem, 1989. **179**(1): p. 8-18.
159. Wang, H.P., et al., *Phospholipid hydroperoxide glutathione peroxidase protects against singlet oxygen-induced cell damage of photodynamic therapy*. Free Radic Biol Med, 2001. **30**(8): p. 825-35.
160. Wang, H.P., et al., *Phospholipid hydroperoxide glutathione peroxidase induces a delay in G1 of the cell cycle*. Free Radic Res, 2003. **37**(6): p. 621-30.
161. Berridge, M.V., P.M. Herst, and A.S. Tan, *Tetrazolium dyes as tools in cell biology: new insights into their cellular reduction*. Biotechnol Annu Rev, 2005. **11**: p. 127-52.
162. Wagner, B.A., S. Venkataraman, and G.R. Buettner, *The rate of oxygen utilization by cells*. Free radical biology & medicine, 2011. **51**(3): p. 700-12.
163. Lin, X., et al., *2-Deoxy-D-glucose-induced cytotoxicity and radiosensitization in tumor cells is mediated via disruptions in thiol metabolism*. Cancer research, 2003. **63**(12): p. 3413-7.
164. Kondo, T., et al., *gamma-Glutamylcysteine synthetase and active transport of glutathione S-conjugate are responsive to heat shock in K562 erythroid cells*. J Biol Chem, 1993. **268**(27): p. 20366-72.
165. Leier, I., et al., *ATP-dependent glutathione disulphide transport mediated by the MRP gene-encoded conjugate export pump*. Biochem J, 1996. **314** (Pt 2): p. 433-7.
166. Zhang, K. and K.P. Wong, *Active transport of glutathione S-conjugate in human colon adenocarcinoma cells*. Cancer Lett, 1996. **108**(1): p. 143-51.

167. Brechbuhl, H.M., et al., *Glutathione transport is a unique function of the ATP-binding cassette protein ABCG2*. J Biol Chem, 2010. **285**(22): p. 16582-7.
168. Rothnie, A., et al., *Mechanistic differences between GSH transport by multidrug resistance protein 1 (MRP1/ABCC1) and GSH modulation of MRP1-mediated transport*. Mol Pharmacol, 2008. **74**(6): p. 1630-40.
169. Olive, C. and P. Board, *Glutathione S-conjugate transport by cultured human cells*. Biochim Biophys Acta, 1994. **1224**(2): p. 264-8.
170. Yang, W.S., et al., *Regulation of ferroptotic cancer cell death by GPX4*. Cell, 2014. **156**(1-2): p. 317-31.
171. Bhowmick, D. and G. Mugesh, *Insights into the catalytic mechanism of synthetic glutathione peroxidase mimetics*. Org Biomol Chem, 2015. **13**(41): p. 10262-72.
172. Zhang, F., S.S. Lau, and T.J. Monks, *The cytoprotective effect of N-acetyl-L-cysteine against ROS-induced cytotoxicity is independent of its ability to enhance glutathione synthesis*. Toxicol Sci, 2011. **120**(1): p. 87-97.
173. Morrison, J.P., et al., *Thiol supplementation in aged animals alters antioxidant enzyme activity after heat stress*. Journal of applied physiology, 2005. **99**(6): p. 2271-7.
174. Fink, B.D., et al., *A mitochondrial-targeted coenzyme q analog prevents weight gain and ameliorates hepatic dysfunction in high-fat-fed mice*. J Pharmacol Exp Ther, 2014. **351**(3): p. 699-708.
175. Antonenko, Y.N., et al., *Penetrating cations enhance uncoupling activity of anionic protonophores in mitochondria*. PLoS One, 2013. **8**(4): p. e61902.
176. Sosman, J.A. and K.A. Margolin, *Inside life of melanoma cell signaling, molecular insights, and therapeutic targets*. Current oncology reports, 2009. **11**(5): p. 405-11.
177. Jacobs, J.F., et al., *Regulatory T cells in melanoma: the final hurdle towards effective immunotherapy?* Lancet Oncol, 2012. **13**(1): p. e32-42.

178. Carlino, M.S., et al., *(18)F-labelled fluorodeoxyglucose-positron emission tomography (FDG-PET) heterogeneity of response is prognostic in dabrafenib treated BRAF mutant metastatic melanoma*. Eur J Cancer, 2013. **49**(2): p. 395-402.
179. Sonveaux, P., et al., *Targeting lactate-fueled respiration selectively kills hypoxic tumor cells in mice*. J Clin Invest, 2008. **118**(12): p. 3930-42.
180. Zito, C.R. and H.M. Kluger, *Immunotherapy for metastatic melanoma*. J Cell Biochem, 2012. **113**(3): p. 725-34.
181. Spagnolo, F. and P. Queirolo, *Upcoming strategies for the treatment of metastatic melanoma*. Arch Dermatol Res, 2012. **304**(3): p. 177-84.
182. Shieh, J.M., et al., *Activation of c-Jun N-terminal kinase is essential for mitochondrial membrane potential change and apoptosis induced by doxycycline in melanoma cells*. Br J Pharmacol, 2010. **160**(5): p. 1171-84.
183. Altman, M.K., et al., *Targeting melanoma growth and viability reveals dualistic functionality of the phosphonothionate analogue of carba cyclic phosphatidic acid*. Mol Cancer, 2010. **9**: p. 140.
184. Soengas, M.S. and S.W. Lowe, *Apoptosis and melanoma chemoresistance*. Oncogene, 2003. **22**(20): p. 3138-51.
185. Niehr, F., et al., *Combination therapy with vemurafenib (PLX4032/RG7204) and metformin in melanoma cell lines with distinct driver mutations*. J Transl Med, 2011. **9**: p. 76.
186. Grippo, J.F., et al., *A phase I, randomized, open-label study of the multiple-dose pharmacokinetics of vemurafenib in patients with BRAF V600E mutation-positive metastatic melanoma*. Cancer Chemother Pharmacol, 2014. **73**(1): p. 103-11.
187. Corazao-Rozas, P., et al., *Mitochondrial oxidative stress is the Achille's heel of melanoma cells resistant to Braf-mutant inhibitor*. Oncotarget, 2013. **4**(11): p. 1986-98.

188. Yu, L., et al., *Involvement of superoxide and nitric oxide in BRAF(V600E) inhibitor PLX4032-induced growth inhibition of melanoma cells*. Integr Biol (Camb), 2014. **6**(12): p. 1211-7.
189. Haq, R., et al., *Oncogenic BRAF regulates oxidative metabolism via PGC1alpha and MITF*. Cancer Cell, 2013. **23**(3): p. 302-15.
190. Rustin, P., et al., *Biochemical and molecular investigations in respiratory chain deficiencies*. Clin Chim Acta, 1994. **228**(1): p. 35-51.
191. Birch-Machin, M.A., et al., *An evaluation of the measurement of the activities of complexes I-IV in the respiratory chain of human skeletal muscle mitochondria*. Biochemical medicine and metabolic biology, 1994. **51**(1): p. 35-42.
192. Kruger, N.J., *The Bradford method for protein quantitation*. Methods Mol Biol, 1994. **32**: p. 9-15.
193. Benit, P., et al., *Three spectrophotometric assays for the measurement of the five respiratory chain complexes in minuscule biological samples*. Clinica chimica acta; international journal of clinical chemistry, 2006. **374**(1-2): p. 81-6.
194. Baumhover, N.J., et al., *Improved synthesis and biological evaluation of chelator-modified alpha-MSH analogs prepared by copper-free click chemistry*. Bioorganic & medicinal chemistry letters, 2011. **21**(19): p. 5757-61.
195. Martin, M.E., et al., *"Click"-cyclized (68)Ga-labeled peptides for molecular imaging and therapy: synthesis and preliminary in vitro and in vivo evaluation in a melanoma model system*. Recent Results Cancer Res, 2013. **194**: p. 149-75.
196. Martin, M.E., et al., *A DOTA-peptide conjugate by copper-free click chemistry*. Bioorganic & medicinal chemistry letters, 2010. **20**(16): p. 4805-7.
197. Jara, J.A., et al., *Antiproliferative and uncoupling effects of delocalized, lipophilic, cationic gallic acid derivatives on cancer cell lines. Validation in vivo in syngenic mice*. J Med Chem, 2014. **57**(6): p. 2440-54.

198. Atkinson, J., et al., *A mitochondria-targeted inhibitor of cytochrome c peroxidase mitigates radiation-induced death*. Nat Commun, 2011. **2**: p. 497.
199. Constant-Urban, C., et al., *Triphenylphosphonium salts of 1,2,4-benzothiadiazine 1,1-dioxides related to diazoxide targeting mitochondrial ATP-sensitive potassium channels*. Bioorg Med Chem Lett, 2013. **23**(21): p. 5878-81.
200. Ripcke, J., et al., *Small-molecule targeting of the mitochondrial compartment with an endogenously cleaved reversible tag*. Chembiochem, 2009. **10**(10): p. 1689-96.
201. Kim, D.Y., et al., *Comparison of ¹⁸F-labeled Fluoroalkylphosphonium Cations with ¹³N-NH₃ for PET Myocardial Perfusion Imaging*. J Nucl Med, 2015.
202. Sakai, T., et al., *Development of radioiodinated lipophilic cationic compounds for myocardial imaging*. Nucl Med Biol, 2015. **42**(5): p. 482-7.
203. Gurm, G.S., et al., *4-[¹⁸F]-tetraphenylphosphonium as a PET tracer for myocardial mitochondrial membrane potential*. JACC Cardiovasc Imaging, 2012. **5**(3): p. 285-92.
204. Li, Z., et al., *A (^{99m}Tc)-labeled triphenylphosphonium derivative for the early detection of breast tumors*. Cancer Biother Radiopharm, 2009. **24**(5): p. 579-87.
205. Lee, H., et al., *A gradient-loadable (⁶⁴Cu)-chelator for quantifying tumor deposition kinetics of nanoliposomal therapeutics by positron emission tomography*. Nanomedicine, 2015. **11**(1): p. 155-65.
206. Rockey, W.M., et al., *Synthesis and radiolabeling of chelator-RNA aptamer bioconjugates with copper-64 for targeted molecular imaging*. Bioorg Med Chem, 2011. **19**(13): p. 4080-90.
207. Ferreira, C.L., et al., *Evaluation of bifunctional chelates for the development of gallium-based radiopharmaceuticals*. Bioconjug Chem, 2010. **21**(3): p. 531-6.

208. Schjoeth-Eskesen, C., et al., *[(64) Cu]-labelled trastuzumab: optimisation of labelling by DOTA and NODAGA conjugation and initial evaluation in mice*. J Labelled Comp Radiopharm, 2015. **58**(6): p. 227-33.
209. Liu, Q., et al., *Targeting of MMP2 activity in malignant tumors with a Ga-labeled gelatinase inhibitor cyclic peptide*. Nucl Med Biol, 2015.
210. Burke, B.P., et al., *Chelator free gallium-68 radiolabelling of silica coated iron oxide nanorods via surface interactions*. Nanoscale, 2015. **7**(36): p. 14889-96.
211. Autio, A., et al., *Absorption, distribution and excretion of intravenously injected (68)Ge/ (68)Ga generator eluate in healthy rats, and estimation of human radiation dosimetry*. EJNMMI Res, 2015. **5**(1): p. 117.